

POLITECNICO DI TORINO

Master's Degree program in Electrical Engineering



Master's Thesis

Development of a test protocol for remanufacturing of automotive batteries and model-based cell repurposing

Supervisors:

Prof. Paolo Guglielmi

Prof. Francesco Maltoni

Candidate

Luca Vacca

March 2020



This thesis was presented at the Chair of Production Engineering of E-Mobility Components (PEM) at RWTH Aachen.

Master Thesis

Name: Luca Vacca

Matr.-No.: 414023

Title: Development of a test protocol for remanufacturing of automotive batteries and model-based cell repurposing

Supervising assistant: Dipl.-Ing. Francesco Maltoni

1. Examiner: Prof. Dr.-Ing. Achim Kampker

2. Examiner: Dr.-Ing. Dipl.-Wirt.-Ing. Heiner Hans Heimes

Aachen, February 22, 2020

The contents and the result of this thesis are for internal use only. All copyrights remain with RWTH Aachen. This thesis or parts of it are not to be transferred to a third party without the express authorization of the supervising professor.

I Table of contents

I	Table of contents	i
II	Symbols and acronyms	iv
III	List of the figures	vi
IV	List of tables	xii
1	Introduction	15
1.1	Background and Motivation.....	15
1.2	Structure, Objectives and Limitations of the thesis	17
2	General overview	19
2.1	Battery systems	19
2.1.1	Modelling.....	24
2.2	Remanufacturing.....	33
2.3	Re-use and second life	36
3	State of the art	40
3.1	Relaxation.....	40
3.2	Parametrization of the battery	41
3.3	Self-discharge.....	46
3.3.1	Potentiostatic method.....	47
3.4	Capacity.....	49
3.4.1	Research question	52
4	Technical approach	53
4.1	Battery pack.....	53
4.2	Modules	57
4.3	Cells.....	59
4.3.1	Voltage vs SOC.....	60
5	Testing procedure	62
5.1	Testing equipment	62
5.2	Relaxation.....	63
5.3	Pulse tests	67
5.4	Self-discharge.....	74
5.5	Available capacity	76

5.6	Final testing protocol.....	77
6	Results and discussion.....	81
6.1	Main results	81
6.1.1	Battery pack #1	81
6.1.2	Battery pack #2	84
6.1.3	Battery pack #3	87
6.2	Overall results.....	90
6.2.1	SOH	90
6.2.2	EEC parameters.....	94
6.2.3	R_0	95
6.2.4	R_1	96
6.2.5	R_2	97
6.2.6	C_1	98
6.2.7	C_2	100
6.2.8	R_{tot}	100
6.3	Distributions over the SOH.....	101
7	Correlation between parameters and SOH	107
7.1	SOH Self-discharge	108
7.2	SOH and EEC parameters.....	109
7.2.1	SOH- R_0	110
7.2.2	SOH- R_1	112
7.2.3	SOH- R_2	114
7.2.4	SOH- C_1	116
7.2.5	SOH- C_2	118
7.2.6	SOH- R_{tot}	120
7.3	Overall correlation trends	122
8	EEC Simulations	129
8.1	Simulink model.....	129
8.2	Energy losses	135
8.2.1	Full charge (0-100%).....	136
8.2.2	20-80% Charge	138
8.2.3	35-65% charge.....	144

I Table of contents	iii
9 Conclusions and future work.....	150
9.1 Conclusions	150
9.2 Future work.....	152
V Bibliography.....	154

II Symbols and acronyms

Acronym	Description
AC	Alternate Current
AESC	Automotive Energy Supply Corporation
Ah	Ampere hour
AVG	Average
BEV	Battery Electric Vehicle
BMS	Battery Management System
BP	Battery Pack
C	Capacitance
CC	Constant Current
C-rate	Current Rate
CV	Constant Voltage
DC	Direct Current
DOD	Depth of Discharge
EEC	Electric Equivalent Circuit
EIS	Electrochemical Impedance Spectroscopy
EOL	End-of-Life
EES	Energy Storage Systems
EMS	Energy Management System
EV	Electric Vehicle
GHG	Greenhouse Gas
HEV	Hybrid Electric Vehicle
I	Current
ICE	Internal Combustion Engine
Li-Ion	Lithium-Ion
OCV	Open Circuit Voltage
OEM	Original Equipment Manufacturer
PHEV	Plug-in Hybrid Electric Vehicles
PV	Photovoltaic
R	Resistance

RES	Renewable Energy Source
RUL	Remaining Useful Life
SD	Self-discharge
SOC	State of Charge
SOH	State of Health
STD DEV	Standard Deviation
TSO	Transmission System Operator
(UNFCCC)	United Nations Framework Convention on Climate Change
V	Voltage
Wh	Watt hour

III List of the figures

Figure 2.1 Li-Ion cell operation during the discharging process Vgl. Yuping Wu (Lithium-Ion Batteries: Fundamentals and Applications) 2015.	20
Figure 2.2 Li-Ion cell operation during the charging process Vgl. Yuping Wu (Lithium-Ion Batteries: Fundamentals and Applications) 2015.	21
Figure 2.3 OCV vs SOC plots with different C-rates.	24
Figure 2.4 The most simple EEC model used to simulate the behaviour of a cell of a Li-ion battery.	28
Figure 2.5 Three types of EEC models, <i>Internal resistance model</i> , <i>Thevenin model</i> , and <i>Double parametrization model</i>	29
Figure 2.6 Example of the DC current pulse to extract the parameters for <i>the Double polarization model</i> Vgl. Stroe (Master of Research (MRES) - Introduction to Battery Models) 2018.	32
Figure 2.7 Scheme of the steps of the second life process.	34
Figure 2.8 Example of the production, utilization, and second life use processes of a battery pack.	37
Figure 2.9 Raw power profile vs power smoothing of a PV power plant.	38
Figure 3.1 Example of voltage profile during the relaxation pause (1 minute) at 20% SOC after a charging state with 1.5 C.	41
Figure 3.2 Electrical Equivalent Circuit used to model the Li-Ion battery.	42
Figure 3.3 Example of voltage drop due to a current pulse of 1.5 C at 35% SOC.	45
Figure 3.4 Example of self-discharge evaluation using the potentiostatic method Vgl. Keysight Technologies (Evaluate Lithium Ion Self-Discharge of Cells in a Fraction of the Time Traditionally Required).	48
Figure 3.5 Profile of the voltage during the discharging (100%-0%) (module from Nissan Leaf 2011 Edition's battery pack).	51
Figure 4.1 Division in 3 subpacks of the battery pack.	54

Figure 4.2 Scheme of the electrical connection of the modules inside the battery pack of the Nissan Leaf 2011 Edition.....	56
Figure 4.3 Position of the battery pack in the Nissan Leaf 2011 Edition.....	57
Figure 4.4 Disposition of the four cells inside the module of the Nissan Leaf 2011 Edition. ...	59
Figure 4.5 Cell used to manufacture the battery pack of the Nissan Leaf 2011 Edition.....	60
Figure 4.6 Nissan Leaf 2011 Edition cell's polarization curve Vgl. AESC Corp (Specifications Nissan Leaf 2011 Edition) 2011.	61
Figure 5.1 Voltage during the pulse tests at 20% SOC.	70
Figure 5.2 Voltage during the pulse tests at 50% SOC.	70
Figure 5.3 Voltage during the pulse tests at 95% SOC.	71
Figure 5.4 Polarization curve, during the charging process, of the module from the battery pack of the Nissan Leaf 2011 Edition (1 C).....	73
Figure 5.5 Polarization curve, during the charging and discharging processes, of the module from the battery pack of the Nissan Leaf 2011 Edition (1 C).	74
Figure 5.6 Graph of the results of the introductory tests for the self-discharge.	75
Figure 5.7 Voltage and Current profiles during the capacity test.	76
Figure 5.8 Division of the phases that form the final testing protocol used for all the testing of the modules	78
Figure 5.9 Three Nissan Leaf 2011 Edition (24 kWh) modules during the testing.	79
Figure 6.1 Gauss distribution of the SOH of the first battery pack.....	82
Figure 6.2 Division of the SOH of the modules of the battery pack #1, sorted by subpacks. .	84
Figure 6.3 Gauss distribution of the SOH of the second battery pack.....	85
Figure 6.4 Division of the SOH of the modules of the battery pack #2, sorted by subpacks. .	87
Figure 6.5 Gauss distribution of the SOH of the third battery pack (BP #3).....	88
Figure 6.6 Division of the SOH of the modules of the battery pack #3, sorted by subpacks. .	90

Figure 6.7 Distribution of the SOH percentages between the three battery packs tested.	92
Figure 6.8 SOH percentages sorted by module number and divided in the three battery packs.	93
Figure 6.9 Comparison of the plots of the values of R_0 of the modules with the maximum and minimum SOH.	96
Figure 6.10 Comparison of the plots of the values of R_1 of the modules with the maximum and minimum SOH.	97
Figure 6.11 Comparison of the plots of the values of R_2 of the modules with the maximum and minimum SOH.	98
Figure 6.12 Comparison of the plots of the values of C_1 of the modules with the maximum and minimum SOH.	99
Figure 6.13 Comparison of the plots of the values of C_2 of the modules with the maximum and minimum SOH.	100
Figure 6.14 Comparison of the plots of the values of R_{tot} of the modules with the maximum and minimum SOH.	101
Figure 6.15 Distribution of R_{tot} at different SOC levels, sorted by battery pack, over the available remaining capacity.	103
Figure 6.16 Distribution of R_{tot} (m Ω) over the available remaining capacity (Ah) sorted by battery packs.	104
Figure 6.17 Distribution of the self-discharge rate (%/h) over the available remaining capacity (Ah) sorted by battery packs.	105
Figure 7.1 Comparison of the correlation indexes between SOH and self-discharge for the three battery packs.	108
Figure 7.2 Correlation between SOH and R_0 for BP #1 using different C-rates and SOC levels.	110
Figure 7.3 Correlation between SOH and R_0 for BP #2 using different C-rates and SOC levels.	111
Figure 7.4 Correlation between SOH and R_0 for BP #3 using different C-rates and SOC levels.	112

Figure 7.5 Correlation between SOH and R_1 for BP #1 using different C-rates and SOC levels. 113

Figure 7.6 Correlation between SOH and R_1 for BP #2 using different C-rates and SOC levels. 113

Figure 7.7 Correlation between SOH and R_1 for BP #3 using different C-rates and SOC levels. 114

Figure 7.8 Correlation between SOH and R_2 for BP #1 using different C-rates and SOC levels. 115

Figure 7.9 Correlation between SOH and R_2 for BP #2 using different C-rates and SOC levels. 115

Figure 7.10 Correlation between SOH and R_2 for BP #3 using different C-rates and SOC levels. 116

Figure 7.11 Correlation between SOH and C_1 for BP #1 using different C-rates and SOC levels. 117

Figure 7.12 Correlation between SOH and C_1 for BP #2 using different C-rates and SOC levels. 117

Figure 7.13 Correlation between SOH and C_1 for BP #3 using different C-rates and SOC levels. 118

Figure 7.14 Correlation between SOH and C_2 for BP #1 using different C-rates and SOC levels. 119

Figure 7.15 Correlation between SOH and C_2 for BP #2 using different C-rates and SOC levels. 119

Figure 7.16 Correlation between SOH and C_2 for BP #3 using different C-rates and SOC levels. 120

Figure 7.17 Correlation between SOH and R_{tot} for BP #1 using different C-rates and SOC levels. 121

Figure 7.18 Correlation between SOH and R_{tot} for BP #2 using different C-rates and SOC levels. 121

Figure 7.19 Correlation between SOH and R_{tot} for BP #3 using different C-rates and SOC levels. 122

Figure 7.20 Correlation between the SOH and the parameters of the EEC measured at 10% using 1.5 C.	123
Figure 7.21 Correlation between the SOH and the parameters of the EEC measured at 50% using 1.5 C.	124
Figure 7.22 Correlation between the SOH and the parameters of the EEC measured at 95% using 1.5 C.	126
Figure 7.23 Highest correlation indexes for the different parameters extracted from the testing procedure.	127
Figure 8.1 Simulink dynamic model of the EEC of the module of the Nissan Leaf 2011 Edition.	130
Figure 8.2 Particular of the Simulink model, it represents the behaviour of the R_1C_1 parallel branch during the use of the battery.	131
Figure 8.3 Trends of the change of the total resistance R_{tot} with at different C-rates for M35 BP #1.	133
Figure 8.4 Trends of the change of the total resistance R_{tot} with at different C-rates for M11 BP #2.	134
Figure 8.5 Trends of the change of the total resistance R_{tot} with at different C-rates for M13 BP #3.	134
Figure 8.6 Comparison between the energy loss experienced by the module during a full charge using different C-rates.	138
Figure 8.7 Energy losses due to the resistive parameters in the 20-80% charge with different C-rates.	140
Figure 8.8 Energy losses due to the resistive parameters R_0 , R_1 , and R_2 , in the 20-80% charge with 0.1 C (6.6 A).	142
Figure 8.9 Energy loss due to the resistive parameters R_0 , R_1 , and R_2 , in the 20-80% charge with 1 C (66 A).	143
Figure 8.10 Energy losses due to the resistive parameters in the 35-65% charge with different C-rates.	145
Figure 8.11 Energy loss due to the resistive parameters R_0 , R_1 , and R_2 , in the 35-65% charge with 0.5 C (33 A).	146

Figure 8.12 Energy loss due to the resistive parameters R_0 , R_1 , and R_2 , in the 35-65% charge with 1 C (66 A)..... 147

Figure 8.13 Energy loss due to the resistive parameters R_0 , R_1 , and R_2 , in the 35-65% charge with 4 C (264 A)..... 148

IV List of tables

Table 4.1 Numeration of the modules in between the subpacks.	54
Table 4.2 Main specification of the battery pack Nissan Leaf 2011 Edition.	55
Table 4.3 Main specifications of the module of the Nissan Leaf 2011 Edition.	58
Table 4.4 Main specifications of the cell of the Nissan Leaf 2011 Edition	59
Table 4.5 Conversion between C-rate and current for the cell used in the pack of the Nissan Leaf 2011 Edition.	60
Table 5.1 Digatron BNT 50-100-6BDBT specifications.	62
Table 5.2 List of the SOC levels at which the relaxation phenomenon has been tested during the introductory tests.	64
Table 5.3 Results of the trials of the introductory tests for the relaxation processes.	65
Table 5.4 Voltage levels prior to and after the relaxation for the SOC levels object of the pulse tests.	67
Table 5.5 List of the testing cases used to extract the parameters for the EEC using the pulse tests.	68
Table 5.6 Conversion of the SOC levels, percentages, to voltage levels (V).	69
Table 5.7 Conversion from the parameters of the battery to the physical ones.	70
Table 5.8 Comparison between the voltage drops at that occur 20%, 50%, and at 95% with 0.5 C current pulse.	71
Table 5.9 Comparison between the voltage drops that occur at 20%, 50%, and at 95% with 1 C current pulse.	72
Table 5.10 Comparison between the voltage drops that occur at 20%, 50%, and at 95% with 1.5 C current pulse.	72
Table 5.11 Test performed to determine the best self-discharge test to be implemented in the final testing protocol.	75
Table 6.1 Main findings first battery pack.	83

Table 6.2 Comparison of the available capacity of the subpacks for battery pack #1.....	83
Table 6.3 Main findings second battery pack.....	85
Table 6.4 Comparison of the available capacity of the subpacks for battery pack #2.....	86
Table 6.5 Main findings third battery pack.	89
Table 6.6 Comparison of the available capacity of the subpacks for battery pack #3.....	89
Table 6.7 Average SOH percentage of the modules of the three battery packs.....	92
Table 6.8 Standard deviation values of the main parameters sorted by battery packs.....	94
Table 6.9 Data of the module with the overall highest SOH percentage between the three battery packs.	95
Table 6.10 Data of the module with the overall lowest SOH percentage between the three battery packs.	95
Table 7.1 Correlation indexes between SOH and self-discharge for the three battery packs.	109
Table 7.2 Correlation between the SOH and the parameters of the EEC measured at 10% using 1.5 C.	123
Table 7.3 Correlation between the SOH and the parameters of the EEC measured at 50% using 1.5 C.	125
Table 7.4 Correlation between the SOH and the parameters of the EEC measured at 95% using 1.5 C.	126
Table 7.5 Summary of the highest correlation indexes (absolute values) found for the overall case study, between SOH and the parameters extracted from the tests.	127
Table 8.1 Characterization of the SOC levels for the internal resistive parameters of the EEC model.....	130
Table 8.2 List of the study cases performed during the simulations using the Simulink EEC model.....	133
Table 8.3 Modules used in the Simulink simulations.....	135
Table 8.4 Results for the full charge of B1 M35 (90.97% SOH).	136

Table 8.5 Results for the full charge of B2 M11 (71.848%SOH).	137
Table 8.6 Results for the full charge of B3 M13 (81.667%SOH).	137
Table 8.7 Comparison of the energy losses during the charge (20-80%) using 2 C.....	141
Table 8.8 Comparison of the energy losses during the charge (20-80%) using 0.1 C.....	142
Table 8.9 Comparison of the energy losses during the charge (20-80%) using 1 C.....	144
Table 8.10 Comparison of the energy losses during the charge (35-65%) using 0.5 C.....	146
Table 8.11 Comparison of the energy losses during the charge (35-65%) using 1 C.....	147
Table 8.12 Comparison of the energy losses during the charge (35-65%) using 4 C.....	149

1 Introduction

1.1 Background and Motivation

According to Vgl. Hans Eric Melin (The lithium-ion battery end-of-life market – A baseline study) 2019¹ in the next years, the second life use of Electric Vehicles' battery pack will go from 1 GWh in 2018 to more than 16 GWh in 2025, and up to 45 GWh in 2030. These increases will be because of the increase in the market share of EVs. The number of EVs will increase, within a few years the number of used EVs will increase even more Vgl. Brennan et al. (Battery Electric Vehicles vs. Internal Combustion Engine Vehicles) November, 2016².

This transition from traditional Internal Combustion Engines (ICE) to EV is caused by different factors. In 2015, most of the so-called developed countries agreed to reduce their impact on the environment and accepted their responsibility during the Climate Conference that took place in Paris. There, 195 countries adopted a legally binding global climate deal United Nations Framework Convention on Climate Change (UNFCCC) Vgl. Masson et al. (A Snapshot of Global PV (1992-2017)) 2017³. The most significant part of this agreement is to maintain the global temperature increase below 2°C, achieving the peak of the greenhouse gas (GHG) emission as soon as possible and a fast reduction afterward. Although promising, this solution might not be sufficient for the continuity of many regions and ecosystems that are currently in danger because of the GHG emissions. Furthermore, the capacity of the countries involved and society to apply it generates some doubts.

However, the ongoing decarbonization process of electricity generation is compulsory to achieve the planned goals. In fact, decarbonization has already started in Europe, for example, the U.K. has done the largest reform since privatization to increase renewable share, Denmark plans major investments to generate 50% of electricity from wind by 2020 and Netherlands increased the subsidies in renewable energy generation Vgl. Farinet et al. (Battery Lifetime Analysis for Residential PV-Battery System used to Optimize the Self Consumption - A Danish Scenario) 2019⁴.

In addition, if Renewable Energy Sources (RES) would increase their share in the energy production mix, they would need Energy Storage Systems (ESS) to provide them more stability and reliability. Indeed, RES depends on resources (sun, wind, water, etc.) that are not constant over the seasons and cannot be controlled in any way (with the exception of pumped hydro)

¹ Vgl. Hans Eric Melin (The lithium-ion battery end-of-life market – A baseline study) 2019.

² Vgl. Brennan et al. (Battery Electric Vehicles vs. Internal Combustion Engine Vehicles) November, 2016.

³ Vgl. Masson et al. (A Snapshot of Global PV (1992-2017)) 2017.

⁴ Vgl. Farinet et al. (Battery Lifetime Analysis for Residential PV-Battery System used to Optimize the Self Consumption - A Danish Scenario) 2019.

Vgl. Farinet et al. (Battery Lifetime Analysis for Residential PV-Battery System used to Optimize the Self Consumption - A Danish Scenario) 2019. Battery systems are one of the energy storage technologies which can provide part of the expected electricity grid services. In particular, Li-Ion batteries, which have wider working opportunities, are still too expensive for a broad static installation.

On the other hand, most of the commercialized electric vehicles (EV, including Plug-in Hybrid Electric Vehicles (PHEV) and full electric vehicles (BEV)) use Lithium-ion batteries as ESS. These batteries achieve their End-of-Life (EOL) when their capacity is reduced by 20% or, in other words, when they reach 80% of their State of Health (SOH). Thus, used EV battery packs could be considered for re-use while their available capacity is above 80% of their nominal capacity Vgl. Kampker et al. (Remanufacturing of electric vehicles batteries up to the cell level) 2019⁵.

An opportunity for second life uses of EV batteries could be to re-use them as stationary EES. This solution could provide low price batteries for stationary applications while, at the same time, this battery selling may provide some revenue back to car manufacturers and remanufacturers. Moreover, these additional incomes may revert in lower EV selling prices, making EVs more competitive Vgl. Jiao et al. (Business Models for Sustainability: The Case of Second-life Electric Vehicle Batteries) 2016⁶. Thus, there is a need to manage these second life batteries.

From 2010 to 2015 were available more than 20 different electric car models, during that period in the total 405.426 BEV and PHEV were sold in Europe. This statistic shows that there could be more than 20 different types of battery packs used for EVs; this diversity increases the difficulty of the repurposing strategy Vgl. Casals et al. (Second life of electric vehicle batteries: relation between materials degradation and environmental impact) 2017⁷. With this scenario, the remanufacturing processes become at the same time trickier and more sustainable. The diversity of the battery packs requires different plans and industrial plants to first disassemble them and then re-assemble them. At the same time, the growth of the share of EVs bears an improvement for what concerns the awareness between the citizens and induces a reduction in the cost of EVs.

In order to be sustainable from the economical point-of-view, different analysis about second life opportunities have to be carried out, exploring more precisely the EOL of batteries. Furthermore, possible remanufacturing and re-use plans and strategies have to be found.

⁵ Vgl. Kampker et al. (Remanufacturing of electric vehicles batteries up to the cell level) 2019.

⁶ Vgl. Jiao et al. (Business Models for Sustainability: The Case of Second-life Electric Vehicle Batteries) 2016.

⁷ Vgl. Casals et al. (Second life of electric vehicle batteries: relation between materials degradation and environmental impact) 2017.

1.2 Structure, Objectives and Limitations of the thesis

In this thesis, the development and design process of a test protocol for used automotive battery packs are described. The test protocol is designed and referenced according to the specifications of the battery pack of the Nissan Leaf 2011 Edition (24 kWh).

In the second Chapter (General overview) the main characteristics of Li-Ion battery packs for EVs are listed and described. There are presented the remanufacturing and the re-use processes for used EV's battery packs. In Chapter 3 (State of the art) are presented the most recent testing procedures for Li-Ion batteries.

In Chapter 4 (Technical approach) the description of the battery packs used for the research is made, from the pack level to the cell level, with particular attention to the description of the structure of the modules. The structure of the battery pack is essential for second life purposes.

Using the information listed in Chapter 2 (General overview) and the pre-test performed in the early stages of the project, a new test protocol of used EV's battery packs is developed.

The description of the design and the development process of the protocol is described in Chapter 5 (Testing procedure). The testing procedure has been first tested, to evaluate the possible flaws and issues, and then it has been applied to all the modules of the three available battery packs. The total number of trials for the developed testing procedure is 144; this gives the possibility to evaluate the real reliability of the protocol, the limitations, and the possible issues.

The results of the research are divided into two chapters, Chapter 6 (Results and discussion) and Chapter 7 (Correlation between parameters and SOH), to have a better overview of all the results and the processes evaluated with the tests. In Chapter 6 (Results and discussion) are shown the main results of the tests, the remaining available capacity of the modules and the principal parameters extracted from the other tests. In addition, a comparison of the outcomes of the tests performed on the three battery packs of the Nissan Leaf 2011 Edition (24 kWh) is performed and different evaluations are made. In Chapter 7 (Correlation between parameters and SOH) are evaluated the relationships between the parameters and the available remaining capacity of the modules of the battery pack.

In Chapter 8 (EEC Simulations) are presented the simulations of some relevant study cases. There, the data collected with the test illustrated in Chapter 5 and presented in Chapters 6 and 7 are used to parametrize the model and the simulations. The simulations regard the behaviour of the modules under different circumstances (C-rates and SOC ranges).

In the final Chapter 9 (Conclusions and future work), the final remarks of the thesis are made, giving the possibility to summarize the thesis. In addition to that, the possible future project, studies, and researches are proposed and evaluated.

Since there are only a limited number of test protocols for used automotive battery packs in the literature, and the one previously presented are long and time-consuming. This, of course, leaves space for improvements and future work.

The main objective of the thesis is to design a self-developed test to understand what could be the possible second uses of used EV's battery packs. To understand the possible applications, it is necessary to estimate, in a reliable way, the SOH of the different cells and modules. Unfortunately, the existing procedures to evaluate the SOH of the battery packs for automotive are time-consuming and difficult to perform. This study is mainly focused on finding and proposing a fast and good procedure to make the re-use and remanufacturing of battery packs a cost-effective solution for both the industry (Automotive OEM, Transmission System Operators, Battery Manufacturers, and Remanufacturers) and for the clients (private or industrial).

Since the objects of the study are measurements some limitations come from the used test equipment. In particular, the limitations are in terms of current, and this reduces the possible testing scenarios. As for every test and measurement, there are additional limitations on the precision of the measurement, due to the accuracy and the resolution of the testing equipment. In addition, the entire work is based on testing for Li-Ion battery packs and may not be applicable to different battery technologies.

In addition, the Simulink model used for the simulations is limited and does not take into account different parameters (temperature, degradation, capacity fade, etc.) that could affect the results and the outcome of the simulations.

2 General overview

This chapter of the thesis gives an overview of battery systems that use Lithium-Ion technology. In section 2.1 are presented the battery systems, their main parameters and how their characteristics can be modeled using different equivalent circuits. Section 2.2 gives a detailed overview of what a remanufacturing process for used EV battery packs is and how it has to be performed. In the last part of the chapter, section 2.3, are listed other second life uses for the cells/modules that compose battery packs that are not used for remanufacturing processes.

2.1 Battery systems

A battery is a device that converts the chemical energy contained in its active materials directly into electric energy by means of an electrochemical oxidation-reduction (redox) reaction. The batteries are made of cells where the chemical energy is converted into electrical energy and vice versa. The desired battery voltage, as well as current levels, are obtained by electrically connecting the cells in series and parallel. With the electrical connection of a number of cells it is possible to create battery systems that can be used for many different applications.

The batteries are rated in terms of their energy (Wh) and power capacities (W). Some of the important features and characteristics of a battery system are Vgl. Davide Andrea (Battery Management Systems for Large Lithium-Ion Battery Packs) 2010⁸:

- voltage (V);
- capacity (Ah);
- C-rate (C);
- efficiency, the ratio between the amount of energy needed to charge the battery and the actual energy that can be used;
- life span (stated in terms of number of cycles and time);
- operating temperature, depth of discharge (batteries are generally not discharged completely and Depth of Discharge (DOD) refers to the extent to which they are discharged);
- self-discharge (some batteries cannot retain their electrical capacity when stored in a shelf and self-discharge represents the rate of discharge);
- energy capacity (Wh);
- energy density (Wh/L) in terms of volume;
- energy density (Wh/kg) in terms of weight;
- power capacity (W);
- power density (Wh/L) in terms of volume;
- power density (Wh/kg) in terms of weight.

⁸ Vgl. Davide Andrea (Battery Management Systems for Large Lithium-Ion Battery Packs) 2010.

For most of the battery types, the power and energy capacities are not independent, indeed, they are fixed (within limited ranges) and therefore they cannot be changed during the design and the development of the battery system. All these parameters and indexes could be different depending on the type and technology of the battery used.

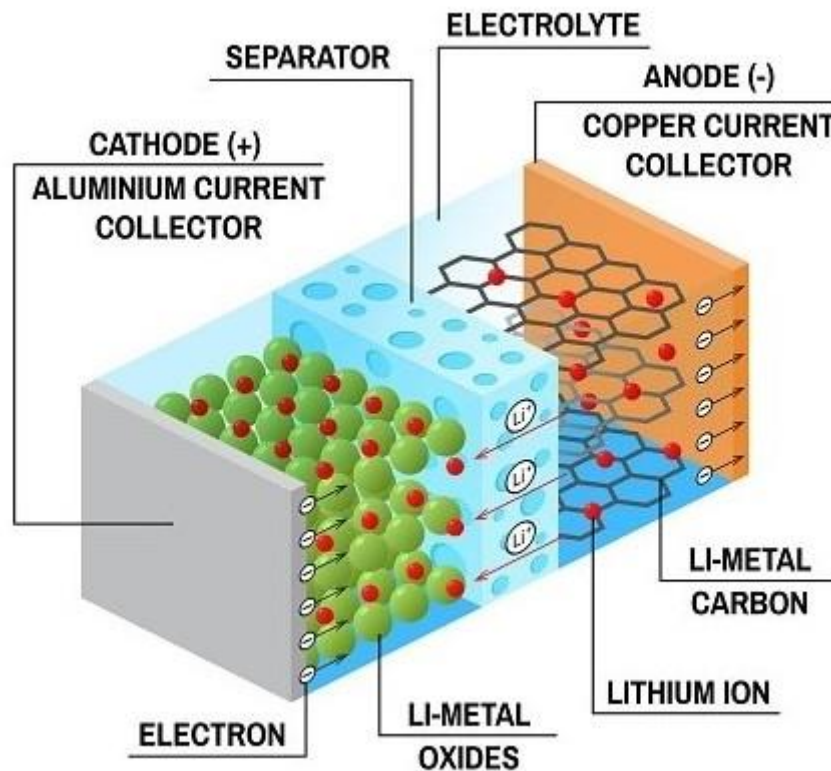


Figure 2.1 Li-Ion cell operation during the discharging process Vgl. Yuping Wu (Lithium-Ion Batteries: Fundamentals and Applications) 2015⁹.

In Lithium-Ion (Li-Ion) cells, as can be deduced from the name, there is a great use of lithium. Lithium is the lightest of all metals, it has the greatest electrochemical potential and it provides the largest energy density in terms of weight (Wh/kg). For these reasons, the development of Li-Ion batteries had a great development during the last decades. Right now, the majority of the electronic devices (smartphones, laptops, tablets, etc.), Hybrid Electric Vehicles and EVs use batteries equipped with Li-Ion technology Vgl. van Schalkwijk et al. (Advances in Lithium Ion Batteries) 2002¹⁰ Vgl. Diouf et al. (Potential of lithium-ion batteries in renewable energy) April 2015¹¹.

⁹ Vgl. Yuping Wu (Lithium-Ion Batteries: Fundamentals and Applications) 2015.

¹⁰ Vgl. van Schalkwijk et al. (Advances in Lithium Ion Batteries) 2002.

¹¹ Vgl. Diouf et al. (Potential of lithium-ion batteries in renewable energy) April 2015.

Figure 2.1 and Figure 2.2 show the Li-Ion operation of the cells during the charging and discharging phases. The cell is composed of different elements, the Cathode, the Li-Metal Oxides, the Separator, the electrolyte, the Li-Metal carbon, and the Anode. The Cathode and the anode, respectively the positive and the negative ends of the battery are the points at which the wiring harness is connected. When the cell is being charged the electrons flow from the anode to the cathode through the separator.

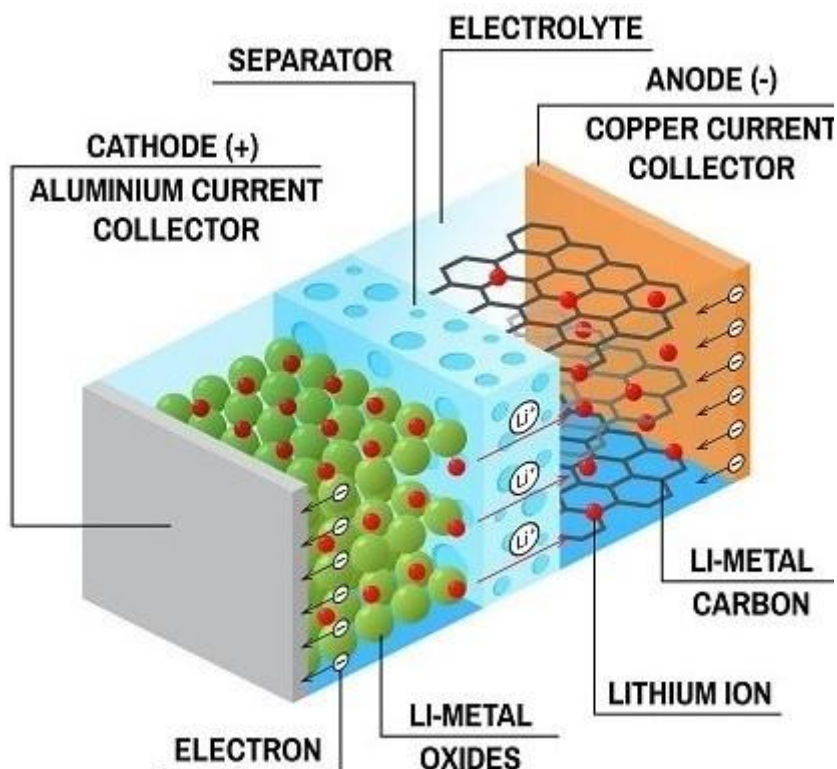


Figure 2.2 Li-Ion cell operation during the charging process Vgl. Yuping Wu (Lithium-Ion Batteries: Fundamentals and Applications) 2015¹².

The quantity of electricity that can be delivered by a battery is its capacity, and it is measured in units of ampere-hours or amp-hours (Ah). It quantifies for how long a battery will last, in hours, keeping constant the discharge current, measured in Amperes (A). The charging or discharging rate of a cell or battery is expressed in terms of its total storage capacity in Ah.

Therefore, a rate of 1 C means that the transfer of all the stored energy from the battery occurs in one hour (ideally, this works from the mathematical point of view). A C-rate of 0.1 C means 10% transfer in one hour or full transfer in 10 hours. The calculation of the C-rate, for every type and technology of battery, can be made using the equation (2.1).

¹² Vgl. Yuping Wu (Lithium-Ion Batteries: Fundamentals and Applications) 2015.

$$C - rate = \frac{(Ah)}{time} \quad (C) \quad (2.1)$$

<i>C - rate</i>	Measured using (C)
<i>Ah</i>	Capacity of the battery (Ah)
<i>time</i>	Time needed to charge/discharge the battery (h)

A drawback of the battery systems which are equipped with Li-Ion cells is that this technology suffers from various degradation processes. There are different types of degradation for Li-Ion batteries, and they depend on different factors.

The main factors that cause the degradation processes can be divided into:

- time, which causes the calendar aging;
- usage, which causes the cycle aging.

The degradation that occurs with aging (due to the time, months and years) of the battery is called the aging process or calendar aging. With time the internal parameters of the battery change, causing an increase of the internal resistance of the cells. This process decreases the efficiency of the battery, Γ , that can be calculated using the equation (2.2). This occurs because the energy used to charge the battery is being partly dissipated on the internal parameters (resistances) of the cells. Therefore, the amount of usable energy E_U reduces and it becomes smaller than the energy used to charge the battery E_C .

Li-Ion batteries are not ideal devices, therefore even when the battery is new Γ is already smaller than 1 (usually high values 0.96-0.98). Then, it decreases with the aging and with the usage of the system Vgl. Farinet et al. (Battery Lifetime Analysis for Residential PV-Battery System used to Optimize the Self Consumption - A Danish Scenario) 2019¹³.

$$\Gamma = \frac{E_U}{E_C} \cdot 100 \quad (2.2)$$

Γ	Efficiency of the battery (%)
E_U	Energy at disposal of the battery after the charge (Wh)
E_C	Energy used to charge the battery (Wh)

There is another factor that influences the degradation of the battery and it is the usage. This phenomenon is denominated Cycle-life, which is greatly influenced by the operating conditions at which the battery system works. The charging states influences the cycle life, while the discharging has a lower impact on it. High charge cut-off voltages and a long float-charge

¹³ Vgl. Farinet et al. (Battery Lifetime Analysis for Residential PV-Battery System used to Optimize the Self Consumption - A Danish Scenario) 2019.

period at 4.2 V or above have the most severe effects on cycle-life, indeed, the operating conditions of the cells have to be chosen very carefully. Another condition which greatly influences the degradation of the internal parameters of the cells is the use of high charge rates (above the 1 C rate) Vgl. Seok Choi et al. (Factors that affect cycle-life and possible degradation mechanisms of a Li-ion cell based on LiCoO₂) 2002¹⁴. These values of the charging rates lead the temperature of the cells to rise causing premature degradations and therefore a reduction for what concerns the lifetime.

As shown in Figure 2.3, the Open Circuit Voltage (OCV) profile could have different patterns based on the C-rate used to extract the OCV curve. It can be noticed that the OCV profile extracted with 1.5 C generally Li-Ion has lower voltage values in comparison with the other smaller C-rates used (0.5 C and 1 C). If the battery is charged with a lower C-rate the profile of the voltage is higher than the ones that are extracted with the use of higher C-rates. The data used to develop the OCV vs SOC (State of Charge) graph come from the testing of the modules of the Nissan Leaf 2011 Edition. As shown, the plot OCV vs SOC is influenced by the C-rate used, at the same time the profile is influenced also by the SOH of the battery. This relationship is essential when a battery pack is either designed, tested, used or evaluated.

Indeed, the relationship between the OCV over the SOC is essential for battery modeling, battery lifetime estimations and cell performance control with Battery Management System (BMS). The OCV increases with the increases of the SOC, therefore the voltage is generally used to estimate the SOC of the battery. Of course, this technique is not very precise, and it has to be refined with further tests and evaluations. Another process that can be used to estimate the SOC, while the battery is being used, is presented in section 2.1.1.

¹⁴ Vgl. Seok Choi et al. (Factors that affect cycle-life and possible degradation mechanisms of a Li-ion cell based on LiCoO₂) 2002.

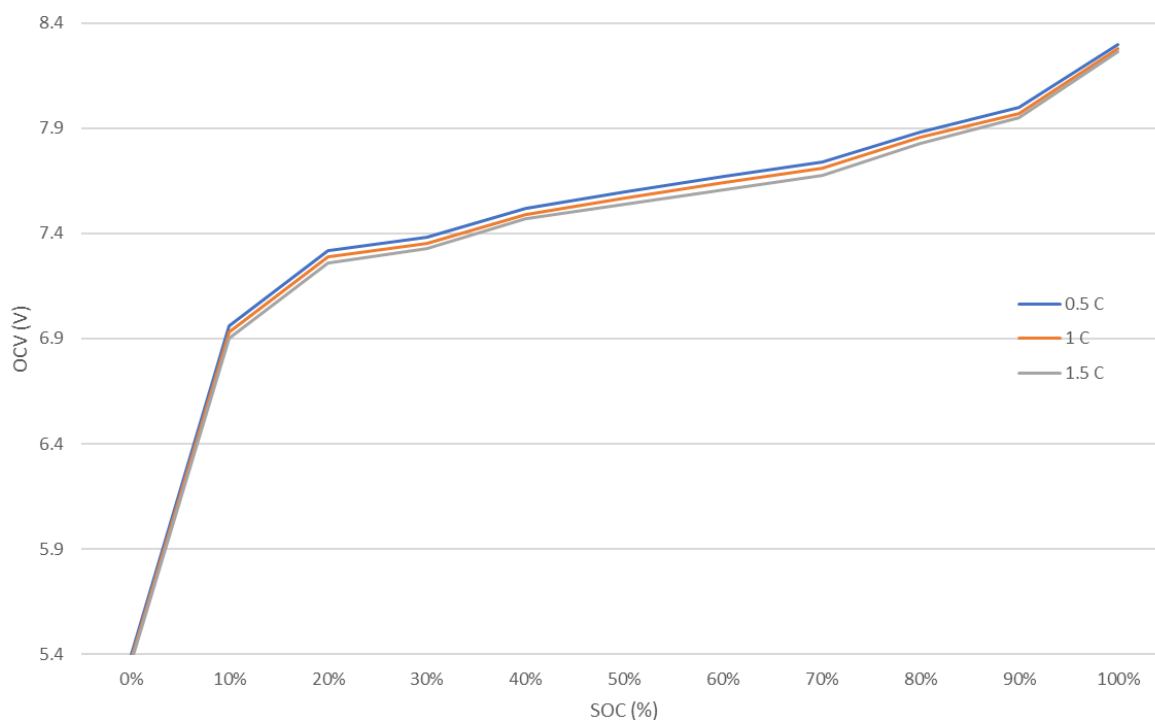


Figure 2.3 OCV vs SOC plots with different C-rates.

As stated in Chapter 1, the battery packs of EVs reach the EOL when the reduction of the available capacity is greater than 20%. This capacity fade is due to different internal processes that occur either when the battery is not being used (calendar aging) and also while the battery is used (cycling aging). The estimation, the description and the evaluation of the phenomena and processes that occur are given in the next chapters.

2.1.1 Modelling

The modelling of batteries is essential, for many different reasons. First of all, it enables to describe the behaviour of the system in different operating conditions, some of which may not be replicable in real cases (due to safety, equipment reasons). Indeed, in many cases, it is not possible to perform test cases due to limitations of the equipment (voltage limits, current limits, dimension limits etc.), and with the use of models and simulations, it is possible to estimate the behaviour of the cells.

Battery modelling is crucial during the sizing and the design of battery packs for every application. In particular, for Li-Ion batteries the voltage is dependent on different parameters (C-rate, temperature, SOC, SOH), therefore it is essential to know in advance its characteristics under various working conditions. Battery modeling is a complex process as batteries are highly non-linear electrochemical devices with many phenomena occurring in parallel. Modelling gives the opportunity to simulate them and have a better understanding of the ongoing processes. Moreover, due to the composition of battery cells, many inner battery parameters are not directly measurable and have to be estimated and determined using tests and simulations.

The choice of the model type is always a compromise between the required accuracy and the parametrization effort (computation burden and cost). The use of performance models is in some cases needed due to the duration, in time, that the testing procedures for batteries take. Using a model enables us to simulate different scenarios with a limited amount of time, compared to the one that would be requested for real-time testing. Indeed, the testing of battery systems takes a large amount of time (months, even years), because it includes a large number of tests and procedures. With the use of models, the main parameters can be extracted with introductory tests (days, weeks depending on the type of parameters), which then are used to parametrize the models Vgl. Stroe (Master of Research (MRES) - Introduction to Battery Models) 2018¹⁵. In addition to the reduction of the time, the use of models for the batteries increases the safety of the tests, because there is no need test battery at critical conditions. At the same time, it is possible to test the operation of the Battery Management System (BMS) without any danger Vgl. Davide Andrea (Battery Management Systems for Large Lithium-Ion Battery Packs) 2010¹⁶.

State of Charge (SOC) is a parameter that describes the available remaining capacity of the battery and is determined through the Ah-balance as shown in the equation (2.3). This parameter can be very useful because it is calculated using percentages. With the percentage of the SOC, the available capacity in Ah can be determined. In addition to the capacity in Ah the SOC percentage gives the amount of energy (Wh) that is available in the battery. Therefore, with one value, the SOC, two of the key parameters of the battery can be determined.

As can be seen in equation (2.3), the SOC is a function of the time and it varies with the variation of the current I_{batt} . It is interesting to notice that, since I_{batt} can be either negative or positive, the SOC can either increase or decrease (within the boundaries 0% and 100%) its value. Therefore, equation (2.3) can be used for both the charging and the discharging states Vgl. Davide Andrea (Battery Management Systems for Large Lithium-Ion Battery Packs) 2010¹⁷.

$$SOC(t) = \left[SOC_0 + \frac{1}{C_N} \int_0^t I_{batt} \cdot dt \right] \cdot 100 \quad (2.3)$$

SOC	State of Charge over the time (%)
SOC_0	State of Charge at the beginning of the process (%)
C_N	Nominal capacity of the battery (As)

¹⁵ Vgl. Stroe (Master of Research (MRES) - Introduction to Battery Models) 2018.

¹⁶ Vgl. Davide Andrea (Battery Management Systems for Large Lithium-Ion Battery Packs) 2010.

¹⁷ Vgl. Davide Andrea (Battery Management Systems for Large Lithium-Ion Battery Packs) 2010.

I_{batt}	Current of the battery (A)
t	Time (seconds)

The capacity of the battery is dependent on the battery's discharge current; the relationship between the battery capacity and discharge current is not linear and less Ah can be recovered with the use of a higher discharge rate. For a one-ampere (1 A) discharge rate, Peukert's law is applied as shown in the equation (2.4). Ideally, the parameter "k" should be equal to 1, but in real applications, the Peukert coefficient "k" is greater than 1 (between 1.1 and 1.3 for lead-acid batteries and close to 1 for Li-Ion batteries) Vgl. Stroe (Master of Research (MRES) - Introduction to Battery Models) 2018¹⁸.

$$C_p = I^k \cdot t \quad (2.4)$$

C_p	Capacity at a one-ampere discharge rate
I	actual discharge current (A)
k	Peukert constant
t	Actual time to discharge the battery

For what concerns the battery modelling there are different possibilities available, depending on the required accuracy level, such as:

- Electrochemical;
- Electrical;
- Mathematical.

The electrochemical model simulates the physic-chemical properties of the battery's electrodes (positive and negative) and electrolyte, it is also known as the "physic-chemical" model. The electrochemical model is used for the identification of the processes that limit the battery cell performance and for the determination of the correct way to maximize the performance of the battery. This model has high accuracy and from it the macroscopic parameters can be extracted, as well as the microscopic parameters. The model gives a good knowledge of the electrochemical battery behavior, determining over 50 parameters of the battery (structure, chemical composition, etc.) Vgl. Farinet et al. (Battery Lifetime Analysis for Residential PV-Battery System used to Optimize the Self Consumption - A Danish Scenario) 2019¹⁹ Vgl. Stroe et al. (Generalized Characterization Methodology for Performance Modelling of Lithium-Ion

¹⁸ Vgl. Stroe (Master of Research (MRES) - Introduction to Battery Models) 2018.

¹⁹ Vgl. Farinet et al. (Battery Lifetime Analysis for Residential PV-Battery System used to Optimize the Self Consumption - A Danish Scenario) 2019.

Batteries) 2016²⁰. On the other hand, it has a great computational burden and it quite hard to design and use (complex equipment needed). Due to the main aims of this research, this type of model is not evaluated anymore, since it is too complicated for both the extraction of the parameters and for the characterization of the cell. In addition, the available equipment for the introductory tests does not reach the required accuracy and precision needed to develop such a model.

The second model that can be used is the Electrical Model, which uses an Equivalent Electrical Circuit (EEC) to predict the static and dynamic performance behavior of the battery. The EEC is composed of a combination of voltage sources, resistors, capacitances other electrical parameters Vgl. Hongwen et al. (Evaluation of Lithium-Ion Battery Equivalent Circuit Models for State of Charge Estimation by an Experimental Approach) 2011²¹. These parameters provide information about the battery's macroscopic quantities, such as voltages and currents. The accuracy (i.e., 1-5%) is quite high, depending on the number of RC parallel networks (order of the EEC) and on the load profile that is applied to the battery Vgl. Yuping Wu (Lithium-Ion Batteries: Fundamentals and Applications) 2015²². Electrical models (EEC) are regarded as a trade-off solution since they offer relatively high accuracy and a moderate modeling and parametrization complexity.

In Figure 2.4 is shown the basic circuit of the EEC for a Li-Ion battery. The Open Circuit Voltage (OCV) is modelled as a DC voltage source, which is SOC dependent. The behaviour of the battery is simulated using the impedance Z_{ECC} . The composition of Z_{ECC} depends on the accuracy that the model is designed to have. The parameter V_{batt} represents the voltage of the battery after the voltage drop, ΔV_{ECC} , that occurs over the impedance Z_{ECC} . The formulas used to determine the value ΔV_{ECC} and V_{batt} are reported in the equations (2.5) and (2.6).

²⁰ Vgl. Stroe et al. (Generalized Characterization Methodology for Performance Modelling of Lithium-Ion Batteries) 2016.

²¹ Vgl. Hongwen et al. (Evaluation of Lithium-Ion Battery Equivalent Circuit Models for State of Charge Estimation by an Experimental Approach) 2011.

²² Vgl. Yuping Wu (Lithium-Ion Batteries: Fundamentals and Applications) 2015.

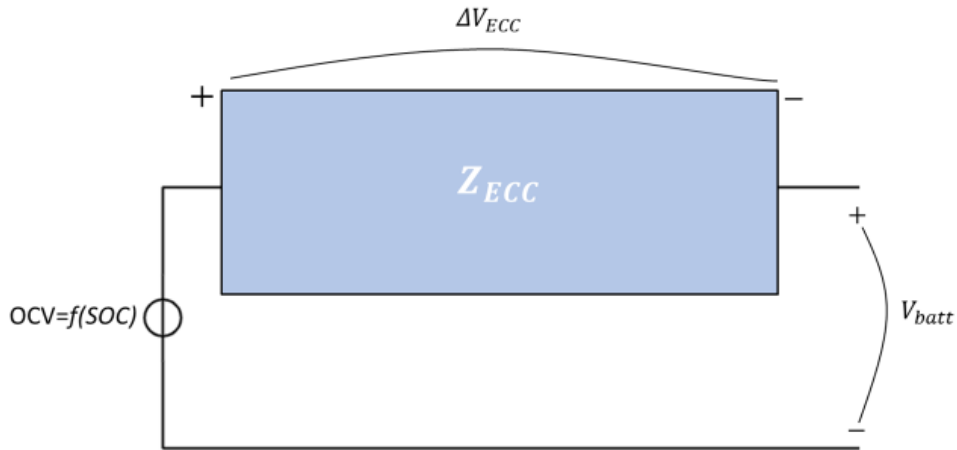


Figure 2.4 The most simple EEC model used to simulate the behaviour of a cell of a Li-ion battery.

$$\Delta V_{ECC} = Z_{ECC} \cdot I_{batt} \quad (2.5)$$

$$V_{batt} = OCV + \Delta V_{ECC} \quad (2.6)$$

ΔV_{ECC}	Voltage drop over Z_{ECC} (V)
Z_{ECC}	Equivalent impedance of the circuit (Ω)
OCV	Open Circuit Voltage (V)
I_{batt}	Current of the battery (can be + or -) (A)
V_{batt}	Voltage after the Z_{ECC} (V)

The inputs of the EEC are the initial SOC, SOC_0 , the current, I_{batt} , and the temperature (T). Certainly, prior to the use of the model, the parameters of the battery (OCV and Z_{ECC}) have to be extracted from the introductory tests. The outputs that are obtained from the simulations of the model are the voltage profile and the SOC, during the use of the battery.

The Z_{ECC} can have different configurations depending on the modeling requirements and purposes, such as model accuracy, computational time and physic-chemical meaning. The V_{ECC} , calculated with equation (2.5), represents the voltage drop that occurs while I_{batt} flows through the impedance Z_{ECC} , according to the state (charging or discharging) of the battery the current can be positive or negative. The OCV describes the voltage of the battery at no-load condition (when no loads are applied at the ends of the battery), while V_{ECC} describes the dynamics that occurs while the battery is being used.

As previously stated, the impedance Z_{ECC} can be implemented using different electrical configurations depending on the degree of accuracy that the model aims to reach, as shown in Figure 2.5.

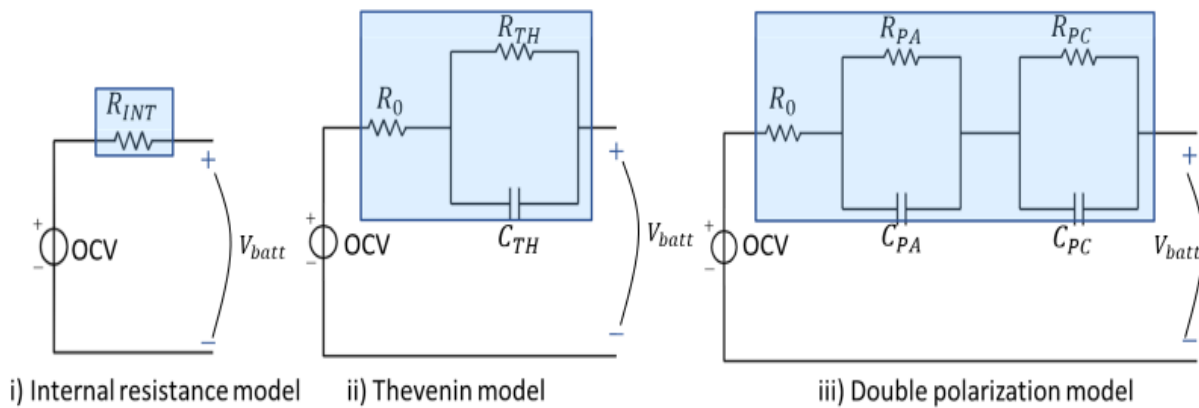


Figure 2.5 Three types of EEC models, *Internal resistance model*, *Thevenin model*, and *Double parametrization model*.

Indeed, Figure 2.5 illustrates the three EEC versions of the model object of this study, in the following order:

- *Internal resistance model i)*;
- *Thevenin model ii)*;
- *Double parametrization model iii)*.

According to the different types of uses, one of the three listed models can be chosen. The three options are listed in order of accuracy and data needed. Thus, the *Internal resistance model* (Figure 2.5, i)) represents the simplest model, and it describes only the ohmic behaviour of the cell. Indeed, it does not describe the dynamics that occur while the battery is used (either during the charging, discharging and idling states). The model is quite basic and can be used for introductory studies or for researches that focus only on the internal resistance, modelled with R_{INT} .

The second model of Figure 2.5 (ii), *Thevenin model*, adds an RC parallel branch in series to the *Internal resistance model*, as shown in Figure 2.5 (ii). This model has a higher complexity compared to the previous one (*Internal resistance model*), and it enables to describe the dynamics of the battery. The latter model shown in Figure 2.5 (iii) is the *Double polarization model*. This configuration enables us to better describe the dynamics of the battery in comparison with the previous ones.

In comparison with the *Thevenin model*, it has a second RC parallel branch in series to the previous one. The use of these two parallel RC branches describes the dynamics of the battery in a more complete way. The resistor R_0 models the ohmic behaviour of the battery, as occurred for the first two models, the *Internal resistance model* and the *Thevenin model* presented above. This model allows differentiating the behaviour of the two polarizations, electrochemical polarization, and concentration polarization.

Indeed, the first RC parallel branch, which includes R_{PA} and C_{PA} , is used to model the electrochemical polarization, with R_{PA} that describes the charge transfer resistance. The other parameter of the RC branch, the capacitance C_{PA} , is used to describe the transient states that occur while the battery is being used.

The second RC parallel branch is composed of R_{PC} and C_{PC} , which are used to model the diffusion process that takes place when the battery is charged (or discharged). As well as the first RC branch the capacitance C_{PC} is used to describe the transient state of the diffusion process.

Since the data available in the battery datasheet is not enough for the parametrization of an EEC-based battery model, the determination of the parameters has to be done using two different experimental tests Vgl. Böttiger et al. (Systematic experimental pulse test investigation for parameter identification of an equivalent based lithium-ion battery model) 2017²³. The two protocols are quite different, since the first one is based on Alternate Current (AC) signals, while the second one is based on DC signals.

The first one is done using the Electrochemical Impedance Spectroscopy (EIS). This technique, presented in Vgl. Stroe et al. (Generalized Characterization Methodology for Performance Modelling of Lithium-Ion Batteries) 2016²⁴ and in Vgl. Andre et al. (Characterization of high-power lithium-ion batteries by electrochemical impedance spectroscopy. II: Modelling) 2011²⁵. During EIS experiments, a small amplitude AC signal is applied to the battery system which is being studied. EIS is a non-destructive technique that evaluates and analyzes a wide range of materials, such as coatings, anodized films, corrosion inhibitors, batteries, and can provide information on the systems under examination.

Parameters such as corrosion rate, electrochemical mechanisms and reaction kinetics, battery life performance can all be determined from these data. It may be performed in either galvanostatic (constant current) or potentiostatic (constant voltage) Vgl. Shih et al. (Electrochemical Impedance Spectroscopy for Battery Research and Development) 1996²⁶.

The AC current pulses can be either charging or discharging ones. For what concerns the ranges of the frequency of the pulses, they may vary from battery to battery. Indeed, the range of frequencies evaluated could be quite wide, from Hz to kHz Vgl. Galeotti et al. (Performance analysis and SOH (state of health) evaluation of lithium polymer batteries through electrochemical impedance spectroscopy) 2015²⁷. The results of the EIS provide an evaluation of the change that occurs to the impedances with the aging and the usage of the battery. The wider

²³ Vgl. Böttiger et al. (Systematic experimental pulse test investigation for parameter identification of an equivalent based lithium-ion battery model) 2017.

²⁴ Vgl. Stroe et al. (Generalized Characterization Methodology for Performance Modelling of Lithium-Ion Batteries) 2016.

²⁵ Vgl. Andre et al. (Characterization of high-power lithium-ion batteries by electrochemical impedance spectroscopy. II: Modelling) 2011.

²⁶ Vgl. Shih et al. (Electrochemical Impedance Spectroscopy for Battery Research and Development) 1996.

²⁷ Vgl. Galeotti et al. (Performance analysis and SOH (state of health) evaluation of lithium polymer batteries through electrochemical impedance spectroscopy) 2015.

is the spectrum of frequencies used during the test, the higher is the reliability and accuracy of the test. The EIS test enables us to distinguish the real and the imaginary parts of the impedance.

As previously stated, the second technique uses DC current pulses and it is presented in Vgl. Stroe et al. (Generalized Characterization Methodology for Performance Modelling of Lithium-Ion Batteries) 2016. The battery is discharged (charged) to a certain voltage level (SOC level), then, at that voltage level, a DC current pulse is applied to the battery. The DC current pulse is applied for a short time (in the range of seconds) and the voltage drop (rise) is evaluated, as shown in Figure 2.6. Figure 2.6 refers to a discharge current pulse, therefore the voltage of the battery decreases. Both charging and discharging current pulses can be applied to the battery, to extract the parameters for the EEC, depending on the accuracy of the model in which the parameters will be used. In Figure 2.6, it is shown how the three components of the EEC are extracted from the test, to be then used to create the three EEC models. The first voltage drop represents and models the voltage drop that occurs on the first resistance of the *Double polarization model*.

The performed tests have to be very precise, because the performance parameters, on which the EEC circuit is based, are very sensitive to the operating conditions (i.e., temperature, load current, SOC). Figure 2.6 shows how the parameters' extraction is performed, using the DC current pulses. As shown, as the current pulse is applied the voltage drops with a great rate, this first voltage drop, from V_{OC} to V_{OHMIC} , represents the R_0 shown in Figure 2.5. It can be calculated using the equation (2.7) Vgl. Stroe (Master of Research (MRES) - Introduction to Battery Models) 2018²⁸.

Then a second voltage drop can be noticed, from V_{OHMIC} to $V_{CH.TRAN}$, which represents the first RC branch of the *Double polarization model*. The second voltage drop that occurs while the current pulse is applied can be calculated using the equation (2.8) Vgl. Stroe (Master of Research (MRES) - Introduction to Battery Models) 2018. The last voltage drop, described by the equation (8.3), going from $V_{CH.TRAN}$ to V_{DIFF} , represents the voltage drop that occurs over the second RC parallel branch of the model, Z_{DIFF} Vgl. Stroe (Master of Research (MRES) - Introduction to Battery Models) 2018.

²⁸ Vgl. Stroe (Master of Research (MRES) - Introduction to Battery Models) 2018.

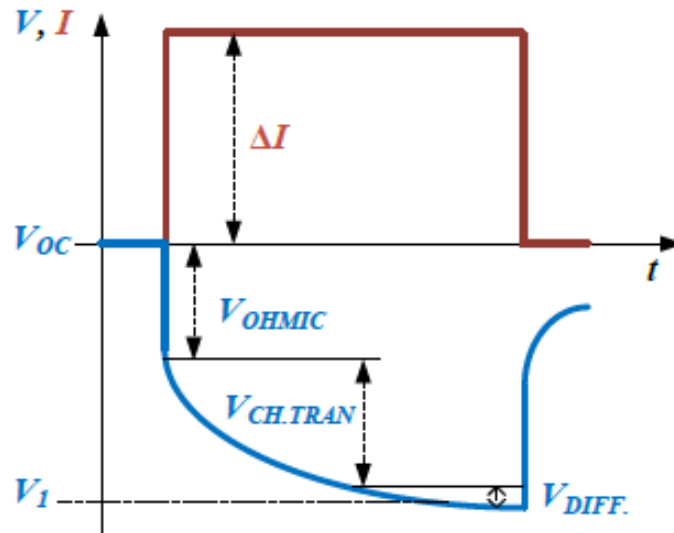


Figure 2.6 Example of the DC current pulse to extract the parameters for the *Double polarization model* Vgl. Stroe (Master of Research (MRES) - Introduction to Battery Models) 2018²⁹.

$$\Delta V_{OHMIC} = OCV - V_{OHMIC} = I_{batt} \cdot R_{OHMIC} \quad (2.7)$$

$$\Delta V_{CH.TRAN} = V_{OHMIC} - V_{CH.TRAN} = I_{batt} \cdot Z_{CH.TRAN} \quad (2.8)$$

$$\Delta V_{DIFF} = V_{CH.TRAN} - V_1 = I_{batt} \cdot Z_{DIFF} \quad (2.9)$$

ΔV_{OHMIC}	Voltage drop over R_{OHMIC} (V)
OCV	Open Circuit Voltage (V)
V_{OHMIC}	Voltage after R_{OHMIC} (V)
I_{batt}	Current of the battery (+ or -) (A)
R_{OHMIC}	Ohmic resistance (Ω)
$\Delta V_{CH.TRAN}$	Voltage drop over $Z_{CH.TRAN}$ (V)
$V_{CH.TRAN}$	Voltage after $Z_{CH.TRAN}$ (V)
$Z_{CH.TRAN}$	Impedance representing the charge transfer (Ω)
ΔV_{DIFF}	Voltage drop over Z_{DIFF} (V)
V_1	Voltage at the end of the current pulse (V)
Z_{DIFF}	Impedance representing the diffusion process (Ω)

The computation time increases exponentially with increasing the number of RC parallel networks and the EEC parametrization is more difficult for the increased number of RC networks.

²⁹ Vgl. Stroe (Master of Research (MRES) - Introduction to Battery Models) 2018.

The accuracy increases with increasing the number of RC parallel networks. On the other hand, the number of RC parallel networks influences the accuracy of the voltage during the transient states.

2.2 Remanufacturing

As stated in Chapter 1, the batteries used for the EV applications reach the EOL when their available capacity reaches 80% of the rated one. The battery pack, which is one of the most important components of EVs, has a great impact on the environment and faces recycling issues Vgl. Casals et al. (Second life of electric vehicle batteries: relation between materials degradation and environmental impact) 2017³⁰. For these reasons, it is important to evaluate and study the different options that could decrease the environmental impact that EV battery packs have.

One solution to this issue could be to remanufacture the used EV battery packs into new battery packs. This process consists of collecting different used battery packs, evaluate their SOH and their characteristics, create, use the modules/cells to create renewed battery packs.

To fully evaluate the actual available remaining capacity, and therefore its SOH, of the battery pack a full disassembly of it is needed. The pack has to be demounted from the EV and brought into a safety room (a special space where the disassembly can be performed according to high-security standards). In the safety room, the disassembly is performed by trained and specialized personnel, because of the hazardous equipment. The disassembly could take a few hours, depending on the design of the battery pack, because the operations are time consuming and hazardous.

Indeed, usually, the voltage of the battery packs of the EVs are at 400 V, but right now there are new car models that have battery packs with 800 V Vgl. Lie et al. (The electric vehicle: a review) 2017³¹. These voltage levels require very careful operations and specific equipment Vgl. Li (Systematic analysis of an automatic disassembly process of automotive batteries) 2018³².

The disassembly could be performed at different levels, depending on the design of the battery pack and on the different goals of the tests that have to be performed on the components of the battery pack. For instance, for what concerns the pack that equips the Nissan Leaf 2011 Edition, the pack is divided into three subpacks. Two of which have the same number of modules (left and right subpacks), 12, and one with 24 modules (rear subpack). This type of battery

³⁰ Vgl. Casals et al. (Second life of electric vehicle batteries: relation between materials degradation and environmental impact) 2017.

³¹ Vgl. Lie et al. (The electric vehicle: a review) 2017.

³² Vgl. Li (Systematic analysis of an automatic disassembly process of automotive batteries) 2018.

ack can be therefore disassembled into three subpacks that can be remanufactured into new packs or reused for different applications. From the subpack level, the pack can be disassembled to a lower level. Hence, the three subpacks can be disassembled to the module level. A module is a set of cells, electrically connected to reach the voltage and the capacity levels required.

Disassembling the pack into modules requires more time than the subpack level, but it provides more flexibility for second life uses. Indeed, the tests that can be performed on the single modules can be more focused on certain parameters and they can show any variation in the SOHs of the modules of the pack. With this type of disassembly, the modules, after the tests and evaluations, can be used for different purposes according to their degradation and SOH. From the module level, there is a lower level of disassembly, the cell level. This kind of disassembly can be performed after the module level is reached.

The modules, which usually have different cells connected in series and in parallel, are disassembled to the cell level. The cells are then tested and analyzed, to find abnormalities in their degradation. For what concerns the battery pack of the Nissan Leaf 2011 Edition, to reach the cell level the modules have to be opened by cutting (and therefore breaking) their cover shell. By breaking their cover, the modules become unusable, therefore the cells contained inside them have to be inserted into other shells (or other types of containers). This process is very time consuming and it is difficult to perform, also due to the fact that there is a large number of modules inside one pack (48 for the Nissan Leaf 2011 Edition). The disassembly of the modules can be performed by different operators (or robots) at the same moment, thus decreasing the total amount of time needed for the disassembly.

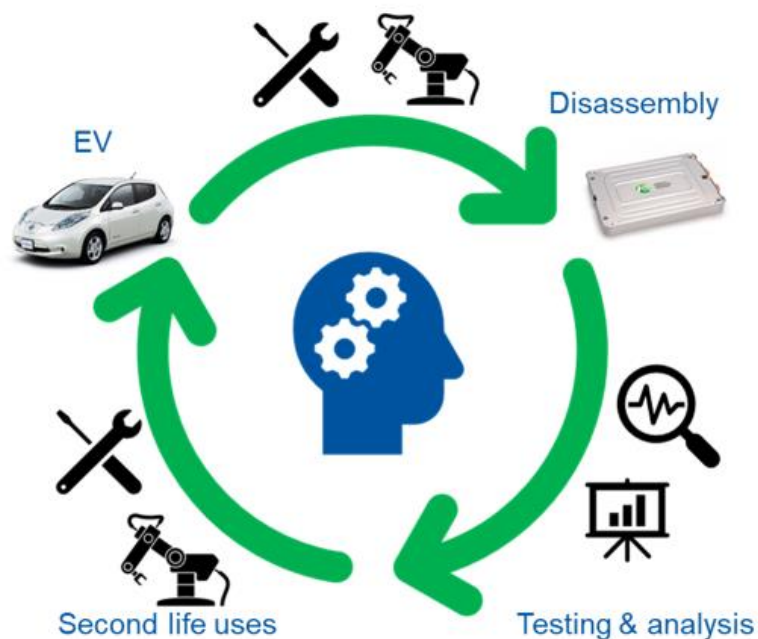


Figure 2.7 Scheme of the steps of the second life process.

In Figure 2.7 are presented the main steps that have to be performed in order to re-use and remanufacture the used battery packs of EVs. As previously stated, the first step is to collect the used EV, and then the battery pack has to be demounted from it. When the pack has been demounted, it has to be disassembled to the module or cell level (depending on the second life use and on the design of the battery pack). Then the modules/cells have to be tested and their data analyzed, to establish their degradation rate and SOH. When the usage of the pack has been evaluated, the different second life uses can be applied to the elements of the battery pack.

Certainly, the lower is the disassembly level, the more are possibilities that could be feasible for second life uses. On the other hand, at the same time, reaching a deeper level is more complex and thus more time-consuming. The different disassembly levels have to be chosen according to the possible second life uses of the modules and the cells.

The process of remanufacturing consists of disassembling a large number of battery packs coming from EV applications into modules or cells. After the disassembly process, the modules/cells have to be tested, the tests are different according to the type of second use (remanufacturing or re-use), therefore the length of the testing procedure varies Vgl. Keeli et al. (Optimal use of second life battery for peak load management and improving the life of the battery) 04/03/2012 - 08/03/2012³³. The most common tests are the ones previously presented in this chapter.

One of the second life uses is the remanufacturing process. Remanufacturing of battery packs consist of first disassembly the packs to a certain level (subpacks, modules, cells), then test them to evaluate their degradation and their SOH and of the last step to remanufacture them into new battery packs. The remanufacturing process may have different goals, depending on the type of battery packs. One of them could be to upgrade the capacity of the battery packs, by adding modules to a (used) existing pack.

An example of this scenario is the new Volkswagen ID.3, which has three capacities (45 kWh, 58 kWh, and 77 kWh), but it uses the same shell for the battery packs Vgl. Tim Fronzek (New ID.3 and future ID. models to be equipped with batteries offering the highest capacity – and an eight-year warranty) 2019³⁴. Since the external dimensions of the pack are the same, any user with a car equipped with a smaller battery could easily upgrade the capacity of his battery, using the modules from other ID.3s. This case is only an example of the direction in which the designs EV's battery packs are leaning to. In the future, more and more battery packs will be designed modular architecture, to avoid waste and to recycle the majority of the equipment of the vehicle. Of course, this process has to be taken out by the OEM or by specialized remanufacturer companies.

³³ Vgl. Keeli et al. (Optimal use of second life battery for peak load management and improving the life of the battery) 04/03/2012 - 08/03/2012.

³⁴ Vgl. Tim Fronzek (New ID.3 and future ID. models to be equipped with batteries offering the highest capacity – and an eight-year warranty) 2019.

The remanufacturing process can be used also in case of great differences between the different cells (in terms of capacity, internal parameters, etc.) of the battery pack. To sort out the differences that characterize the cells, different tests have to be performed, both at the module and cell level. When great differences between the components of the same pack are found the battery packs do not work properly, this situation causes an anticipated degradation of the pack and its components Vgl. Martinez-Laserna et al. (Evaluation of lithium-ion battery second life performance and degradation) 18/09/2016 - 22/09/2016³⁵.

The substitution of the damaged cells with new ones enables the battery to work at a better operating point, increasing the performances of the pack. This solution can be very powerful and useful if anomalies and precocious degradation occur, without remanufacturing the performances of the pack would decrease. In addition to the decrease of the performances, anomalies and degradation would rapidly lead to a reduction of the useful lifetime of the battery pack, thus reaching the EOL sooner than expected. By replacing only the *bad* modules the pack would last longer and with better performances.

Remanufacturing can be performed after a car wreck that has damaged the car, but it has not entirely destroyed the pack. After the accident the pack has to be tested, the results evaluated and then the modules can be used for remanufacturing of other battery packs.

In general, the use of remanufacturing prolongs the lifespan of the battery packs, because it eliminates the cells that may cause damages and degradation to the battery. The main issue of remanufacturing is that it is a time-consuming step (the disassembly, the testing, and the re-assembly). Another issue is that the process requires a large number of packs, and to store them great facility is needed. In addition to the storage rooms, which have to be safe and *ad hoc*, a large number of testing platforms is required, in order to perform the tests in a more productive way.

2.3 Re-use and second life

As well as the remanufacturing processes the second life uses are different depending on the degradation of the battery. The re-use of used EV's battery packs means to use the entire pack, or part of it, for applications that are not automotive. The first steps of the re-use are the same as the remanufacturing. The battery pack has to be taken out from the EV, then it has to be stored in a safe room. Afterward, the pack needs to be disassembled to either the module or cell level Vgl. Martinez-Laserna et al. (Evaluation of lithium-ion battery second life performance and degradation) 18/09/2016 - 22/09/2016³⁶. Then based on the specifications of the modules and the possible second life options different testing procedures can be performed.

³⁵ Vgl. Martinez-Laserna et al. (Evaluation of lithium-ion battery second life performance and degradation) 18/09/2016 - 22/09/2016.

³⁶ Vgl. Martinez-Laserna et al. (Evaluation of lithium-ion battery second life performance and degradation) 18/09/2016 - 22/09/2016.

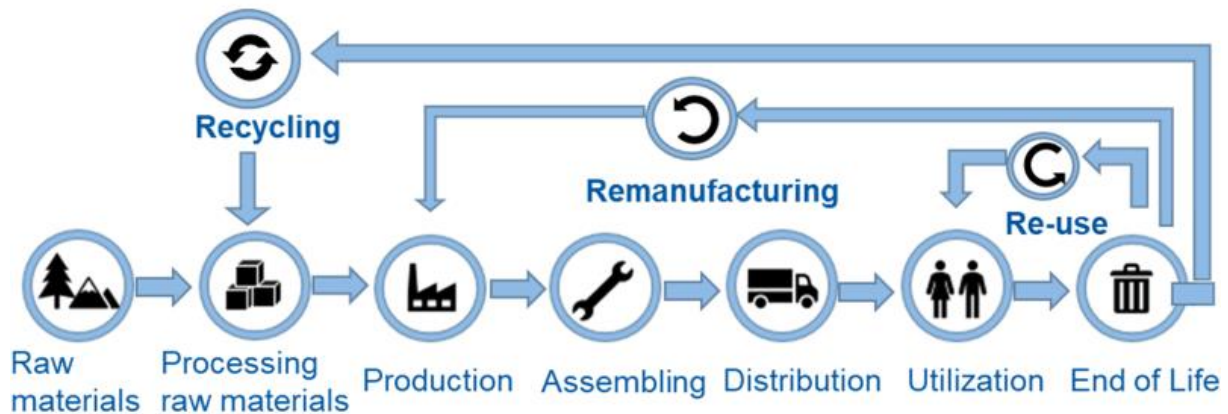


Figure 2.8 Example of the production, utilization, and second life use processes of a battery pack.

In Figure 2.8 is reported the scheme of the processes that occur to a battery pack during its lifetime, from the extraction of the raw materials to the EOL, passing through the assembling process, and the utilization. As shown, at the EOL there are different options, such as re-use, remanufacturing and recycling of the materials. The best option among the three is chosen according to various parameters such as the usage of the pack, the degradation, and the other possible second life uses.

For instance, a second life option could be to use the pack as an energy storage system for a private household. In this case, the Li-Ion cells are used to store the energy produced by a renewable source (solar photovoltaic (PV), wind turbines, micro-hydroelectric power plants, etc.). In this scenario, the use of the storage systems enables us to find the match between the production and the consumption of energy, which are generally not matched (production occurs during the day and the consumption during the night, for the solar PV case). An EES could be useful in countries that have different tariffs according to the periods/hours of the day. In this way, the energy can be bought, and stored, when the prices are low, and then used when the prices are high Vgl. Farinet et al. (Battery Lifetime Analysis for Residential PV-Battery System used to Optimize the Self Consumption - A Danish Scenario) 2019³⁷. Using this technique, the electricity bill can be reduced. Of course, the two solutions, production and storage, and storage at low prices could be combined to maximize the profit.

From the point of view of the Transmission System Operator (TSO), the battery packs can be used for different applications. For instance, the applications of Li-Ion batteries for TSOs, such as:

- Large energy storage systems;
- Power smoothing.

³⁷ Vgl. Farinet et al. (Battery Lifetime Analysis for Residential PV-Battery System used to Optimize the Self Consumption - A Danish Scenario) 2019.

In the first case, they can be used as storage systems, to provide energy when energy production is not enough. For this use the amount of energy and power that the battery banks need to deliver increases very much, in the range of MWh and MW, while the energy capacity and power capacity needed are the range of kWh and kW. In both cases, the use of storage systems stabilizes the balance between the production and the consumption of energy in areas in which the penetration of RES is high.

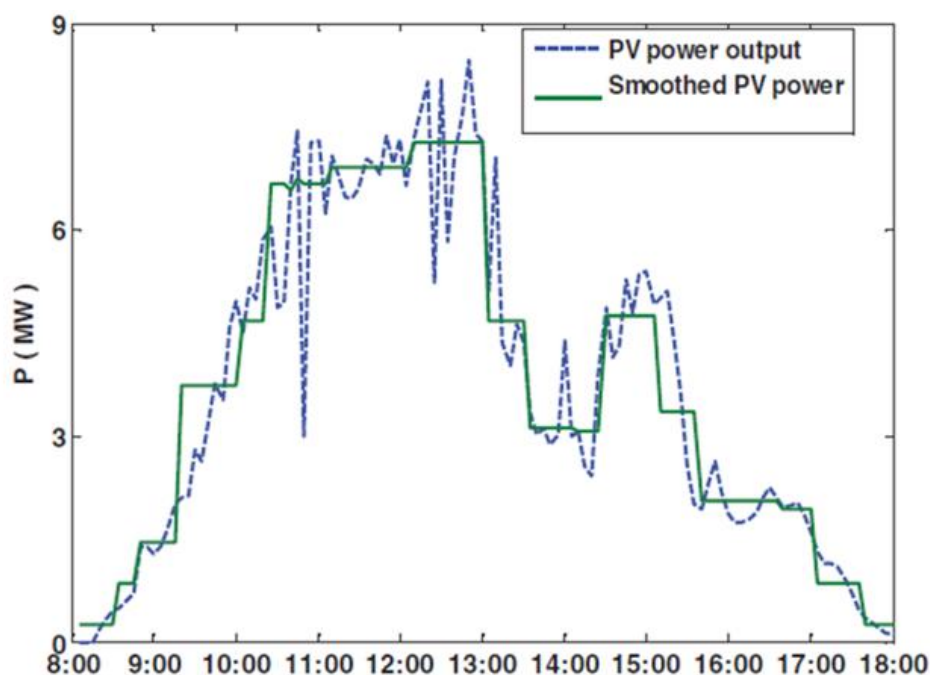


Figure 2.9 Raw power profile vs power smoothing of a PV power plant.

For what concerns the power smoothing application, the Li-Ion batteries are mostly used in renewable energy production. Indeed, the power produced by RESs can have a high harmonic component, which makes the power quality very poor Vgl. Bo Liu et al. (Control Strategy of BESS for Smoothing Fluctuation)³⁸. With the implementation of battery systems, it is possible to store the energy and then re-power it to the electrical grid with better power quality. When it is applied to PV systems it reduces the harmonic component of the energy and thus the power quality is increased. The power generated from the RES flows into the battery and then it is ready to be used. Of course, in the case of PV generators, the electrical connection between the battery system and the PV plant could be made with a DC/DC converter, while for other types of RES (hydro, wind, etc.) the connection has to be made using an AC/DC interface.

In Figure 2.9 it is shown the power profile of a large PV power plant. The blue dashed line represents the power actually produced by the plant; it can be noticed that the profile fluctuates

³⁸ Vgl. Bo Liu et al. (Control Strategy of BESS for Smoothing Fluctuation).

very much during the hours of the day. This condition is not ideal for the electrical grid, especially if the area in which the PV plant is located has a high penetration rate of RES. For instance, at 11 there is a great drop in the production, from 6 MW to 3 MW, that could create serious problems to the grid. With the use of a battery system, the power profile can be smoothed, and the fluctuation of the power could be stabilized. The green line represents the power injected into the grid from the PV+storage system Vgl. Farinet et al. (Battery Lifetime Analysis for Residential PV-Battery System used to Optimize the Self Consumption - A Danish Scenario) 2019³⁹. The profile has a solid behaviour and it does not have sudden rises and drops. Nevertheless, the profile of the output power can be easily controlled with the use of an Energy Management System (EMS), enabling better management of the power flow during the different hours of the day.

This process is useful especially when it is applied to large PV power plants, which have a great harmonic distortion. In addition to the harmonic distortion, large PV power plants have enormous fluctuations in the power produced during the different periods of the day (due to atmospheric and weather conditions).

³⁹ Vgl. Farinet et al. (Battery Lifetime Analysis for Residential PV-Battery System used to Optimize the Self Consumption - A Danish Scenario) 2019.

3 State of the art

In this chapter are presented the main processes and tests that are relevant for this thesis. The examples are taken from the existing literature and previous researches performed at RWTH (Production Engineering of E-Mobility Components (PEM) institute). Thus, are evaluated the following tests:

- Relaxation (3.1);
- Parametrization of the battery (3.2);
- Self-discharge (3.3);
- Capacity of the battery (3.4).

3.1 Relaxation

As seen previously, the OCV versus SOC relationship is crucial for battery cells. The more the curve is accurate and the more reliable are the results of the tests. To extract the OCV vs SOC curve the relaxation phenomenon must be considered. Relaxation is a process that occurs when the battery changes its state, and it is more appreciable when the battery is on a steady-state (either after a charging or discharging process). If a charging state has been applied to the cell, at the end of the charge, the OCV would decrease. On the contrary, if the battery was discharging, at the end of it the OCV would increase Vgl. Petzl et al. (Advancements in OCV Measurement and Analysis for Lithium-Ion Batteries) 2013⁴⁰.

As presented in Vgl. Petzl et al. (Advancements in OCV Measurement and Analysis for Lithium-Ion Batteries) 2013 the relaxation process could have great influence during the testing of battery cells. As stated in the study the amount of voltage decrease/increase depends on the type of battery technology used. The impact of this process is greater the higher is the resolution and accuracy needed during the test. For these reasons, it is necessary to add pauses between the charging and discharging processes.

The value of the voltage drop/increase could depend on the SOC, on the temperature of the battery and on the C-rate used during the charging/discharging process. In Figure 3.1, it is shown the voltage during the relaxation pause after a charging state. The voltage drop starts from 7.39 V and it occurs as soon as the charging stops. Then the voltage moves among 7.38 V and 7.37 V, and then, after a few seconds, it stabilizes at 7.37 V. The voltage then remains constant at 7.37 V for more than 50 seconds until the discharging process starts.

As can be noticed the voltage goes up and down at the beginning of the relaxation, which occurs because of the resolution limit of the testing equipment that has been used. With a higher resolution, the voltage profile during the relaxation would be different, with a steep drop at the beginning and then a slower voltage drop, in the second part.

⁴⁰ Vgl. Petzl et al. (Advancements in OCV Measurement and Analysis for Lithium-Ion Batteries) 2013.

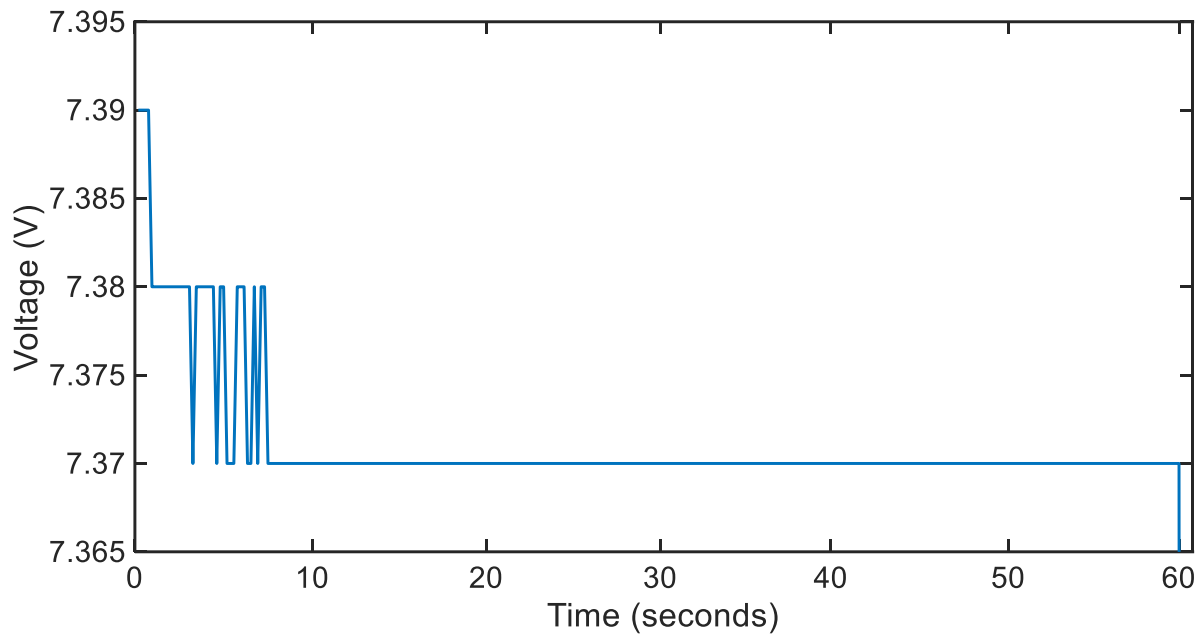


Figure 3.1 Example of voltage profile during the relaxation pause (1 minute) at 20% SOC after a charging state with 1.5 C.

Of course, relaxation is not a symmetrical process, therefore the behaviour of the OCV after a charging state could be different, in terms of absolute values, from the behaviour after a discharging state. For these reasons, the relaxation process has to be considered, and possibly it has to be evaluated and studied with further tests, during the development of a test protocol for Li-Ion batteries.

3.2 Parametrization of the battery

According to the researches Vgl. Madani et al. (An Electrical Equivalent Circuit Model of a Lithium Titanate Oxide Battery) 2019⁴¹ and Vgl. Stroe et al. (Lithium-Ion Battery Dynamic Model for Wide Range of Operating Conditions) 2017⁴² the best trade-off between the parametrization of the battery and the accuracy of the model is to use an Equivalent Electric Circuit (EEC). This type of model is used to study the behaviour of Li-Ion batteries. The model is based on the equivalence between the electrical parameters DC voltage source, resistances, and capacitances. To model the behaviour of the battery the voltage profile of the pulse tests is evaluated. Using these it is possible to model a wide range of characteristics of Li-Ion batteries.

As shown in Figure 3.2, the EEC model has four different electrical parameters, such as:

⁴¹ Vgl. Madani et al. (An Electrical Equivalent Circuit Model of a Lithium Titanate Oxide Battery) 2019.

⁴² Vgl. Stroe et al. (Lithium-Ion Battery Dynamic Model for Wide Range of Operating Conditions) 2017.

- Open Circuit Voltage (OCV) modeled as a Direct Current (DC) voltage source;
- R_0 ;
- R_1 and C_1 ;
- R_2 and C_2 ;

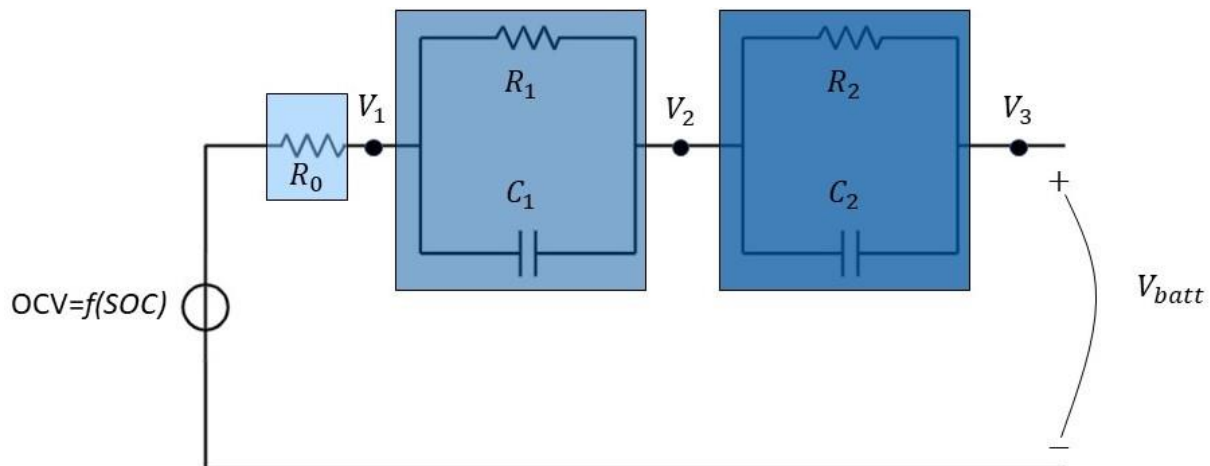


Figure 3.2 Electrical Equivalent Circuit used to model the Li-Ion battery

R_0 represents the ohmic resistance and therefore the resistive behaviour of the battery cell. The first RC parallel, R_1 and C_1 , demonstrated the small-time constant of the battery cell feedback, and it represents the effect of the double-layer capacitance and of the charge transfer procedures. While the second RC parallel, R_2 and C_2 , shows the lengthy-time one was employed to model the diffusion operation.

These parameters are not constant for all the batteries that use Li-Ion technology; indeed, they are different based on the kind of cells used. Since the value of the parameters is not constant it is necessary to evaluate each time the cells and to extract the parameters.

The evaluation of the parameters that form the EEC is important because from them, and from the results of other batterie tested it is possible to give a first estimation of the SOH. Indeed, the value of R_0 increases significantly with the aging and the usage of the battery.

On this matter, there are different researches, such as Vgl. Stroe et al. (Lithium-Ion Battery Dynamic Model for Wide Range of Operating Conditions) 2017⁴³ and Vgl. Sarasketa-Zabala et al. (Cycle ageing analysis of a LiFePO4/graphite cell with dynamic model validations: Towards realistic lifetime predictions) 2015⁴⁴. Those present different methodologies to extract the parameters. As stated previously the OCV is a function of the SOC (and the C-rate) and

⁴³ Vgl. Stroe et al. (Lithium-Ion Battery Dynamic Model for Wide Range of Operating Conditions) 2017

⁴⁴ Vgl. Sarasketa-Zabala et al. (Cycle ageing analysis of a LiFePO4/graphite cell with dynamic model validations: Towards realistic lifetime predictions) 2015.

therefore its value varies depending on the moment of use of the battery. For the same reasons the values of the parameters used in the EEC have different values.

To extract the EEC parameters the presented studies, use various DC current pulses at different SOC. The current pulses are applied for a short time (seconds) and can be either charging or discharging pulses Vgl. Böttiger et al. (Systematic experimental pulse test investigation for parameter identification of an equivalent based lithium-ion battery model) 2017⁴⁵.

The formulas used to determine the parameters are listed in the equations (3.1), (3.2), (3.3), (3.4), (3.5), (3.6), (3.7), (3.8), (3.9) and (3.10).

Where t_i is the time at which the voltage V_i is measured and I_{batt} is the value of current at which the pulse is applied.

$$\Delta V_1 = OCV - V_1 (V) \quad (3.1)$$

$$\Delta V_2 = V_1 - V_2 (V) \quad (3.2)$$

$$\Delta V_3 = V_2 - V_3 (V) \quad (3.3)$$

$$R_0 = \frac{(OCV - V_1)}{I_{batt}} (\Omega) \quad (3.4)$$

$$R_1 = \frac{(V_1 - V_2)}{I_{batt}} (\Omega) \quad (3.5)$$

$$R_2 = \frac{(V_2 - V_3)}{I_{batt}} (\Omega) \quad (3.6)$$

$$C_1 = \frac{(t_2 - t_1) \cdot I_{batt}}{(V_2 - V_1) \cdot \ln\left(\frac{V_2}{V_1}\right)} (F) \quad (3.7)$$

$$C_2 = \frac{(t_3 - t_2) \cdot I_{batt}}{(V_3 - V_2) \cdot \ln\left(\frac{V_3}{V_2}\right)} (F) \quad (3.8)$$

$$\tau_1 = R_1 C_1 (s) \quad (3.9)$$

$$\tau_2 = R_2 C_2 (s) \quad (3.10)$$

OCV	Open Circuit Voltage
V_1	Voltage of the module at t_1 (V)
V_2	Voltage of the module at t_2 (V)
V_3	Voltage of the module at t_3 (V)
ΔV_1	Voltage drop between OCV and V_1 (V)
ΔV_2	Voltage drop between V_1 and V_2 (V)

⁴⁵ Vgl. Böttiger et al. (Systematic experimental pulse test investigation for parameter identification of an equivalent based lithium-ion battery model) 2017.

ΔV_3	Voltage drop between V_2 and V_3 (V)
I_{batt}	Current used for the pulse (A)
R_0	Ohmic resistance (Ω)
R_1	Small constant resistance, first parallel branch (Ω)
R_2	Diffusion resistance, second parallel branch (Ω)
C_1	Small constant capacitance, first parallel branch (F)
C_2	Long constant capacitance, second parallel branch (F)
τ_1	Time constant of the first RC branch (s)
τ_2	Time constant of the first RC branch (s)

The total resistance R_{tot} can be also calculated by adding all of the resistances R_0 , R_1 , and R_2 , as shown in the equation (8.3).

$$R_{tot} = \sum_{i=0}^{i=2} R_i \quad (\Omega) \quad (3.11)$$

R_{tot} Total equivalent internal resistance (Ω)

i Order of the model

In order to have the parameters to create the EEC of the battery, a pulse test has to be performed. As stated in Vgl. Madani et al. (An Electrical Equivalent Circuit Model of a Lithium Titanate Oxide Battery) 2019⁴⁶ the current pulses can be either using charging or discharging ones. To have a better representation of the behaviour of the battery and the processes that occur during the usage many current pulses are applied (with different C-rates and at various SOCs). The more trials made the more accurate can be the model created to simulate the characteristics of the battery Vgl. Sarasketa-Zabala et al. (Cycle ageing analysis of a LiFePO4/graphite cell with dynamic model validations: Towards realistic lifetime predictions) 2015⁴⁷. As stated, the more points of measurement there are the more accurate the EEC model will be.

Figure 3.3 shows an example of the pattern of the voltage (V_{batt}) of the battery during a discharging current pulse. The battery being tested is a module of the Nissan Leaf 2011 Edition (66 Ah), the current pulse is of 1.5 C (99 A) and the SOC at which the pulse is applied is 35%.

⁴⁶ Vgl. Madani et al. (An Electrical Equivalent Circuit Model of a Lithium Titanate Oxide Battery) 2019.

⁴⁷ Vgl. Sarasketa-Zabala et al. (Cycle ageing analysis of a LiFePO4/graphite cell with dynamic model validations: Towards realistic lifetime predictions) 2015

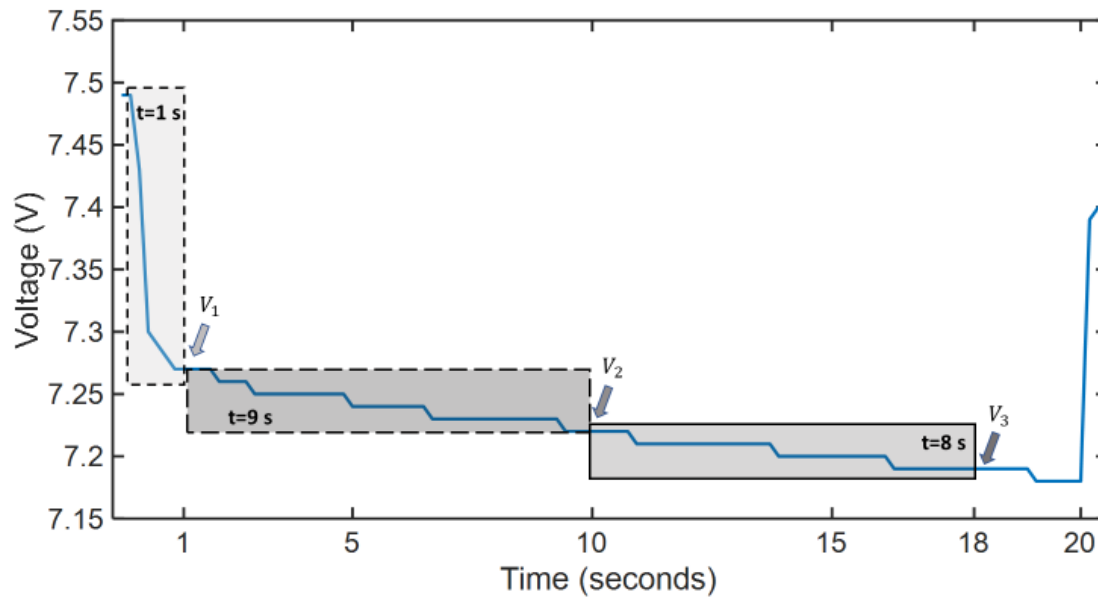


Figure 3.3 Example of voltage drop due to a current pulse of 1.5 C at 35% SOC.

The procedure of extraction of the parameters is made by charging (or discharging) the battery to the established voltage level. Then, the current is set to the established level (positive to charge or negative discharge) and is kept constant for a certain amount of time. In the case reported in Figure 3.3 the current pulse has a duration of 20 seconds, but the duration of the test can be either longer or shorter, according to the different types of batteries Vgl. Farinet et al. (Battery Lifetime Analysis for Residential PV-Battery System used to Optimize the Self Consumption - A Danish Scenario) 2019⁴⁸.

While the current pulse is being applied the voltage levels are registered. With the measurement of the voltage, it is possible to determine different “transient states” during the pulse, as shown in the figure above. In particular, after 1 second from the current pulse, the voltage drops significantly, this decrease is due to the Ohmic resistance R_0 , which can be calculated from the equation (3.4). The measurement of the voltage V_1 is taken at $T=T_1$. After this sudden voltage drop, there is a phase where the voltage decreases, but with a lower rate, this behaviour is linked to the first RC branch of the EEC. When the voltage drop rate decreases even more the third transient state starts, this process is the one that gives the parameters to model the second RC branch of the EEC.

The different values of T_1 , T_2 , and T_3 are different for all the batteries, depending on the type of battery and the SOH. Generally, the values of the duration of the test are similar to the ones showed in Figure 3.3.

⁴⁸ Vgl. Farinet et al. (Battery Lifetime Analysis for Residential PV-Battery System used to Optimize the Self Consumption - A Danish Scenario) 2019.

In Vgl. Farinet et al. (Battery Lifetime Analysis for Residential PV-Battery System used to Optimize the Self Consumption - A Danish Scenario) 2019⁴⁹ and Vgl. Stroe et al. (Lithium-Ion Battery Dynamic Model for Wide Range of Operating Conditions) 2017⁵⁰ the voltage steps are applied respectively with 5% and 10% SOC resolution. Vgl. Stroe et al. (Lithium-Ion Battery Dynamic Model for Wide Range of Operating Conditions) 2017 use 8 different C-rates, going from 0.1 C to 9 C (for both the charging and discharging states).

This methodology enables to have great datasets to be used for the creation of the EEC model Vgl. Böttiger et al. (Systematic experimental pulse test investigation for parameter identification of an equivalent based lithium-ion battery model) 2017⁵¹. However, the difference between the values of the parameters of the EEC has to be evaluated according to the different batteries and the type of application for which the battery system is designed. One of the main drawbacks of this technique is that could be very time-consuming if the test has many different C-rates and SOC levels. For instance, the presented test has 20 SOC levels and 8 C-rates, which gives 160 trials for the charging pulses and 160 for the discharging ones, for a total of 320 trials.

3.3 Self-discharge

All the technologies used for batteries are affected by self-discharge. Self-discharge is a characteristic of batteries, of course, the lower is the quality of the manufacturing process, the higher is the impact of this characteristic on the cell. Self-discharge is a permanent process and cannot be reversed, the amount of charge self-discharged is lost and decreases the efficiency of the battery. The self-discharge can be thought as an efficiency coefficient Vgl. Keysight Technologies (Evaluate Lithium Ion Self-Discharge of Cells in a Fraction of the Time Traditionally Required)⁵².

The impact of self-discharge varies according to different conditions. For instance, the same cell can have different self-discharge rates at different SOCs. This parameter varies also with the aging and the usage of the cell.

Cells that use Li-Ion technology have charge loss due to different causes. The losses come from the electrochemical structure of the cells, where the electrical charges have to flow

⁴⁹ Vgl. Farinet et al. (Battery Lifetime Analysis for Residential PV-Battery System used to Optimize the Self Consumption - A Danish Scenario) 2019.

⁵⁰ Vgl. Stroe et al. (Lithium-Ion Battery Dynamic Model for Wide Range of Operating Conditions) 2017

⁵¹ Vgl. Böttiger et al. (Systematic experimental pulse test investigation for parameter identification of an equivalent based lithium-ion battery model) 2017.

⁵² Vgl. Keysight Technologies (Evaluate Lithium Ion Self-Discharge of Cells in a Fraction of the Time Traditionally Required).

through the layers. Because of these movements, there are small energy losses that decrease the overall efficiency of the battery. As for the electrical parameters of the EEC, the self-discharge is not constant over time and it increases its value with the aging and the usage of the battery.

Another test that gives great information about a Li-Ion cell SOH is the Self-discharge test. Indeed, high Self-discharge rates point out that the cells might be damaged or soon to have failures. For this reason, is important to evaluate this aspect in the remanufacturing process. As stated in Vgl. Keysight Technologies (Evaluate Lithium Ion Self-Discharge of Cells in a Fraction of the Time Traditionally Required)⁵³ and Vgl. Zimmerman (Self-discharge losses in lithium-ion cells) 2004⁵⁴ there are different methods to characterize the self-discharge of a Li-Ion cell, such as:

- galvanostatic method;
- potentiostatic method.

The galvanostatic method is based on the voltage drop that occurs over time. As reported Vgl. Keysight Technologies (Evaluate Lithium Ion Self-Discharge of Cells in a Fraction of the Time Traditionally Required) this method is very time-consuming. In addition to that, Li-Ion cells have a limited Self-discharge, therefore, to see the impact of Self-discharge the test must be performed for a long period (several weeks, months). From an industrial point-of-view, this time-consuming process is not ideal. The same goes for the study cases of this research since the number of modules is great a different testing procedure must be found.

3.3.1 Potentiostatic method

In Vgl. Zimmerman (Self-discharge losses in lithium-ion cells) 2004 and Vgl. Keysight Technologies (Evaluate Lithium Ion Self-Discharge of Cells in a Fraction of the Time Traditionally Required) is presented the potentiostatic method to test the Self-discharge, which considers the current that is used to charge the battery during the test. The method consists of charging the cell to an established voltage level (or SOC) when the battery is at that voltage level a CV charge state starts.

It is clear that the Potentiostatic method has many different advantages when used in industrialized processes, such as:

- testing time reduction, from weeks/months to hours;
- enables to have a fast understanding of the cell/module's SOH;
- good reliability.

These characteristics are key features for the testing of a large number of cells and modules, like the ones that come from the disassembly of the used EV's battery packs.

⁵³ Vgl. Keysight Technologies (Evaluate Lithium Ion Self-Discharge of Cells in a Fraction of the Time Traditionally Required).

⁵⁴ Vgl. Zimmerman (Self-discharge losses in lithium-ion cells) 2004.

According to the different types of Self-discharge test, the duration of it may change. In the presented studies the duration of the tests is in the range of hours. During the test, due to the CV charging state, the voltage is kept constant at the established voltage level using a charging current.

In Figure 3.4 is shown the potentiostatic method presented in Vgl. Keysight Technologies (Evaluate Lithium Ion Self-Discharge of Cells in a Fraction of the Time Traditionally Required). As said above this method uses a stable DC voltage source (in the figure on the right) which is kept constant to the value of the voltage of the cell (V_{cell}). Then the current I_{SD} is used to charge the cell and to keep V_{cell} constant.

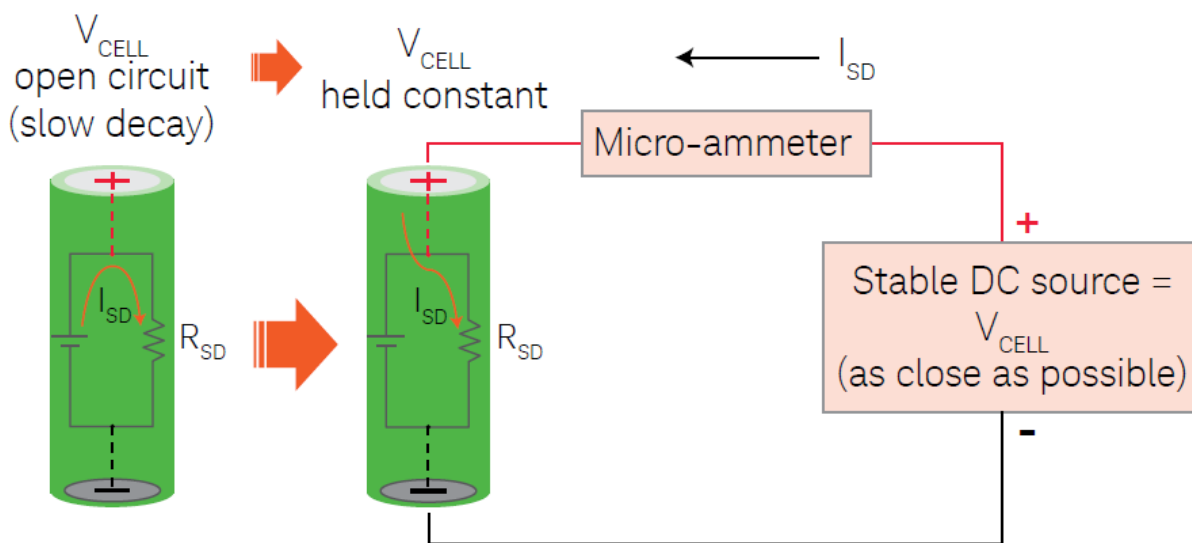


Figure 3.4 Example of self-discharge evaluation using the potentiostatic method Vgl. Keysight Technologies (Evaluate Lithium Ion Self-Discharge of Cells in a Fraction of the Time Traditionally Required)⁵⁵

Self-discharge tests may be applied to the same cell at different SOCs with either equal or different durations in time. The voltage level at which the self-discharge test is applied may depend on a different kind of measurement that has to be made. The self-discharge is then evaluated according to the equation (3.12), where the charging current is integrated over the time of the test. The formula (3.12) gives the self-discharge in As, to change it to Ah the (3.13) can be used. The self-discharge can be referenced also to the rated capacity, as shown in the (8.3).

$$SD = \int_{t_0}^{t_1} i \cdot dt \quad (\text{As}) \quad (3.12)$$

⁵⁵ Vgl. Keysight Technologies (Evaluate Lithium Ion Self-Discharge of Cells in a Fraction of the Time Traditionally Required).

t_0	Beginning of the self-discharge test (seconds)
t_1	Ending of the capacity test (seconds)
i	Current (A)
SD	Self-discharge (As)

$$SD (Ah) = \frac{SD (As)}{3600} \quad (3.13)$$

SD Self-discharge (Ah)

$$SD (\%) = \frac{(SD(Ah) \cdot 100)}{C_N} \quad (3.14)$$

$SD (\%)$ Self-discharge percentage

$C_N (\%)$ Nominal capacity of the cell (Ah)

3.4 Capacity

The most important parameter of any energy storage device is the capacity that is available to the final user. As stated previously the capacity of battery systems depends on the usage and on the aging of them. Therefore, for second life uses, it is important and essential to evaluate the actual available capacity of the batteries.

The End-of-Life (EOL) of batteries is usually reached when the available capacity reaches the 70-80 % Vgl. Ramoni et al. (End-of-life (EOL) issues and options for electric vehicle batteries) 2013⁵⁶ of the rated capacity. In particular, for EV applications the EOL is reached when the capacity drops below 80 %. In the researches Vgl. Ramoni et al. (End-of-life (EOL) issues and options for electric vehicle batteries) 2013 and Vgl. Ecker et al. (Calendar and cycle life study of Li(NiMnCo)O₂-based 18650 lithium-ion batteries) 2014⁵⁷ are presented some examples of the possible test to determine the available capacity of Li-Ion cells.

In the presented researches the tests start with a CC charging state, using a low C-rate (0.1 C, 0.3 C) when the voltage reaches the established voltage level (which corresponds to 100 % SOC) the CC phase ends and the CV phase. During the CV charging state, the current decreases and when the current reaches C/100 (1% of the C-rate) the charging state stops. Then, after a pause phase (minutes) the battery is discharged with a low C-rate (0.1

⁵⁶ Vgl. Ramoni et al. (End-of-life (EOL) issues and options for electric vehicle batteries) 2013.

⁵⁷ Vgl. Ecker et al. (Calendar and cycle life study of Li(NiMnCo)O₂-based 18650 lithium-ion batteries) 2014.

C, 0.3 C). The discharge phase starts with a CC, with the defined current. When the battery voltage level reaches the voltage, which corresponds to the 0% SOC the CC state ends, and the CV state begins. The CV discharging state ends when the current reaches $C/100$ (1% of the C-rate) Vgl. Hongwen et al. (Evaluation of Lithium-Ion Battery Equivalent Circuit Models for State of Charge Estimation by an Experimental Approach) 2011⁵⁸.

This technique is used to fully discharge the battery and to obtain the actual available capacity of the battery. Figure 5.7 shows the profile of the voltage and of the current during the module, during the capacity test, of a module of the Nissan Leaf 2011 Edition. It can be seen the typical shape of the voltage during the discharge. In the figure, the discharge state has been performed using a C-rate of 1 C. The initial decrease of the current during the CV phase is steep, but as soon as the current reaches 10 A the decrease slows down, reaching the set value (1% of 1 C) only 40 minutes after the start of the CV state.

When the CC-CV discharging state ends the available capacity is determined according to (8.3) Vgl. Davide Andrea (Battery Management Systems for Large Lithium-Ion Battery Packs) 2010⁵⁹.

$$Capacity = \int_{t_0}^{t_1} i \cdot dt \text{ (As)} \quad (3.15)$$

t_0	Beginning of the capacity test (seconds)
t_1	Ending of the capacity test (seconds)
i	Discharge current (A)
<i>Capacity</i>	Available capacity (As)

To have an easier and better evaluation and comparison of the capacity between the modules of the packs, the value calculated using equation (3.15) is converted in Ah with equation (3.16).

$$Capacity \text{ (Ah)} = \frac{Capacity \text{ (As)}}{3600} \quad (3.16)$$

<i>Capacity</i>	Available capacity (Ah)
3600	Number of seconds in an hour

⁵⁸ Vgl. Hongwen et al. (Evaluation of Lithium-Ion Battery Equivalent Circuit Models for State of Charge Estimation by an Experimental Approach) 2011.

⁵⁹ Vgl. Davide Andrea (Battery Management Systems for Large Lithium-Ion Battery Packs) 2010.

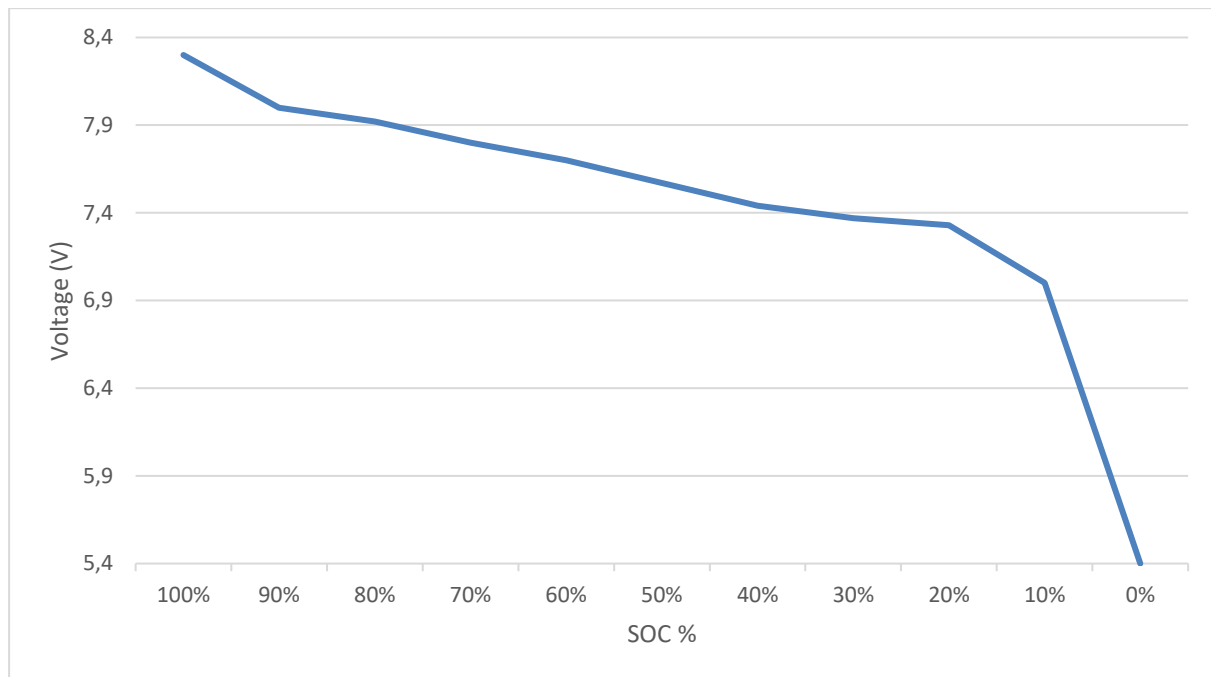


Figure 3.5 Profile of the voltage during the discharging (100%-0%) (module from Nissan Leaf 2011 Edition's battery pack).

As shown in the previous sections of this chapter, the test possibilities are many and so are the parameters that can be extracted from them. The three kinds of tests evaluate in different ways the battery cells. The pulse tests presented in section 3.2 provide the parameters to develop an EEC model to simulate the behaviour of the battery in a various range of conditions. In addition to the dynamic simulations of the battery, the extraction of the parameters of the EEC could provide information on the SOH of the cell. Indeed, by monitoring the values of the parameters a pattern of the degradation of the battery and evaluate the SOH of it. This testing procedure is quite fast (20-30 seconds per pulse) and enables to have a good understanding of the battery. On the other hand, to fully characterize the battery a great number of current pulses have to be applied, using different C-rates, at different SOC's and at different temperatures. Of course, the performance of all these test cases has a great impact on the duration of the tests. The best trade-off between the accuracy of the model and the time at disposal for the testing stage must be found, to do so the purpose of the study must be very specific.

As well as for the pulse test the self-discharge test could be applied to various test cases and scenarios. The duration of a single self-discharge test, using the potentiostatic method described in section 3.3.1, is in the range of hours. For this reason, the voltage levels at which perform the procedure must be found according to the final purpose of the test. As the parameters of the EEC, the self-discharge rate increases with the aging and usage of the battery and it could be used as a sign of the degradation of the battery.

The last testing procedure presented in section 3.4 is the capacity test. This test is the key to evaluate the SOH of the batteries and gives the actual available capacity of the battery tested. The duration depends on the C-rate used to discharge (or charge) the battery, but as

stated in section 3.4 the lower is the C-rate the higher is the quality of the results. Whichever is the C-rate chosen to discharge the battery and whichever is the cut-off value of current for the end of the test the duration of this procedure is in the range of hours.

The presented tests could be performed all to acquire consistent datasets about the SOH of the battery. Combining the information of the tests it is possible to obtain new data about the aging of the battery. For instance, the increase of the resistive components of the EEC (R_0 , R_1 , and R_2) due to the degradation of the battery could be directly linked to the capacity fade. The dataset could be then evaluated, using statistical methods to obtain a correlation among the SOH's intervals and the value of the parameters of the EEC. This could be done studying the correlation between the self-discharge rate and the available capacity.

Certainly, the more cells and modules are tested the more consistent is going to be the results of the correlation among the results of the different tests.

Given the theoretical overview of battery packs for automotive applications, the issues of the used EV battery packs and the possibilities of second life uses, it is clear that there is space for studies and researches. This thesis aims to find a way to test used battery packs in a fast and reliable way. By achieving this the remanufacturing of the packs could be more attractive for automotive OEMs, battery manufacturers, automotive remanufacturers and other types of industries.

3.4.1 Research question

The core questions are all related to the possibility of developing a viable solution for the second life uses of used EV battery packs.

Is it possible to develop a testing strategy that gives good results and being time and cost-effective?

Is it possible to remanufacture a used EV's battery packs, does it give good results? What are the possible applications of the parts that come from the battery of an EV?

Do they change according to the different conditions at which they are found at the time of the remanufacturing process?

4 Technical approach

To develop a definitive test protocol for used automotive battery packs, with the aim of re-using and remanufacture them, it is essential to do some pre-testing and trials. Thus, three Nissan Leaf 2011 Edition (24 kWh) used battery packs have been evaluated in this research. To do so the three packs have been disassembled to the modules level, this process took 3 to 4 hours per pack, depending on the state (rust and degradation of the bolts) of the external cover. The chapter is divided into three sections, based on the architecture of the battery pack of the Nissan Leaf 2011 Edition:

- Battery pack, described in section 4.1;
- Modules, described in section 4.2;
- Cells, described in section 4.3.

The data presented in Table 4.1, Table 4.2, Table 4.3, Table 4.4, and Table 4.5 of this chapter have been taken from Vgl. Gray et al. (2011 Nissan Leaf VIN 0356 Plug-In Hybrid Electric Vehicle Battery Test Results) December 2016⁶⁰ and Vgl. NISSAN NORTH AMERICA (2011 Leaf First Responder's Guide) 2011⁶¹. Part of the data (weights, energy density etc.) has been measured during the disassembly and test processes.

4.1 Battery pack

The battery pack is one of the most important elements of an EV. Indeed, it is a key component and its design and development have to be well thought. For what concerns the Nissan Leaf 2011 Edition the pack is located in the bottom of the car frame, in the center of the vehicle, as shown in Figure 4.3.

Figure 4.1 shows the division of the battery pack in three different subpacks, rear subpack, left subpack and right subpack.

⁶⁰ Vgl. Gray et al. (2011 Nissan Leaf VIN 0356 Plug-In Hybrid Electric Vehicle Battery Test Results) December 2016.

⁶¹ Vgl. NISSAN NORTH AMERICA (2011 Leaf First Responder's Guide) 2011.

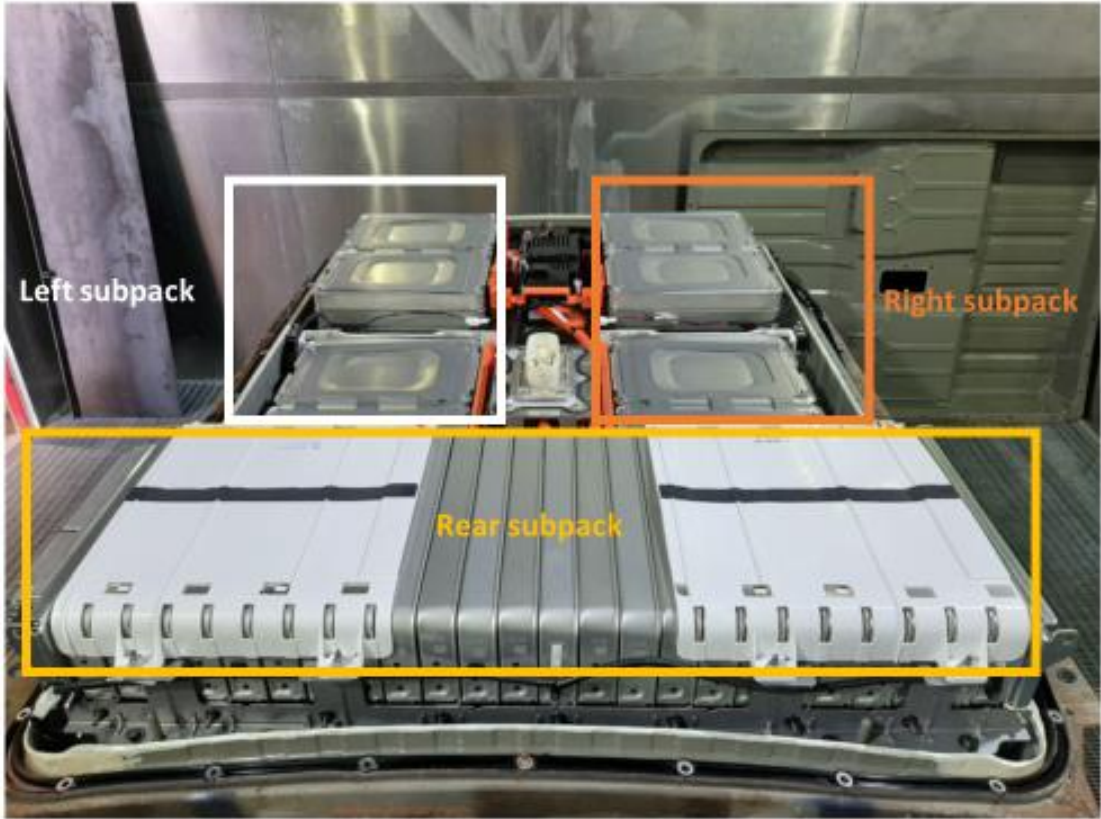


Figure 4.1 Division in 3 subpacks of the battery pack

The total amount of modules, 48, is divided into the subpacks as it follows:

- rear subpack 24 modules;
- left subpack 12 modules;
- right subpack 12 modules.

The subpacks are not only divided in a physical way, indeed, their division is used also electrically. Following the electrical connection from the common “-“ we find the series connection of the all modules from the rear subpack, then the ones from the left subpack and finally the modules of the right subpack. To create the enumeration of the modules of the pack it has been used the electrical connection, therefore the modules have been numbered as listed in Table 4.1.

Table 4.1 Numeration of the modules in between the subpacks.

Subpack	Module number
Rear subpack	1-24
Left subpack	25-36
Right subpack	37-48

The enumeration of the modules follows the electrical connection and goes from the common “-“ end to the common “+” end. Then the module number “1” is the one connected to the common “-“, while the module number “48” is the module connected to the common “+”. From now on, and for all the battery packs tested, this will be the denomination of the modules.

In Table 4.2 are listed the main specifications of the battery pack object of the testing. The operating nominal voltage of the pack is 364.8 V. The nominal capacity is 66 Ah, these two values bring the nominal capacity, measured in kWh, of the pack to 24 kWh. The modules are connected using a series connection.

This type of connection enables the pack to increase and to reach the desired voltage. The total weight of the pack is approximately 294 kg, this weight requires special tools and lifting equipment. Of course, given the voltage level of the pack, the risk of hazard is high, and various precautions must be used.

Table 4.2 Main specification of the battery pack Nissan Leaf 2011 Edition.

Nissan Leaf 2011 Battery pack specifications	
Manufacturer	Automotive Energy Supply Corporation (AESC)
Technology	Lithium-Ion – Laminate type
Cathode / Anode Material	LiMn2O4 with LiNiO2/Graphite
Pack Location	Under the center of the vehicle
Number of Cells	192
Cell Configuration	96 series, 2 parallel, 96 s 2 p
Nominal Cell Voltage	3.8 V
Nominal System Voltage	364.8 V
Rated Pack Energy	24 kWh
Max. Cell Charge Voltage	4.2 V
Min. Cell Discharge Voltage	2.5 V
Cooling	Passive, Sealed Unit
Approximate Pack Weight	294 kg
Dimensions (L x W x H)	1570.5 x 1188 x 264.9 mm
Energy density	81.63 Wh/kg

From the results of the disassembly of the pack it is clear that the Nissan Leaf 2011 Edition battery packs were engineered and designed to facilitate the process of re-use and remanufacturing of the components. Indeed, during the disassembly of the packs only very few components were compromised (cable ties and rusty bolts) and at the same time they were highly

replaceable. This situation makes the future re-use and remanufacturing processes more likely and easier to design.

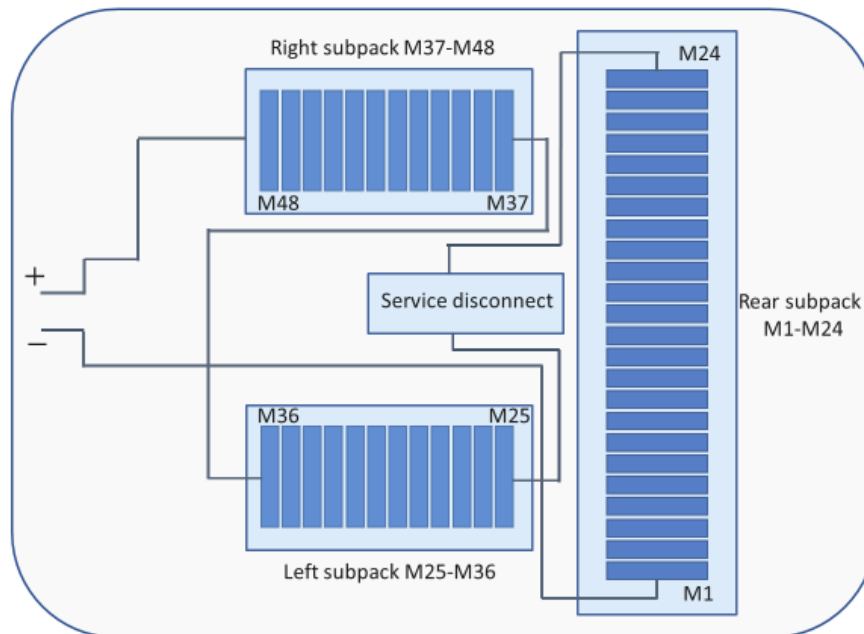


Figure 4.2 Scheme of the electrical connection of the modules inside the battery pack of the Nissan Leaf 2011 Edition.

In Figure 4.2 are illustrated the electrical connection between the three subpacks of the battery pack. As previously stated, starting from the common “-“, the first subpack is the rear one, with the modules from M1 to M24. Then, linked to the module M24 there is the service disconnect. This device is used to disconnect the battery, it has a fuse which breaks if the current exceeds a certain threshold. The disconnection can be made also manually, by pulling out a small box in which is contained the fuse. Coming out from the service disconnect box, there is the connection with the side subpacks, the left and right subpacks. Going out from the service disconnect there is the left subpack, with the modules from M25 to M36. The last 12 modules, from M37 to M48, are contained in the right subpack; lastly from the module 48 there is the electrical connection to the common “+” of the battery.

As shown in Figure 4.3 the battery pack of the Nissan Leaf 2011 Edition is positioned in the center part of the car, under the seats. This choice has been done to balance the weight of the motor, which is placed in the front of the car. In addition to the balance in the distribution of the weight, the low position of the battery pack lowers the center of gravity of the car. A lower center of gravity gives better handling during the driving and prevents the car from overturning while driving on tight and sharp corners.

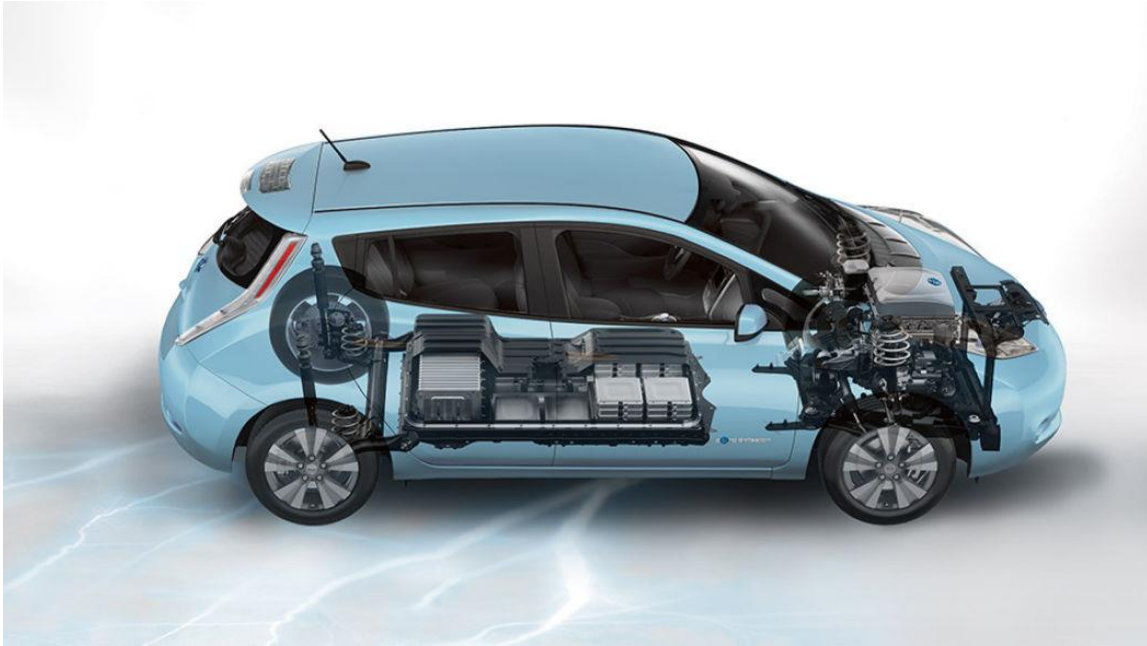


Figure 4.3 Position of the battery pack in the Nissan Leaf 2011 Edition.

The total weight of the 192 cells, considering only the electrochemical devices, is approximately 151 kg, to which the steel boxes, wire harnesses, plates, and electronics add another 143 kg for a total pack weight of approximately 294 kg. This means that half of the weight of the battery pack is composed of the battery itself, while the other half is composed of the accessories that complete the pack.

4.2 Modules

As said in section 4.1 the battery pack is divided 3 subpacks and the total number of modules is 48. The fact that the pack is divided in this way enables different second life purposes because the battery can be disassembled rather easily, and the modules are suitable for re-use and even more for remanufacturing of battery packs.

As outlined, the battery pack is made up of 48 modules that are connected using a series connection. All the 48 modules are formed by 4 Lithium-Ion cells. To create the module the 4 cells are divided into two series branches, that are then connected in parallel. This design brings the module to have a rated voltage (7.6 V) and a good capacity (66 Ah), as shown in equation (4.1) and equation (4.2).

$$V_M = V_C \cdot N_S = 3.8 \cdot 2 = 7.6 \text{ (V)} \quad (4.1)$$

$$C_M = C_C \cdot N_P = 33 \cdot 2 = 66 \text{ (Ah)} \quad (4.2)$$

V_M	rated voltage of the module (V)
V_C	rated voltage of the cell (V)
N_S	number of cells connected in series

C_M	rated capacity of the module (Ah)
C_C	rated capacity of the module (Ah)
N_p	number of cells connected in parallel

$$W_M = V_M \cdot C_M = 7.6 \cdot 66 = 501.6 \text{ (Wh)} \quad (4.3)$$

W_M	rated capacity of the module (Wh)
V_M	rated voltage of the module (V)
C_M	rated capacity of the module (Ah)

In Table 4.3 are listed the main specifications of the modules that make up the battery pack object of the testing. As can be seen, there is a small difference (501.6 Wh and 500 Wh) in the energy of the module from the one calculated in (4.3), this is due to the fact not all the energy at disposal is used during the operation of the battery.

Table 4.3 Main specifications of the module of the Nissan Leaf 2011 Edition.

Nissan Leaf 2011 Module specifications	
Number of Modules per pack	48 (series connection)
Number of Cells	4
Cell Configuration	2 parallel, 2 series, 2 p 2 s
Nominal Voltage	7.6 V
Rated Capacity	66 Ah
Rated Energy	500 Wh
Max. Charge Voltage	8.4 V
Min. Discharge Voltage	5 V
Approximate Weight	3.76 kg
Dimensions (L x W x H)	303 x 223 x 55 mm

Figure 4.4 shows a schematic of how the cells are placed inside the module. As said previously, inside every module there are four cells, they are stacked inside the module. The two “+” ends of the cells placed in the top are connected together in the common positive end of the top part, the same occurs for the “-” ends. The same operation is done for the two cells placed on the bottom of the module. Then, the common ends of the top and the bottom are connected together, “+” with “+” and “-” with “-”, creating a single common positive end and a single negative end for every module. Using this type of connection between the cells the designed voltage level is reached.

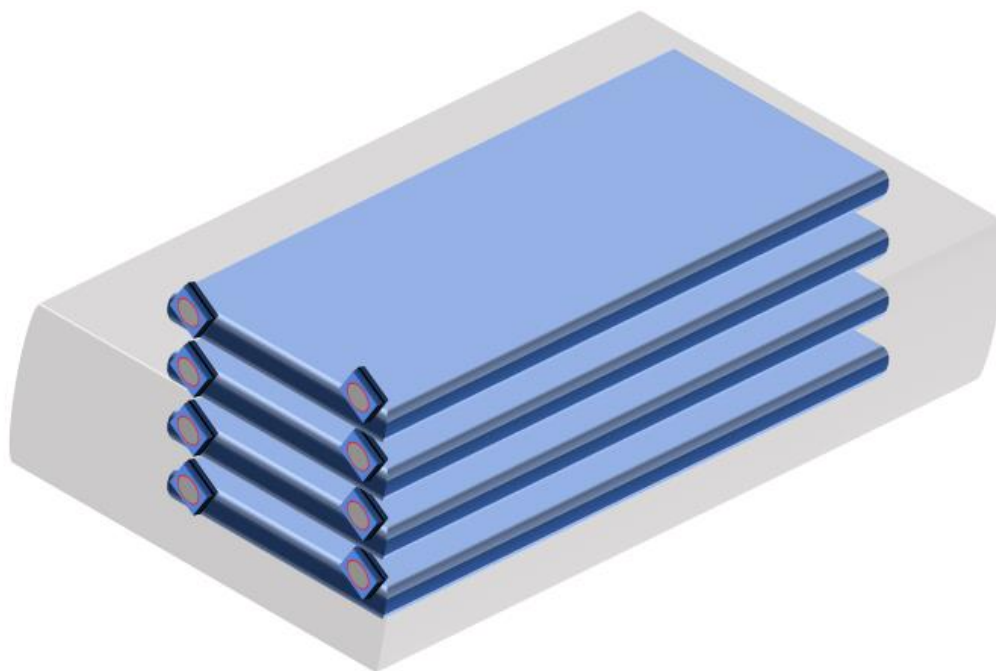


Figure 4.4 Disposition of the four cells inside the module of the Nissan Leaf 2011 Edition.

4.3 Cells

The cells are the most important components of a battery pack. Indeed, the battery pack is based on them and on their specifications. The designed capacity (Ah) and the designed voltage of the battery pack are based on the different connections of the cells (parallel connection or series connection).

In Table 4.4 are listed the main specifications of the cell that make up the modules object of the testing. As stated previously the number of cells contained in the battery pack is 192. The overall connections in the pack are performed through the modules, each one has inside four cells, connected using a series and parallel connection.

Table 4.4 Main specifications of the cell of the Nissan Leaf 2011 Edition

Nissan Leaf 2011 Cell specifications	
Number of Cells	192
Nominal Voltage	3.8 V
Rated Energy	125 Wh
Max. Charge Voltage	4.2 V
Min. Discharge Voltage	2.5 V
Number of cells per module	4
Shape	Pouch
Energy density	320 Wh/L



Figure 4.5 Cell used to manufacture the battery pack of the Nissan Leaf 2011 Edition.

As shown in Figure 4.5, the cells used in the Nissan Leaf 2011 Edition have a pouch form, which enables to stack them easily inside the modules. This choice has been made to increase the modularity of the systems, enabling the possibility to scale the design of the pack to highest capacities without re-designing the entire pack. However, this choice has its own downsides, indeed, the second level of packaging, the modules, is needed between the cells and the pack. This need brings more weight to the pack, decreasing its energy density (Wh/kg). Thus, this choice results in an increase in the weight of the pack and a decrease in the efficiency of the EV.

4.3.1 Voltage vs SOC

In Figure 4.6 are illustrated the polarization curves during the discharge of the cell used to compose the battery pack of the Nissan Leaf 2011 Edition. The plots express the voltage over the discharge capacity. In Figure 4.6 there are 4 plots, sorted by different currents. 90 A, 60 A, 1 C and 1/3 C. In Table 4.5 is made the conversion between C-rate and current levels, for the cell.

Table 4.5 Conversion between C-rate and current for the cell used in the pack of the Nissan Leaf 2011 Edition.

C-rate (C)	Current (A)
1/3 C	11 A
1 C	33 A
1.82 C	60 A
2.73 C	90 A

Figure 4.6 is very important because it shows the behaviour of the voltage of the cell, used for the implementation of the Nissan Leaf 2011 Edition when different discharging currents are applied. The same trends can be found in the plots of the voltage of the entire battery pack, these trends give an understanding of how the voltage profile changes with the different operating conditions (discharging current, SOC, and discharge capacity).

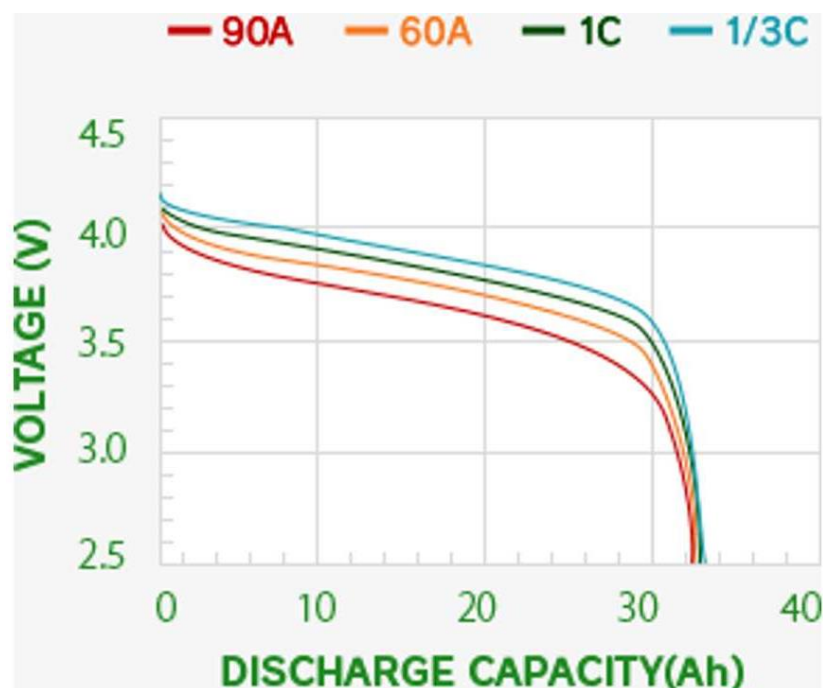


Figure 4.6 Nissan Leaf 2011 Edition cell's polarization curve Vgl. AESC Corp (Specifications Nissan Leaf 2011 Edition) 2011⁶².

The red plot, corresponding to a discharge current of 90 A, has the lowest values for what concerns the voltage, this occurs because the cells are reacting to the severe stress, almost 3 C current, by decreasing the voltage. The second lowest curve is obtained with a discharging current of 60 A. The highest curve is the one obtained with the least discharging current, 1/3 C. It can be assessed that the polarization curve has lower values when the current is higher. Of course, has shown in Figure 4.6 this phenomenon affects the curve in the range from 90% to 15% SOC. The initial voltage level of the discharge does not vary very much with the increase of the discharging current, nor does the ending point (set at 2.5 V). However, some differences can be appreciated if the discharging currents are very different (for example 3 A and 120 A).

⁶² Vgl. AESC Corp (Specifications Nissan Leaf 2011 Edition) 2011.

5 Testing procedure

In this chapter are presented how and with what instruments the testing protocol has been developed. First, the is presented the testing equipment in section 5.1. Then, in the following sections are presented the different tests that have been performed during the introductory tests. Indeed, in section 5.2 is analyzed the relaxation process that occurs when the battery changes state (from either charging or discharging). Then, in section 5.3 are presented the pulse tests, how they are performed and how they are implemented in the testing.

Section 5.4 describes the procedure to determine the self-discharge according to the potentiostatic method presented in section 3.3.1. The last test evaluated is the capacity test, which is presented in section 5.5. The last section of this chapter is section 5.6, where it is presented the final testing protocol based on the tests presented in the previous sections of this chapter. This procedure has been used to test all the modules of the three battery packs object of the study.

5.1 Testing equipment

In order to determine the State of Health (SOH) of the modules different evaluations of the parameters listed and described in Chapter 3 have to be made. To do so several tests have been conducted on the modules object of the project. All the tests have been performed using the Digatron BNT 50-100-6 BDBT.

At first, some introductory tests have been performed on a module, to determine the correct final testing procedure. In particular, the introductory tests gave an idea of the total average amount of time, the possible issues and how to perform the correct measurements during the tests.

Table 5.1 Digatron BNT 50-100-6BDBT specifications.

Digatron BNT 50-100-6 BDBT	
Number of channels	6
Maximum current per channel	± 50 A
Minimum current per channel	± 0.050 A
Maximum voltage	± 100 V
Minimum voltage	± 5 V
Maximum No. of channels in parallel	6

In addition to the time required for the testing, these pre-tests enabled us to understand the behaviour of the modules, and of the Digatron, under different circumstances. The maximum value for the current available for the testing is obtained by connecting in parallel all the 6

channels of the Digatron, but with this procedure, the number of modules tested per day would be very limited.

In the following sections (5.3, 5.4 and 5.5) are listed the different tests performed in order to develop the final testing procedure. All the tests have been first conducted separately for 5 times and then, ascertained the accuracy of each of them they are put together according to the final testing procedure presented in 5.6. All the introductory tests that have been performed were applied to a module of the Nissan Leaf 2011 Edition.

Of course, since all the introductory tests have been performed on a module coming from the first battery pack disassembled, some of the results might be slightly different. This is due to the fact that the three battery packs at disposal have been used in different conditions. Indeed, for the modules of the other two battery packs, some parameters could be different. This solution has been chosen to speed up the testing process since the time for the testing procedures was limited. Indeed, it has been decided to privilege the increase in the number of modules tested, to have a better overview of all the ongoing processes.

5.2 Relaxation

As reported in Chapter 5.2, the relaxation process has to be taken into account, because it could affect the results of the tests very much. If the relaxation of the Li-Ion cells is not considered the voltage levels used for the tests can be different from the one previously set. Indeed, the relaxation process is the phenomenon for which after the battery is being charged the voltage suddenly drops. At the same time, right after the battery is being discharged the voltage suddenly rises. The evaluation of the relaxation behaviour of the Li-Ion battery has to be done very carefully during the introductory tests.

Since the relaxation influences the voltage levels the first thing to do is to determine how much it is and how it could be taken into account. For these reasons, the first steps of the introductory tests have been to consider the effect of the relaxation on the voltage profile of the modules of the Nissan Leaf 2011 Edition. Since these tests have been performed at the beginning of the project the phenomenon has been evaluated at various SOC steps, to have a whole picture of its behaviour.

The evaluation has been made based on different trials, as explained in Table 5.2

. The table shows all the voltage levels at which the relaxation tests have been performed. The test has been run three times for each voltage level, as shown the test was run with a resolution of 5% on the SOC level. Then, the results of the tests have been compared and the average of the voltage drop has been recorded and the data have been stored. Then, prior to the implementation in the final testing protocol, the results have been applied to all of the SOC levels. With this method, the results of the pulse tests, self-discharge, and capacity test are more reliable and could be compared. The relaxation has been fully tested only in the charging way because the tests that are implemented in the final testing protocol are performed while the battery is under a charging process.

The correspondence between the voltage values and the SOC levels was taken from the polarization curve of the cell, reported in Figure 4.6.

Table 5.2 List of the SOC levels at which the relaxation phenomenon has been tested during the introductory tests.

SOC level	Voltage level (V)
0%	5.40 V
5%	6.36 V
10%	7.03 V
15%	7.20 V
20%	7.37 V
25%	7.41 V
30%	7.46 V
35%	7.51 V
40%	7.57 V
45%	7.62 V
50%	7.67 V
55%	7.72 V
60%	7.78 V
65%	7.82 V
70%	7.86 V
75%	7.90 V
80%	7.96 V
85%	8.00 V
90%	8.06 V
95%	8.10 V
100%	8.30 V

As stated above, all the voltage levels from 5% to 100%, with a resolution of 5% have been tested 3 times for the relaxation phenomenon. The test consisted of charging the modules to the established SOC level using 0.5 C. When the level is reached the charging process stops, and it begins an idle phase, during this phase, the battery is neither charged nor discharged. This state is kept for a minute, during this period of time the battery experiences a transient state during which the relaxation process takes place.

As shown in Table 5.3 the values of the voltage drop due to the relaxation process, are quite close to each other, especially in the range from 30% to 90% the values are always constant.

Table 5.3 Results of the trials of the introductory tests for the relaxation processes.

SOC level	Voltage after the relaxation (60 seconds)		
	Trail #1	Trail #2	Trail #3
0% (5.40 V)	5.36 V	5.36 V	5.35 V
5% (6.36 V)	6.30 V	6.30 V	6.30 V
10% (7.03 V)	6.97 V	6.97 V	6.97 V
15% (7.20 V)	7.14 V	7.14 V	7.13 V
20% (7.37 V)	7.31 V	7.31 V	7.31 V
25% (7.41 V)	7.35 V	7.35 V	7.35 V
30% (7.46 V)	7.41 V	7.41 V	7.41 V
35% (7.51 V)	7.46 V	7.46 V	7.46 V
40% (7.57 V)	7.51 V	7.51 V	7.51 V
45% (7.62 V)	7.56 V	7.56 V	7.56 V
50% (7.67 V)	7.61 V	7.61 V	7.61 V
55% (7.72 V)	7.66 V	7.66 V	7.66 V
60% (7.78 V)	7.71 V	7.71 V	7.71 V
65% (7.82 V)	7.75 V	7.75 V	7.75 V
70% (7.86 V)	7.80 V	7.80 V	7.80 V
75% (7.90 V)	7.84 V	7.84 V	7.84 V
80% (7.96 V)	7.90 V	7.90 V	7.90 V
85% (8.00 V)	7.94 V	7.94 V	7.94 V
90% (8.06 V)	8.00 V	8.00 V	8.00 V
95% (8.10 V)	8.04 V	8.03 V	8.04 V
100% (8.30 V)	8.23 V	8.23 V	8.22 V

In all the tests performed the voltage drops that occurred due to the relaxation are smaller than 1% of the voltage level, as shown in the equation (5.1).

$$\Delta V_R = \frac{V_L - V_R}{V_L} \quad (5.1)$$

ΔV_R	Voltage drop due to the relaxation (V)
V_L	Voltage level prior to the relaxation (V)
V_R	Voltage level after the relaxation (60 seconds) (V)

Some examples of the calculation of the voltage drop ΔV_R is shown in the equations (5.2), (5.3), and (5.4), where the voltage drops occurring at 20%, 50% and 90% are measured.

$$\Delta V_R = \frac{7.37 - 7.31}{7.37} = \frac{0.06}{7.37} = 0.841 \% \quad (5.2)$$

$$\Delta V_R = \frac{7.67 - 7.61}{7.67} = \frac{0.06}{7.67} = 0.782 \% \quad (5.3)$$

$$\Delta V_R = \frac{8.06 - 8.00}{8.06} = \frac{0.06}{8.06} = 0.744 \% \quad (5.4)$$

As can be seen from the equations (5.2), (5.3), and (5.4) and from Table 5.3, the relaxation process is responsible for a quite small voltage drop (always below 1%). However, this decrease in the voltage level could deeply affect the results of the tests, especially the ones that are more sensitive to voltage fluctuations (pulse tests).

Given the results of the introductory tests performed to evaluate the relaxation it has been decided to increase the voltage levels for the tests. Indeed, when a test has to be performed at a certain level the module will be charged to a higher voltage level. Then there will be an idle phase, during which the relaxation process will take place, setting the voltage to the right voltage level.

After these first tests, it has been decided to run another set of trials to confirm the reliability of the results obtained with the introductory tests for the relaxation. Therefore, as shown in Table 5.4, a new set of tests was run to assess the right voltage levels for the final testing protocol. In the table are shown, in the second column, the voltage levels at which the modules are charged prior to the relaxation. Then, after the relaxation has taken place, the voltage levels are at the right value, and the next test can be performed. These tests took place only for the eight SOC levels object of the pulse tests, due to the time limitations.

Table 5.4 Voltage levels prior to and after the relaxation for the SOC levels object of the pulse tests.

SOC	Voltage prior relaxation	Voltage after relax. (60 sec)
5%	5.46 V	5.40 V
10%	7.10 V	7.03 V
20%	7.43 V	7.37 V
35%	7.51 V	7.51 V
50%	7.73 V	7.67 V
65%	7.88 V	7.82 V
80%	7.92 V	7.86 V
95%	8.16 V	8.10 V
100%	8.37 V	8.30 V

For instance, when the pulse test is applied to the 50% the module will be charged, using a CC phase with 1 C, to 7.73 V. Then, there is an idling phase, with a duration of 60 seconds, where the relaxation state takes place. At the end of this phase the voltage is at the correct level and the next test can be performed correctly.

5.3 Pulse tests

As stated in Chapter 3 (State of the art) the behaviour and the characteristics of the Li-Ion cells can be simulated using an EEC Vgl. Stroe et al. (Lithium-Ion Battery Dynamic Model for Wide Range of Operating Conditions) 2017⁶³ and Vgl. Farinet et al. (Battery Lifetime Analysis for Residential PV-Battery System used to Optimize the Self Consumption - A Danish Scenario) 2019⁶⁴. To extract the equivalent electrical parameters (resistances and capacitances) of the EEC a current pulse must be applied to the Li-Ion cell.

The transient state that occurs after the pulse provides the information to extract the electrical parameters. As shown in Chapter 3 (State of the art) the value of those parameters varies with the C-rate used for the current pulse and with the SOC at which the current pulse is applied. For these reasons the pulse tests have conducted different SOC's and with different C-rates, in accordance with what it has been presented in Vgl. Böttiger et al. (Systematic experimental

⁶³ Vgl. Stroe et al. (Lithium-Ion Battery Dynamic Model for Wide Range of Operating Conditions) 2017.

⁶⁴ Vgl. Farinet et al. (Battery Lifetime Analysis for Residential PV-Battery System used to Optimize the Self Consumption - A Danish Scenario) 2019

pulse test investigation for parameter identification of an equivalent based lithium-ion battery model) 2017⁶⁵.

The parameters of the pulse tests are listed in Table 5.5. As can 3 C-rates have been evaluated. For what concerns the SOC levels 8 stages have been considered. At first, the SOC levels were 7, with a resolution of 15%, starting from 5% and reaching 95% (5%, 20% 35%, 50%, 65%, 80%, 95%).

As stated in section 5.1 the equipment used for the testing of the modules has some limitations. Indeed, the limitations are mainly due to the current limits, because the current that corresponds to 1 C of the modules is equal to 66 A. The Digatron is equipped with 6 channels, each one with a limit of 50 A, that can be connected in parallel to increase the current rate. To perform a test

Since there was a large number of modules to test (144) and the testing procedure had to be chosen accordingly, to test all the modules properly.

To test that the voltage limits of the battery were not exceeded at all the SOC levels have been applied to the current pulses object of the test. During the preliminary testing the pulse test at 5% the voltage limit where trespassed, with C-rates greater than 0.5 C. For this reason, at 5% the current pulse applied is only one, 0.5 C. To have the electrical parameters of the EEC at low SOC levels, after some tests it has been decided to apply the pulse test at 10%.

In this way, the total number of trials for the pulse test is 22, which gives a good amount of data about the parameters of the EEC.

Table 5.5 List of the testing cases used to extract the parameters for the EEC using the pulse tests.

Test cases performed for the pulse tests			
	C-rate		
	0.5 C	1 C	1.5 C
SOC %	5%	-	-
	10%	10%	10%
	20%	20%	20%
	35%	35%	35%
	50%	50%	50%
	65%	65%	65%
	80%	80%	80%
	95%	95%	95%

⁶⁵ Vgl. Böttiger et al. (Systematic experimental pulse test investigation for parameter identification of an equivalent based lithium-ion battery model) 2017.

Table 5.6 Conversion of the SOC levels, percentages, to voltage levels (V).

SOC level (%)	Voltage level (V)
0%	5.40 V
5%	6.36 V
10%	7.03 V
20%	7.37 V
35%	7.51 V
50%	7.67 V
65%	7.82 V
80%	7.96 V
95%	8.10 V
100%	8.30 V

In Table 5.6 is shown the conversion between the physical voltage levels and the percentage levels used for the SOC. The levels shown are the ones used for the evaluation of the pulse tests. This conversion is needed because the voltage profile of the module of the Nissan Leaf 2011 Edition, and of every Li-Ion battery, is not linear, therefore a conversion between the voltage and the SOC percentages is necessary.

In Figure 5.1 are shown the profiles of the voltage during the pulse test on the module of the Nissan Leaf 2011 Edition. The trials have been performed using three different C-rates (0.5 C, 1 C, and 1.5 C). As stated in the previous chapters, when the current pulse is applied the voltage of the module drops. As shown, the voltage drop increases with the increase of the C-rate. In the figure there is a comparison between three C-rates, the pulses have been applied at 20% SOC (7.37 V). This increase in the drop is more relevant at the beginning of the pulse, then the behaviour of the voltage is quite similar. Indeed, when the current pulse applied is greater, the voltage drop is higher, the relationship between the voltage drop and the current pulse is inverse. The three curves, blue 0.5 C, red 1 C, and yellow 1.5 C show the behaviour of the voltage during the 20 seconds in which the current pulse is applied. When the current pulse stops, the battery is in idling mode (neither charging nor discharging), and the voltage rapidly rises.

Table 5.7 Conversion from the parameters of the battery to the physical ones.

Battery's parameters	Physical parameters
0.5 C	33 A
1 C	66 A
1.5 C	99 A
20%	7.37 V
95%	8.1 V

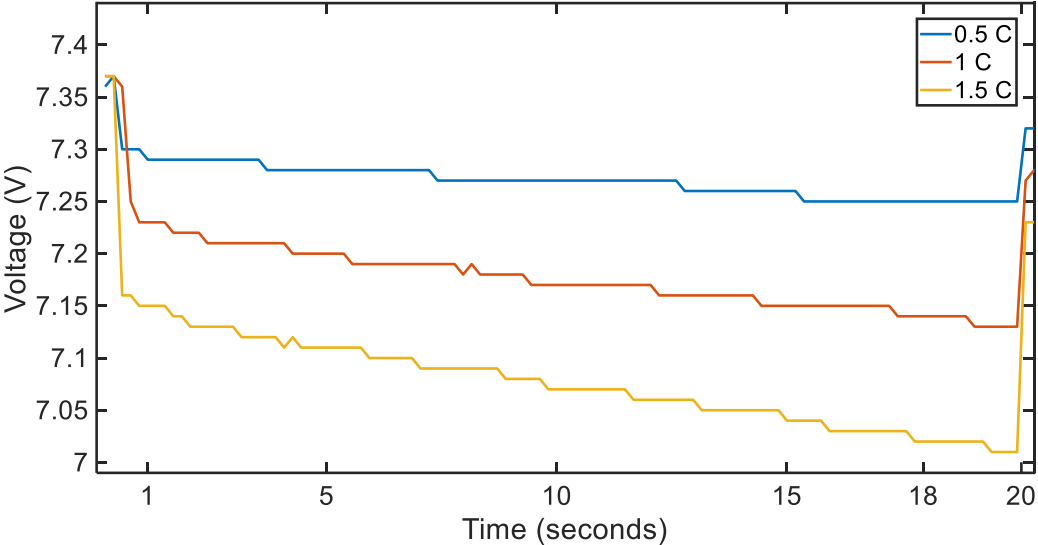


Figure 5.1 Voltage during the pulse tests at 20% SOC.

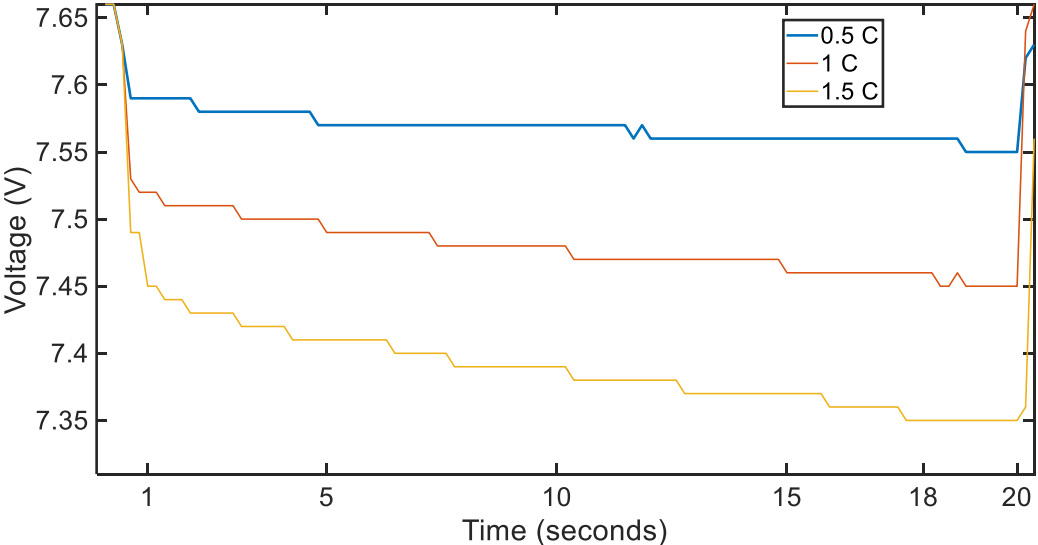


Figure 5.2 Voltage during the pulse tests at 50% SOC.

The magnitude of the voltage drop during the test depends on the magnitude of the C-rate, but it is also highly influenced by the SOC percentage. The voltage drops shown in Figure 5.2 are from pulse tests performed at 50% SOC, while the performed at 95% SOC are shown in Figure 5.3. As well as for Figure 5.1, in Figure 5.2, and in Figure 5.3 there are comparisons of the voltage drops between three C-rates used for the testing.

The same pattern of the voltage found in Figure 5.1, can be seen in Figure 5.2, and in Figure 5.3. The magnitudes of the voltage drop that occur at 50% and 95% SOC are similar with the ones that occur at 20% SOC. Hence, the voltage drop that occurs at 20%, with 1.5 C is of 0.21 V, while at 95%, keeping constant the C-rate, is of 0.19 V.

In Table 5.8, Table 5.9 Table 5.10, are shown the comparison of the voltage drops with respect to the C-rate. To have a better understanding of the tests and of the results of them, in Table 5.7 is presented the conversion between the parameters of the battery (C-rates and SOC) and the physical ones (currents and voltages).

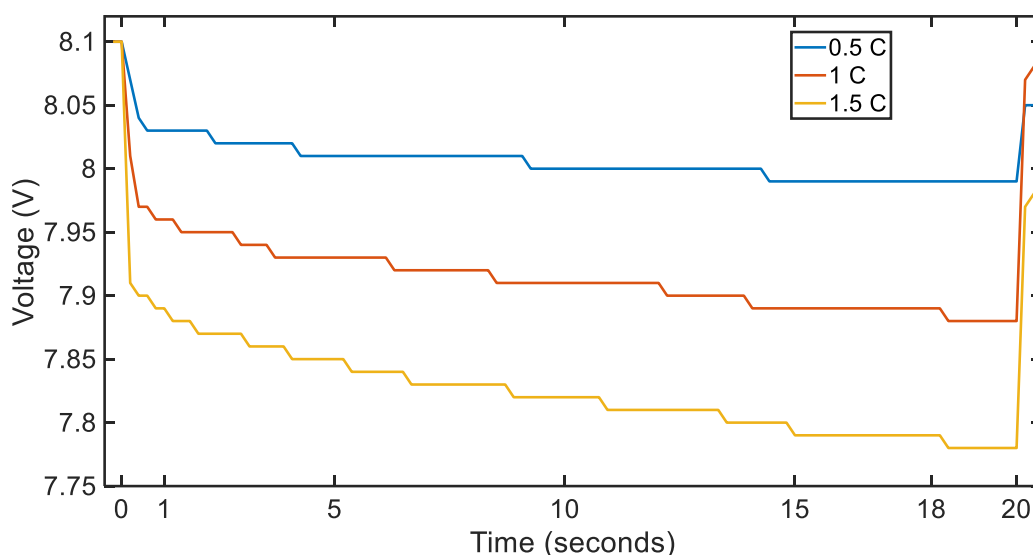


Figure 5.3 Voltage during the pulse tests at 95% SOC.

Table 5.8 Comparison between the voltage drops at that occur 20%, 50%, and at 95% with 0.5 C current pulse.

Current pulse of 0.5 C (33 A)			
	20% SOC	50% SOC	95% SOC
Voltage drop after 1 s	0.07 V	0.08 V	0.07 V
Voltage drop after 10 s	0.10 V	0.10 V	0.09 V
Voltage drop after 18 s	0.12 V	0.12 V	0.11 V

Table 5.9 Comparison between the voltage drops that occur at 20%, 50%, and at 95% with 1 C current pulse.

Current pulse of 1 C (66 A)			
	20% SOC	50% SOC	95% SOC
Voltage drop after 1 s	0.14 V	0.14 V	0.13 V
Voltage drop after 10 s	0.20 V	0.20 V	0.18 V
Voltage drop after 18 s	0.24 V	0.22 V	0.22 V

Table 5.10 Comparison between the voltage drops that occur at 20%, 50%, and at 95% with 1.5 C current pulse.

Current pulse of 1.5 C (99 A)			
	20% SOC	50% SOC	95% SOC
Voltage drop after 1 s	0.21 V	0.18 V	0.19 V
Voltage drop after 10 s	0.30 V	0.28 V	0.28 V
Voltage drop after 18 s	0.36 V	0.32 V	0.32 V

The values presented in the tables above are an example of the pulse tests performed at different SOC levels. As can be seen from Table 5.8, Table 5.9 and Table 5.10 the voltage drops that occur when the pulses are applied are dependent on the C-rate used. The higher is the C-rate the higher the voltage drop will be. Indeed, keeping constant the SOC level, 95% for example, the voltage drop after 10 seconds with 0.5 C is 0.09 V, with 1 C is 0.18 V and with 1.5 C is 0.28 V. The increase in the voltage drop between the pulse with 0.5 C, and the one that occurs with 1.5 C is over 300% (from 0.09 V to 0.28 V). As shown the increment in the voltage drop is not linear. Indeed, it depends on the C-rate used. As stated previously, and how the Figure 5.4 shows, the voltage profile does not have a linear relationship with the percentage of the SOC. The voltage profile presented in the figure has been measured while the module of the Nissan Leaf 2011 Edition (66 Ah) was being charged using a C-rate of 1 C (66 A).

This behaviour has a great impact on the voltage drops because depending on the voltage level at which the current pulse is applied the voltage drop could be very different. Of course, the increase in the voltage drop is compensated by the increase of the current, therefore the extraction of the parameters presented in Parametrization of the battery 3.2 is still valid and reliable Vgl. Hu et al. (Model-Based Dynamic Power Assessment of Lithium-Ion Batteries Considering Different Operating Conditions) 2014⁶⁶.

⁶⁶ Vgl. Hu et al. (Model-Based Dynamic Power Assessment of Lithium-Ion Batteries Considering Different Operating Conditions) 2014.

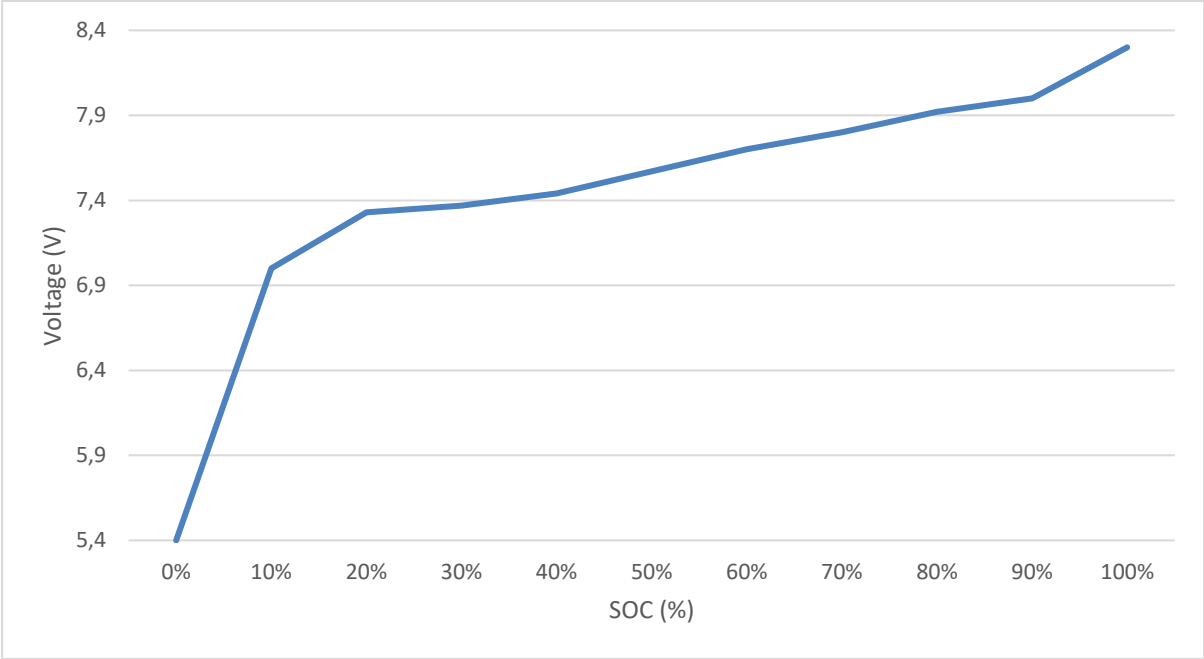


Figure 5.4 Polarization curve, during the charging process, of the module from the battery pack of the Nissan Leaf 2011 Edition (1 C).

Figure 5.5 shows the two polarization curves obtained using a charge state (blue curve) and a discharging state (red curve). As can be seen, there are some minor differences in the two curves, but it can be stated that the trends are quite similar (of course, considering that one is decreasing and the other one is increasing at the increase of the SOC level. The curves have been recorded using 1 C (66 A) in both cases, and they correspond to a module with 89.514% SOH, coming from the first battery pack.

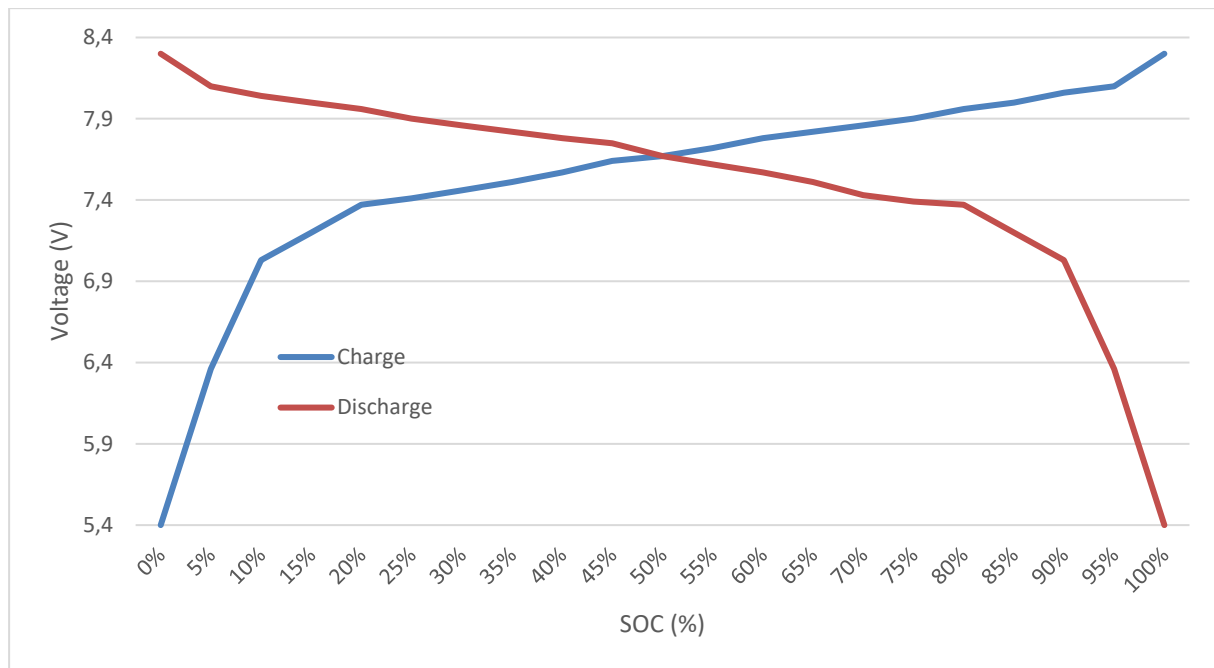


Figure 5.5 Polarization curve, during the charging and discharging processes, of the module from the battery pack of the Nissan Leaf 2011 Edition (1 C).

5.4 Self-discharge

During the first introductory tests different self-discharge tests have been performed. This procedure has been done to determine the best way to test the self-discharge phenomenon. With the evaluation of the results of those tests it was possible to develop the best solution to implement in the final testing protocol to be used on the modules of the three battery packs. Therefore, to design the final test, for the self-discharge part, four different ones have been tested.

All of these four tests are based on the method used to evaluate the self-discharge which has been previously described in the subsection 3.3.1 (Potentiostatic method). The performed tests have the same core procedure, but they are different for what concerns the duration.

To measure the Self-discharge the module is connected to the Digatron BNT 50-100-6 BDBT. When the voltage of the module starts to vary from the established level, the charging process begins, furnishing sufficient current to bring the module to the established voltage and therefore SOC. This voltage level is set to 8.3 V, which corresponds to 100% SOC.

This procedure has been repeated using 4 different periods of time, as reported in Table 5.11. As stated above four different durations have been tested, each with different trials, to evaluate the differences between them. The tests have four different durations, with 15 minutes steps: 15 minutes, 30 minutes, 45 minutes and 60 minutes. All of the durations of the tests have been performed on the same module (with one-hour interval between each trial) for 5 times per duration.

Table 5.11 Test performed to determine the best self-discharge test to be implemented in the final testing protocol.

Length of the introductory self-discharge tests	
Duration	Trials
15 minutes	5
30 minutes	5
45 minutes	5
60 minutes	5

Since the self-discharge has been evaluated with four different durations (15, 30, 45 and 60 minutes) for five times each, the total number of trials of the self-discharge test during the introductory test was 20.

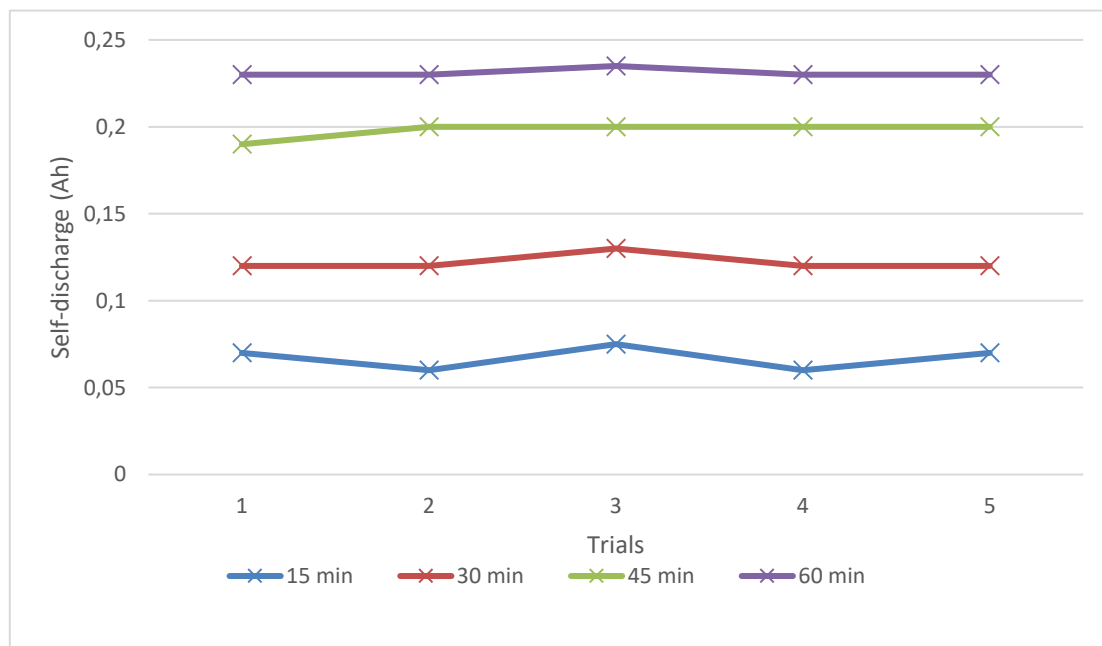


Figure 5.6 Graph of the results of the introductory tests for the self-discharge.

In Figure 5.6 are shown the results of the introductory tests performed to determine the duration of the self-discharge test. As can be seen from the plots, with the increase of the duration of the test the values of self-discharge are more similar to each other. The test with the duration of 15 mins has a fluctuation in the values of self-discharge (measured in Ah). On the other hand, the values of self-discharge measured in the test with the duration of 60 mins, are constant, with the exception of one small deviation.

All the trials have been performed at 100% SOC and on the same module (a module used for the introductory tests) with this setup it is possible to compare the results of the self-discharge

rates. After the trials with different durations it was decided to include in the final testing protocol the test with the duration of 30 minutes. The chosen test is performed with the battery at 100 % SOC for a period of 30 minutes.

This period, 30 minutes, has been chosen as a trade-off between the duration of the test and the accuracy of the procedure. Indeed, with this length of the test, the total duration final testing protocol does not increase very much, enabling the team to test more modules in the same amount of time. In addition, the introductory test performed with the duration of 30 minutes have showed a good reliability of the results, compared to the ones obtained with 45- and 60-minutes duration.

5.5 Available capacity

As explained in the previous sections with the aging and the usage of the battery the value of this parameter decreases. The amount of degradation that occurs depends on different factors, as stated in section Capacity 3.4. To determine the degradation of the battery and the capacity fade, it is necessary to evaluate actual State of Health (SOH) of the modules of the battery packs a capacity test has been performed.

As stated in the previous chapters the available capacity can be assessed by measuring the Ah that occur to either charge or discharge a battery from 0% to 100% or vice versa. For what concerns the tests performed in this research the available capacity is determined by using a discharge process.

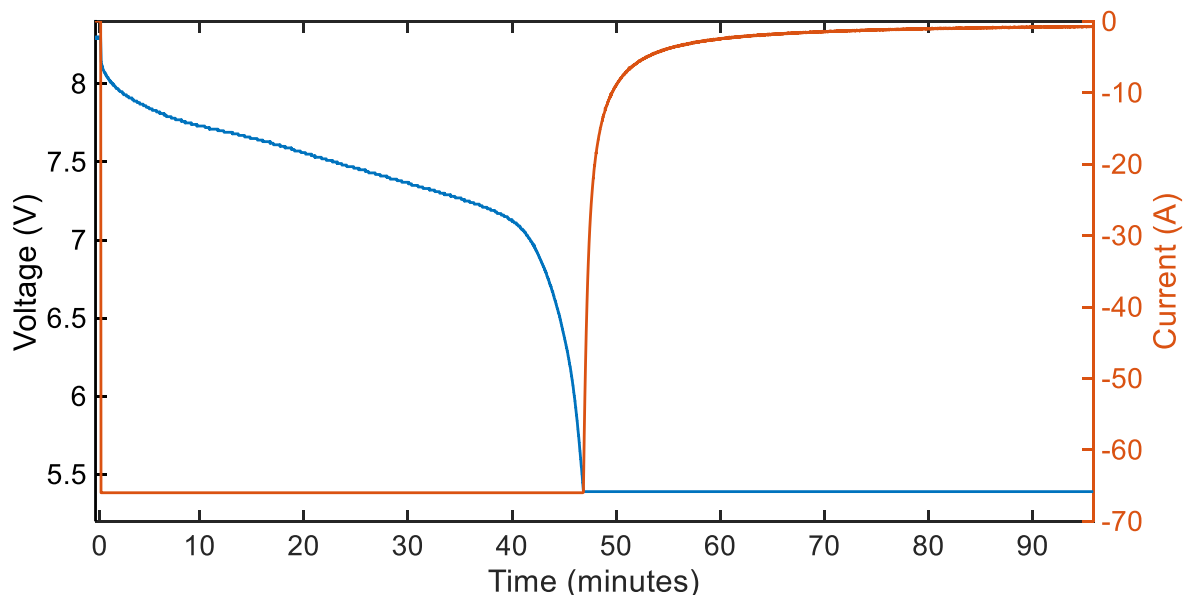


Figure 5.7 Voltage and Current profiles during the capacity test.

In Figure 5.7 are reported the plots of the profiles of the voltage and the current during the capacity test, performed on a module of the first battery pack. The curve is obtained by using the data collected during the discharging, from 100% to 0%. The discharge process has been performed using a Constant Current (CC) phase, using 1 C, which corresponds to 66 A.

When the voltage reaches the value set for the discharging, 0% SOC (5.4 V), the CC phase stops. Then, the test continues with a Constant Voltage (CV) phase, 5.4 V, at the same time the discharge continues with the reduction of the current from 66 A to 0.01 C (0.66 A). This phase is performed to fully discharge battery. These two phases, Constant Current and Constant Voltage (CC-CV), are used to determine the available capacity.

Therefore, the first step of the procedure is to charge the module to 100 % SOC (8.3 V) using a current equal to 33 A (0.5 C). When the voltage level is reached there is a pause of one minute that takes into account the relaxation, as it has been done with the Pulse Tests in section 5.3. After the pause the CC discharge part starts, the module is discharged using CC of 1 C (66 A) until the SOC reaches 0% (5.4 V). When the voltage is equal to 5.4 V the CC discharge stops and the CV part of the test starts. As shown in the graph at first the value of the current decreases rapidly (going from 66 A to 10 A in less than 4 minutes) and then the decreasing process slows down. The CV part of the test ends when the value of the current reaches 0.01 C (1 % of 1 C), which corresponds to 0.66 A.

Summarizing the capacity test that has been implemented in the final testing protocol has the following steps:

- Charge to 100% (8.3 V) using 0.5 C;
- Idle mode for 60 seconds, to take into account the relaxation process;
- CC discharge with 1 C to 0% (5.4 V);
- CV discharge to 5.4 V, reducing the current from 66 A to 0.66 A;
- Measure of the Ah used to fully discharge the battery.

The final value of the CV discharge phase, 0.66 A, has been chosen according to the papers Vgl. Braco et al. (Characterization and capacity dispersion of lithium-ion second-life batteries from electric vehicles) 11/06/2019 - 14/06/2019⁶⁷ and to the introductory tests previously performed. When, during the CV discharge state, the current reaches this value the battery can be considered fully discharged. Thus, the available capacity measurement can be assessed.

5.6 Final testing protocol

From the information and the data collected during the introductory tests it has been possible to develop a final testing procedure. This procedure is composed by the three tests reported in sections (5.3, 5.4 and 5.5). In all the tests included in the final protocol it has been taken into account the relaxation process presented in section 5.2.

⁶⁷ Vgl. Braco et al. (Characterization and capacity dispersion of lithium-ion second-life batteries from electric vehicles) 11/06/2019 - 14/06/2019.

The final testing protocol has an average duration of 8 hours (depending on the initial SOC of the module and on the degradation of the modules). This protocol enables to obtain the following data:

- The 5 electrical parameters (R_0 , R_1 , R_2 , C_1 and C_2) of the EEC of the module at 8 different SOC (5 %, 10 %, 20 %, 35 %, 50 %, 65 %, 80 %, 95 %) and with 3 different C-rates (0.5 C, 1 C and 1.5 C);
- The self-discharge that occurs at 100 % over 30 minutes;
- The actual available capacity of the module.

Along with the data listed above these tests provide large datasets that could be used to create statistics on the relationship between the different parameters. This analysis is made in chapter 6, along with other considerations.

In the Figure 5.9 is shown the setup of the three modules during the testing. To reach the current level designed for the test (1.5 C, 99 A) the modules have been connected to two channels of the Digatron. In addition to the power cables (red for “+” and blue for “-”) two sensors have been connected to the “+” and “-” ends of the module.

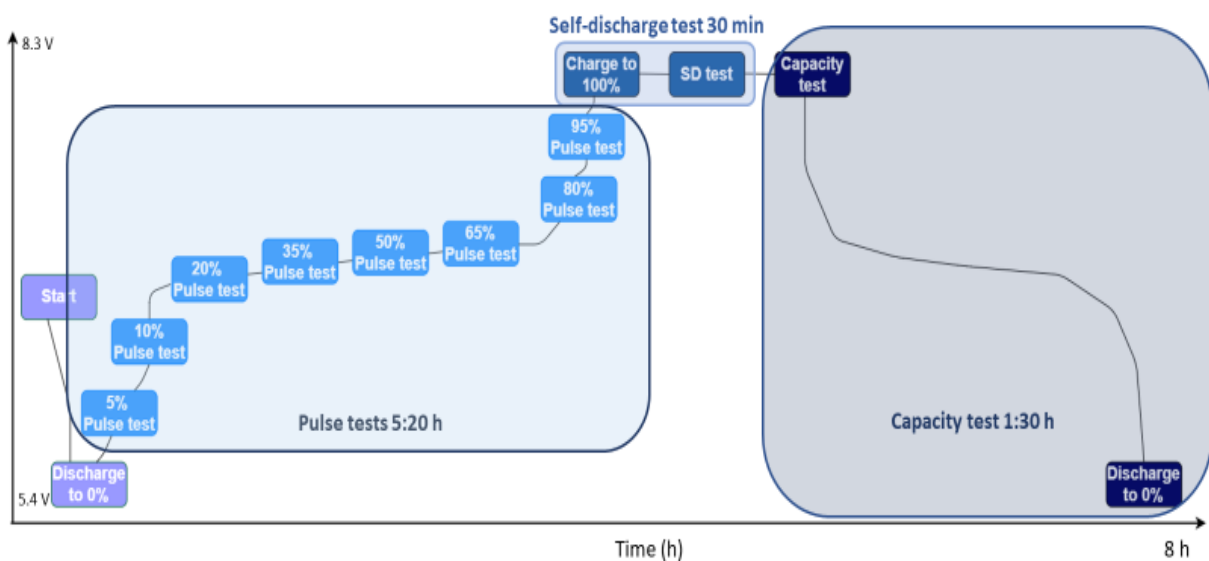


Figure 5.8 Division of the phases that form the final testing protocol used for all the testing of the modules .

As can be seen from Figure 5.8 the final testing protocol is divided in four different phases. The first phase is the discharge of the module from its starting SOC to 0% (5.4 V), this is performed using a current of 1 C. Its duration depends on the starting SOC, but usually it is around 30-40 minutes. Then, after a pause of 5 minutes, there is the second phase, the pulse tests. As shown the tests are performed at different SOC levels (8 different levels). The steps between one level and another are of 15%, with the only exception of 10%, which replaces the measurements at 5% (for 1 C and 1.5 C). For each step of the pulse test are used 3 C-rates (0.5 C, 1 C, and 1.5 C). As stated previously, the C-rate used to charge the module from step

to step is 1 C (66 A). Depending on the SOH of the module the duration of this step can be different, usually in around 5:20 hours.

The third phase of the protocol is the self-discharge test. From the last step of the pulse tests (95%) the battery is charged, using 1 C, up to (100%), using a CC-CV (Constant Current-Constant Voltage) charge. Then, after a pause of 1 minute starts the self-discharge test. The duration of this part is fixed, and it is of 30 minutes. After the self-discharge test, there is a pause of 5 minutes.

Then as shown in the right section of Figure 5.8 there is the last phase of the protocol, the capacity test. This test is performed using a discharge current of 1 C (66 A) and the SOC goes from 100 (8.3 V) to 0% (5.4 V). As occurred for the charge to 100% the discharge is performed using a CC-CV, therefore the current is kept constant until the voltage reaches 5.4 V, then the voltage is kept constant at 5.4 V and the current is reduced from 1 C to 0.01 C (0.66 A). The duration of this phase depends on the SOH of the modules, when the higher is the SOH the longer the test will be. On average the duration of the discharge is of 1 hour and 30 minutes.



Figure 5.9 Three Nissan Leaf 2011 Edition (24 kWh) modules during the testing.

The modules shown in Figure 5.9 are placed in the oven, especially designed for the testing of batteries, which is electrically insulated from the external equipment. It can be noticed that

under the modules there is an additional insulation made with a rubber layer, to increase the safety condition during the testing of the modules. Of course, for all the operation of mounting and demounting of the modules in the testing platform, they were used only insulated tools (wrenches, screwdrivers, etc.).

Prior to the mass testing, the final testing protocol has been tested on a dummy module, to ensure the safety and the reliability of the procedures. The protocol has been run on all the modules that compose the three battery packs object of the testing.

6 Results and discussion

In this chapter are reported the major findings of the tests that have been performed. The tests that have been conducted are all included in the standard test developed and presented in Chapter 5, which is based on the three single tests (Pulse tests, self-discharge and capacity test) that have been presented in Chapter 3. In the first sections of the chapter are presented the main results of the tests, sorted by packs. Thus, the main results of the testing are first presented divided by packs, then all the data are put together and a further analysis is made. Then, in the second part of the chapter an evaluation of the relationships between the parameters is made. The analysis includes the main parameters of the EEC that have been extracted from the testing.

The data reported in this chapter come from the tests performed over October, November and December 2019.

6.1 Main results

This section of the chapter is divided in three parts, which correspond to the three battery packs object of the testing. The focus is on the available remaining capacity of the modules (SOH), on the self-discharge rate and on some of the parameters of the EEC. Then the results of the three packs are combined together, to have a better overview of the data. The packs, and the subsections, are numbered according to the order of the testing.

6.1.1 Battery pack #1

The first battery pack has been tested over the course of 8 working days, with an average of 6 modules per day (three modules in the morning and three in the afternoon). The average duration of the entire testing procedure was of 8 hours and 12 minutes. As stated in 5.6 Final testing protocol different test have been implemented in the final test protocol. The most important parameter is the capacity left in the modules. In the graphs of this chapter the capacity is called SOH, and it is calculated in percentage of the nominal one (66 Ah).

In Figure 6.1 is shown the Gauss curve of the SOH of the modules from the battery pack #1. As the graph reports the SOH is between 88% and 91%, which is a very small range. The majority of the modules has a SOH in between 89% and 90%. In red is shown the Gauss curve that shows the probability of finding a module with a certain SOH. The distribution of the SOHs has a quite small range, thus giving the idea that the pack has degradation that is homogenous overall. This result is evaluated and analyzed with the use of the other test (Self-discharge test) and the parameters of the EEC. The results presented in Figure 6.1 can be found also in Table 6.1, where the maximum, minimum and average SOH percentages are reported. As shown the average SOH of the modules is 89.357%, which corresponds to 58.98 Ah.

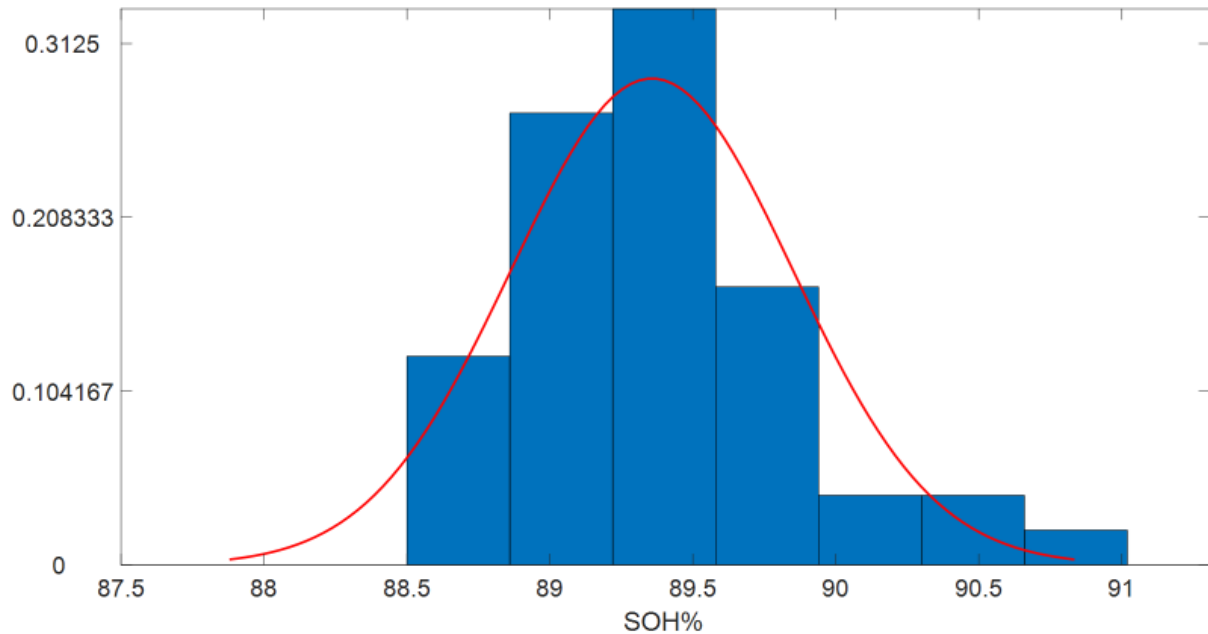


Figure 6.1 Gauss distribution of the SOH of the first battery pack.

In Table 6.1 are reported the main results of the tests performed on the first battery pack. The values are sorted by maximum, minimum and average values. In addition to the values, are reported the module's number which have shown those values. This representation is chosen to give a better understanding of the correlation between the parameters. For what concerns R_0 and R_{tot} the maximum and minimum values are found in the same modules. Indeed, the module number that has the highest R_0 value is M14, 2.2222 m Ω , which is the same module number that has the highest R_{tot} , 2.9293 m Ω . At the same time, the lowest values of R_0 and R_{tot} are found in the same module, M11. These results are due to the fact that, as stated in the first chapters, R_{tot} is the sum of the resistances of the EEC (R_0 , R_1 , and R_2). Thus, this correlation shows that the increase in the value of the resistances occurs for all of them. For what concerns the available remaining capacity and the self-discharge, it can be noticed that the module that has the highest self-discharge is the same that has the lowest SOH (M37). At the same time, the highest SOH and the lowest self-discharge are found in the same module (M35). It can be said that to an increase of R_0 corresponds an increase in the value of R_{tot} . As previously stated in the first chapters.

As stated in the previous sections, the pulse test has been performed at different SOC levels and with different C-rates. The parameters extracted from the tests have therefore 22 different values, depending on the SOC and on the C-rate used for the test. Per every module tested there are 22 values of R_0 and other 22 values for concerns R_{tot} . For these reasons it has been decided to report in the table only two (R_0 and R_{tot}) of the six parameters (R_0 , R_1 , R_2 , C_1 , C_2 and R_{tot}). Since for these two parameters there are different values it was chosen to consider R_0 and R_{tot} at 50% SOC and with a pulse of 1.5 C. The 50% SOC level was chosen because it is half of the capacity of the battery. For what concerns the C-rates it was chosen the highest C-rate available with the testing, to stress the battery the most.

Table 6.1 Main findings first battery pack.

Battery pack #1								
	Cap (Ah/%)		SD Ah (30 m)/h (%)		R ₀ (mΩ)		R _{tot} (mΩ)	
	Max	Min	Max	Min	Max	Min	Max	Min
Mod #	M35	M37	M37	M35	M14	M11	M14	M11
	60.04 Ah	58.46 Ah	0.140	0.100	2.2222	0.5051	2.9293	1.3131
	90.970%	88.576%	0.4242%	0.3030%	-	-	-	-
AVG	58.98 Ah	89.357%	0.124 Ah	0.376%	1.84764		2.61364	

In Figure 6.2 are shown the SOH of the modules of the first battery pack sorted by subpacks. The SOHs have been divided only into three ranges (88-89%, 89-90% and 90-91%), because the percentages of the SOH are similar to each other. From the plots it can be noticed that for all the three subpacks the majority of the modules has a SOH among 89% and 90%. This data is in accordance with the results of the entire pack (average SOH 89.357%). The left subpack, module number from 25 to 36, has the highest average SOH, while the rear subpack has the lowest average SOH. The right subpack, modules from 37 to 48, has an average SOH percentage very close to the average overall SOH. However, the values of the average SOH do not show a particular behaviour in the degradation for what concerns the positioning in the pack. Anyway, this result has to be confirmed with the data of the other two battery packs object of the research.

Table 6.2 Comparison of the available capacity of the subpacks for battery pack #1.

Average available capacity sorted by subpacks BP #1		
Subpack	Average available capacity	Average SOH
Rear	58.853 Ah	89.172%
Left	59.203 Ah	89.701%
Right	58.995 Ah	89.386%
Overall	58.976 Ah	89.357%

These results confirm that the division of the pack into three subpacks does not influence the SOH of the modules. Furthermore, it means that the operating conditions of the modules are the same inside the pack. The homogeneity between the cells, the same operating conditions and a good thermal insulation are key factors for what concerns the degradation of the Li-Ion batteries.

Given the results presented in this subsection, it can be assessed that all the modules from the battery pack #1 have a good remaining useful life (RUL). Indeed, all of them have an available capacity greater than 52.8 Ah (80% SOH). Thus, all of them could be used for remanufacturing of EV battery packs or for other second life uses.

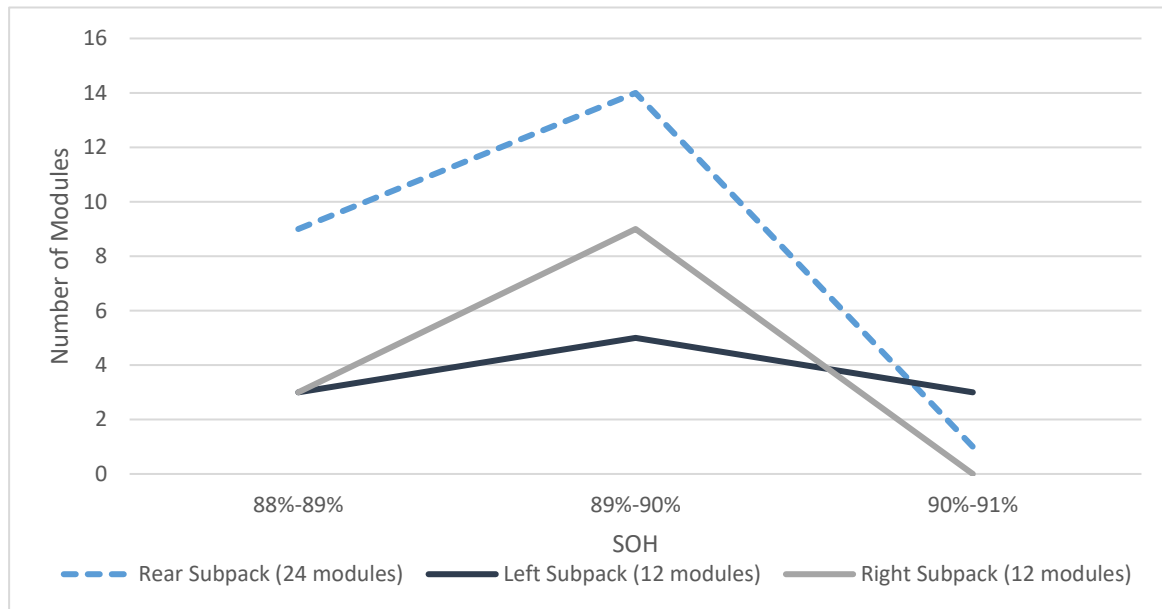


Figure 6.2 Division of the SOH of the modules of the battery pack #1, sorted by subpacks.

6.1.2 Battery pack #2

In this section are evaluated the results of the testing of the second battery pack. As well as for the first pack all the 48 modules have been tested using the protocol described in section 5.6. Since the average SOH percentage of the battery pack is lower than the one of the first battery pack, the average time for the testing was 7 hours and 30 minutes, compared to the 8 hours of the first pack. This is due to the fact that the Ah to charge and to discharge were less and therefore with the current kept constant the time was reduced.

In Figure 6.3 is reported the Gauss distribution of the SOH of the modules of the second battery pack that has been tested. As can be seen the distribution of the SOH of the battery pack #2, is wider with respect to the one of the first battery pack. Indeed, the ranges of the SOH percentages go from 71% to 78%, while the for the first battery the range was 88%-91%. As well as for the ranges also the distribution of the SOH of the modules is different. For the second pack the SOH percentages are more spread among the different levels. For instance, more than 10% of the modules tested have the lowest SOH percentages found (between 71% and 72%).

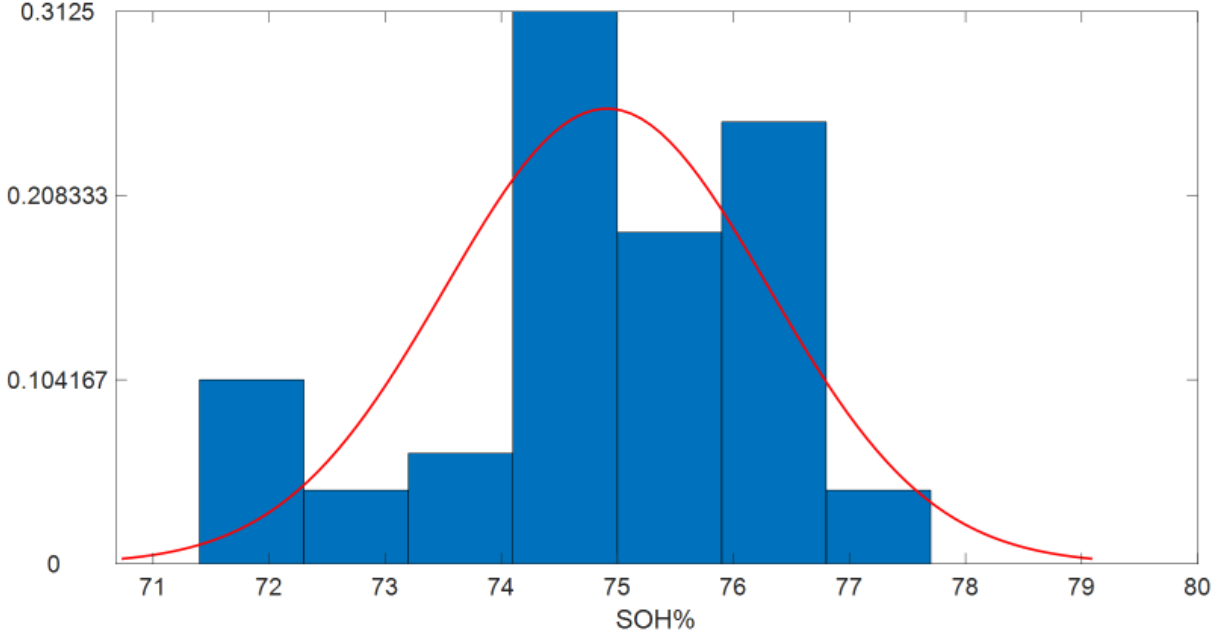


Figure 6.3 Gauss distribution of the SOH of the second battery pack.

The results of Figure 6.3 can be found also in Table 6.3, which gives an overview of the main results and findings of the second battery pack. As well as for the first battery pack, the values of R_0 and R_{tot} are evaluated at 50% SOC and with 1.5 C. The same trends found for the battery pack #1 are found in the results of the second battery pack. Thus, the module which has the highest values of R_0 , 2.8383 mΩ is the same that has the highest R_{tot} 3.7373 mΩ. At the same time, M27 has both the lowest value of R_0 , 2.8383 mΩ, and of R_{tot} , 3.7373 mΩ.

Table 6.3 Main findings second battery pack.

Battery pack #2								
	Cap (Ah/%)		SD Ah (30 m)/h (%)		R_0 (mΩ)		R_{tot} (mΩ)	
	Max	Min	Max	Min	Max	Min	Max	Min
Mod #	M30	M11	M7	M20	M2	M27	M2	M27
	50.87	47.42	0.200	0.160	2.8383	0.7102	3.7373	1.5245
	77.076%	71.848%	0.6061%	0.4848%	-	-	-	-
AVG	49.44 Ah	74.911%	0.179	0.5410%	2.3843		3.2823	

For what concerns the SOH percentage, the highest value is found in module M30, 77.076%, while M11 has the lowest 71.848%. As it has already being stated, the overall SOH percentages of the second battery pack are considerably lower than the ones of the battery pack #1. This means that the degradation processes that have occurred to the pack were greater in comparison with the ones of the first pack. In addition, the higher degradation has created a

wider range in the SOH percentages of the modules. In the first packs the difference between the highest and the lowest SOHs was less than 3%, while for this pack the difference is of 5.228%. In this case, the difference in the available capacity is much greater. This result is due to the fact that with the increase of the usage, and therefore with the increase of the degradation, the resultant decrease in the SOH is not linear and it is not homogeneous among the modules and the cells that form the pack. The average value of the SOH is 74.911, which corresponds to an available remaining capacity of 49.44 Ah.

It is interesting to notice that all the modules coming from the battery pack #2 do not have SOH percentages high enough to be used in remanufacturing. Indeed, all of the SOH values are below the limit set for the EoL for EVs (80% of SOH).

The self-discharge tests have shown an increase in both the values of the self-discharge. Indeed, the maximum SD is 0.20 Ah in 30 minutes, while the minimum value of the SD is 0.16 Ah. It is interesting to noticed that the lowest value of the SD of the BP #2 is greater than the highest one of the BP #1, this is due to the highest difference in the SOH.

Table 6.4 Comparison of the available capacity of the subpacks for battery pack #2.

Average available capacity sorted by subpacks BP #2		
Subpack	Average available capacity	Average SOH
Rear	48.995 Ah	74.234%
Left	50.172 Ah	76.016%
Right	49.604 Ah	75.158%
Overall	49.441 Ah	74.911%

Table 6.4 summarizes the differences in the average available capacity and in the SOHs between the subpacks of the second battery pack. The value of the average SOH for the overall pack is 74.911%, value that can be found also in Figure 6.3. As it was found in the first battery pack the rear subpack has the lowest average SOH, 74.234%. The right subpack has an average SOH, 75.158%, which is very close to the overall one, 74.911%. The highest average value of the SOH comes from the left subpack, 76.016% which corresponds to 50.172 Ah.

As well for the first battery pack the results sorted by subpacks do not present anomalies, the average values of the SOH are close to each other. It is interesting to notice that, as it was for the first battery pack, the highest average SOH was found in the left subpack, the right subpack had the closest to the overall one and the rear subpack had the lowest average SOH. However, the differences between the values are not such to form a statistical theory.

The data reported in Table 6.4 are presented and plotted in Figure 6.4. In order to compare the results, the modules are sorted by subpacks and by SOH range. Since the ranges are seven the SOHs of the modules are spread among them. The findings of the Table 6.4 are reflected in the plots, indeed, the majority of the modules of the left subpack (dark line) are

found in the range 76%-77%. At the same time, the plot of the right subpack (grey line) confirms the fact that its average SOH is close to the average overall SOH (with 5 modules, out of 12, in the range 74%-75%). The plot that represents the rear subpack (dashed line) has two peaks, one in the range 72%-73% and one in 74%-75%. This situation brings this subpack to have the lowest average SOH among the three subpacks of the second battery pack.

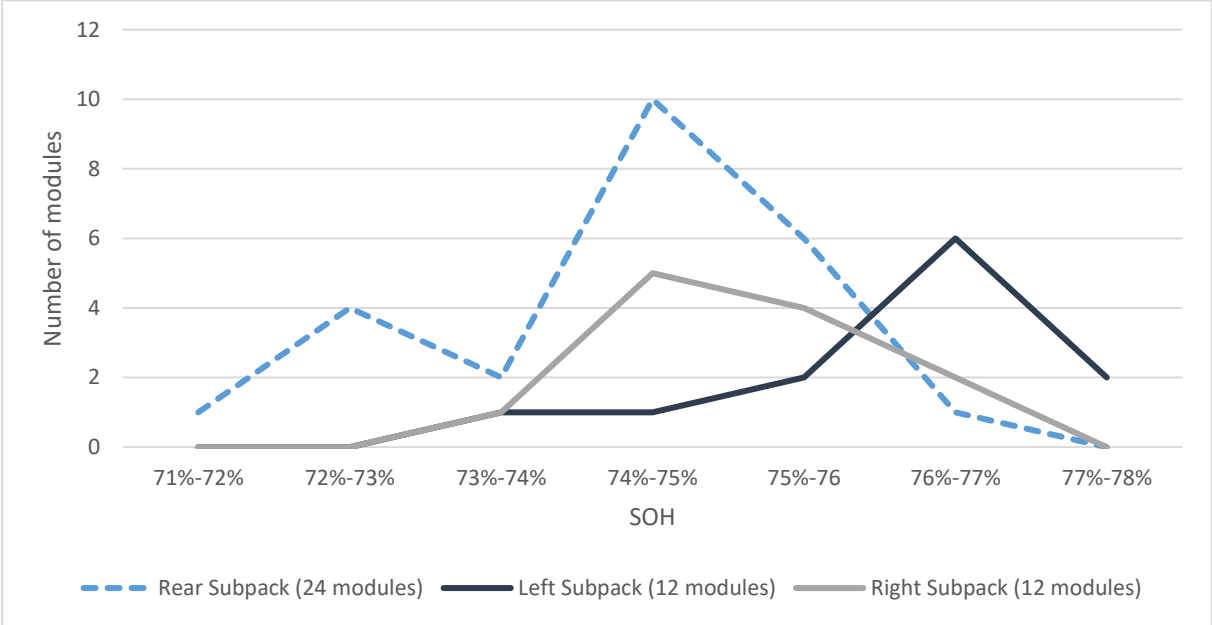


Figure 6.4 Division of the SOH of the modules of the battery pack #2, sorted by subpacks.

6.1.3 Battery pack #3

In this section the results of the testing on the third battery pack are presented. As for the previous sections the focus is on the SOH percentages, on the main parameters and how the SOHs are distributed in the pack. As it happened for the second battery pack the average testing procedure had a duration of 7 hours and 43 minutes. This value is between the duration of the first pack, 8 hours and 12 minutes, and the one of the second pack, 7 hours and 30 minutes.

This parameter, the average duration of the test, gives already a good idea of which battery pack has the greatest SOH. Of course, in order to compare the durations, the initial SOC percentage and the testing procedure must be identical. Indeed, a slightly different initial SOC or procedure could create a great variation in the duration of the test. From the information stated above it is possible to determine that the highest average SOH is found in the first pack, right after the first there is the third BP and lastly the lowest average SOH is found during the testing of the second battery pack. Certainly, these evaluations are relevant if the number of modules tested is large and statistically relevant.

Figure 6.5 reports the Gauss distribution of the SOH of the modules of the third battery pack. The SOH ranges are from 81% to 88%, with the majority of the modules that are found between

83% and 84%. Indeed, as confirmed in Table 6.5, the average SOH percentage is 83.443%, which is highlighted by the maximum of the red curve plotted in Figure 6.5. As well as for the first battery pack, the Gauss distribution of the SOHs shows that over 40% of the tested modules has a SOH close to 83%. Since the all the SOH percentages are higher than the EOL threshold all of the modules could be used for second life uses. Of course, the applications may be different from the ones of the first BP, because the SOH of some modules is slightly above the EOL limit (80%).

Another interesting fact is that, even if the SOH range of Figure 6.5 is the same as the one in Figure 6.3, 6%, the distribution of the SOHs is different. This situation is due to the fact that with the decrease of the SOH the degradation becomes less predictable and it depends more and more on physical differences of the cells. Indeed, the bars of the BP #3 follow more the Gauss curve (red plot in Figure 6.5), while the bars of BP #2 are more distant from the ideal Gauss curve.

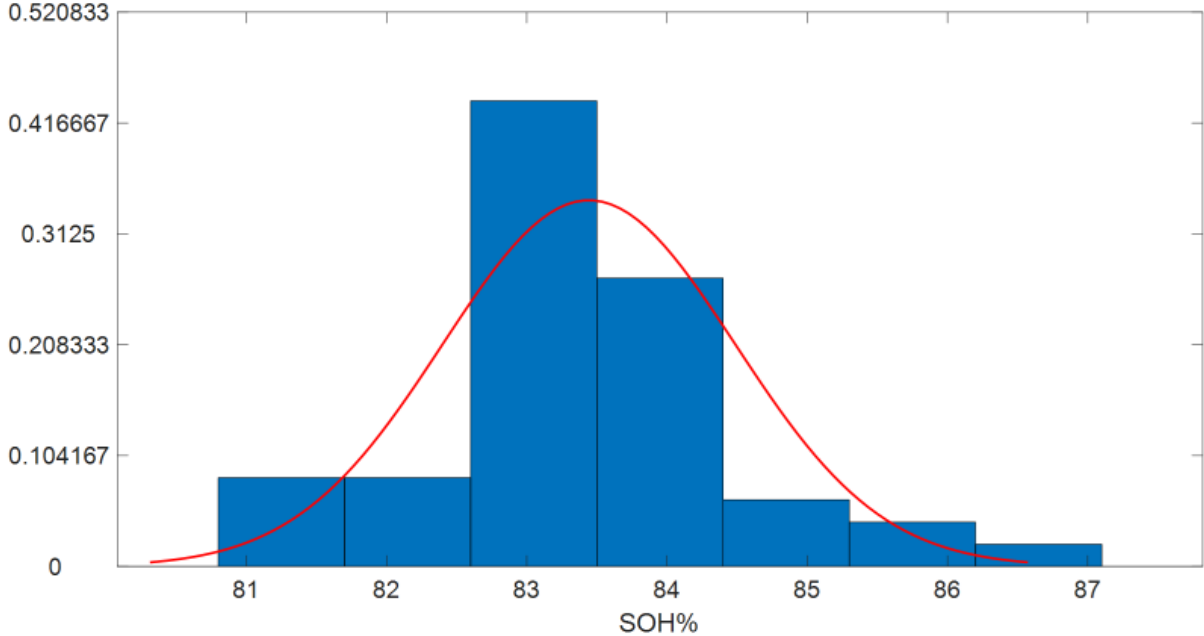


Figure 6.5 Gauss distribution of the SOH of the third battery pack (BP #3).

Table 6.5 reports the main findings of the testing of the third battery pack. As introduced in the previous paragraph the SOHs go from 81.409% to 87.091%. The average available capacity is 55.07 Ah, corresponding to 83.443% SOH. As occurred for the first battery pack, the module that has the highest SOH, M29 is the same that has the lowest self-discharge rate (0.4242%/h). The relationship among the available remaining capacity and the self-discharge rate is evaluated in the next sections.

The self-discharge goes from 0.14 Ah, measured in 30 minutes, of the module M29, to the 0.20 Ah of module M25. The average SD is 0.168 Ah, which corresponds to an hourly rate of 0.5082%/h. For what concerns the parameters of the EEC shown in Table 6.5, R_0 and R_{tot} , have been measured at 50% SOC using 1.5 C (66 A). As it was found in the first two battery

packs the same modules that have the highest and lowest values of R_0 have the highest values of R_{tot} . Indeed, M37 has the highest values of R_0 and R_{tot} , respectively 2.4242 m Ω and 3.2323 m Ω , while M11 has the lowest measurements, 1.4141 m Ω for R_0 and 2.2222 m Ω for R_{tot} . It is interesting to notice that the average values of R_0 and R_{tot} , respectively 2.2664 m Ω and 3.0408 m Ω , are closer to the maximum values than to the minimum ones. This situation could mean the fact that there are only few modules that have experienced a less intense degradation, while in general the other modules have undergone more degradation and thus, they have experienced an increase in the resistive parameters.

Table 6.5 Main findings third battery pack.

Battery pack #3								
Mod #	Cap (Ah/%)		SD Ah (30 m)/h (%)		R_0 (m Ω)		R_{tot} (m Ω)	
	Max	Min	Max	Min	Max	Min	Max	Min
	M29	M42	M25	M29	M37	M11	M37	M11
	57.48 Ah	53.73 Ah	0.20 Ah	0.14 Ah	2.4242	1.4141	3.2323	2.2222
	87.091%	81.409%	0.6060%	0.4242%	-	-	-	-
AVG	55.07 Ah	83.443%	0.168 Ah	0.5082%	2.2664		3.0408	

In Table 6.6 are presented the average SOH percentages sorted by subpack. As it occurred for the first two battery packs the highest average SOH is found in the left subpack, 84.398%. The rear and right subpacks, respectively 83.245% and 82.885% have average SOHs that are lower than the overall one, 83.443%, which corresponds to 55.073 Ah. However, the average SOHs of the three subpacks are not very different from each other (1 Ah difference between the left and right subpacks). These findings can be compared with Figure 6.6, which gives a visual overview of the distribution of the results.

Table 6.6 Comparison of the available capacity of the subpacks for battery pack #3.

Average available capacity sorted by subpacks BP #3		
Subpack	Average available capacity	Average SOH
Rear	54.942 Ah	83.245%
Left	55.703 Ah	84.398%
Right	54.704 Ah	82.885%
Overall	55.073 Ah	83.443%

Indeed, Figure 6.6 shows the distribution of the SOH of the third battery pack sorted by the three subpacks, rear, left and right subpack. It is interesting to notice that the majority of the

modules of the rear subpack (17 out of 24) have a SOH in the range 83%-84%, while there are not modules in the ranges 85%-86% and 86%-87%. For all the three subpacks the highest number of modules is found in the range 83%-84%, which contains the average SOH percentage of the pack 83.443%. Even though the left (dark plot) and right (grey plot) subpacks have a half of the modules, 12, of the rear pack (dashed line), 24, their ranges of the SOHs are wider.

As occurred for the first two battery packs that have been tested the differences in the SOH percentages among the three subpacks are not relevant enough to prove that there are different operating conditions inside the battery pack.

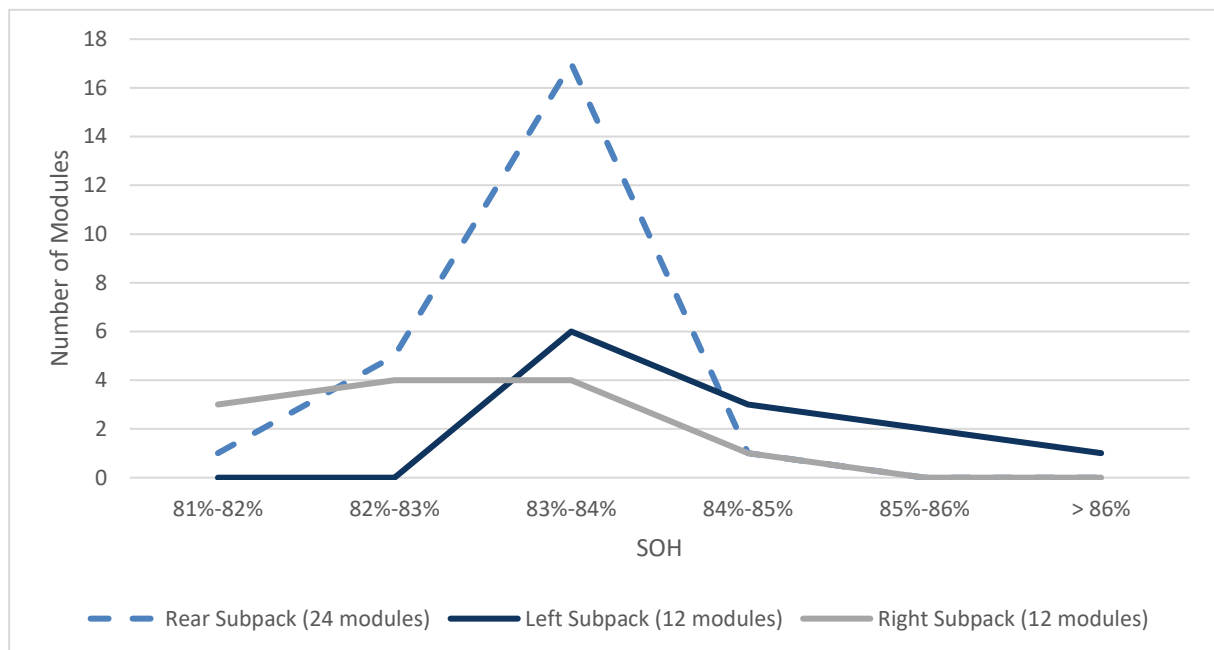


Figure 6.6 Division of the SOH of the modules of the battery pack #3, sorted by subpacks.

6.2 Overall results

In this section a comparison of the results of the testing of the three battery packs is performed. As occurred with the previous sections 6.1.1, 6.1.2, and 6.1.3, the focus is on the SOH of the modules. In addition, the main parameters of the EEC of the modules are evaluated, as well as the self-discharge rate.

6.2.1 SOH

Figure 6.7 shows the distribution of the SOH percentages between the three battery packs that have been tested during the testing campaign. As stated previously, the SOHs of the three packs are not coincident, as the figure shows. Indeed, the distributions of the available remaining capacity do not intercept each other. For these reasons, it is not possible to create a fourth

battery pack, with the 48 modules that have the highest SOH percentages. With the data presented in Figure 6.7 it is clear that the remanufactured battery pack would have the same modules that equip the battery pack #1. Thus, the remanufacturing process, for this scenario, is not viable and the process would not have sense from the economical point of view.

Of course, this scenario is due to the fact that only three battery packs have been disassembled and then tested. If the testing campaign would have had a large number of packs the possibility of finding packs with SOH distribution that cross each other and therefore enabling the remanufacturing process.

Another evaluation that can be made in regards to Figure 6.7 is that with the general decrease in the SOHs its range widens. Indeed, the battery pack #1 (dark blue bars), which has the highest SOHs is divided only in three bars, from 88% to 91%. The BP #3, which has the second highest average SOH, 83.443%, has the distribution (light blue bars) that is composed by 6 different bars. In addition, the range of its SOHs, goes from 81% to 88%.

The second battery pack has the lowest average SOH percentage, 74.911%, and its distribution is divided into 7 different ranges. Another interesting result is the fact that, for each battery, the number of modules that are in the range of the average SOH reduces with the reduction of the overall SOH. Indeed, for the first battery pack the highest number of modules is 28 (dark blue bar), while for the third battery pack the peak is reached with 27 (light blue bar). For the latter battery pack the greatest number of modules in the same range decreases to 16. This is another result of the reduction in the SOH percentages.

As introduced in the previous section, these results confirm the fact that with the decrease of the overall SOH, the values of the SOHs of the modules become more spread around the average value. This phenomenon is one of the reasons why the threshold for the EOL is set to 80% of the initial rated capacity of the battery.

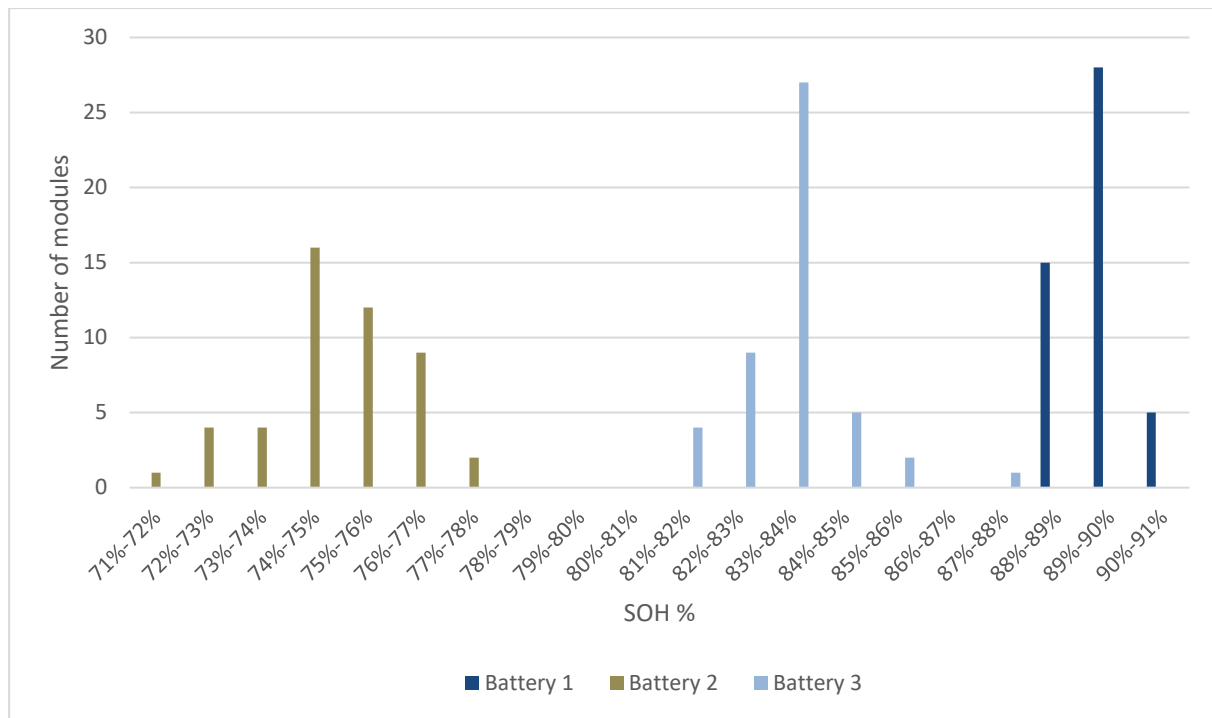


Figure 6.7 Distribution of the SOH percentages between the three battery packs tested.

The results previously presented in the current section and in Figure 6.7 are summarized in Table 6.7

Table 6.7 Average SOH percentage of the modules of the three battery packs.

Average SOH of the modules	
Battery pack #1	89.357%
Battery pack #2	74.911%
Battery pack #3	83.443%

In Figure 6.8 are shown four different plots, the three thinner ones are of the three battery packs, while the thickest one is the average of the three packs. The plots represent the trend of the SOH percentages sorted by battery packs. In the x-axis is shown the module number, the numeration start with the first module connected to the common “-“ of the battery.

As previously stated, the first 24 modules are contained in the rear subpack, the modules from M25 to M36 come from the left subpack and the modules from M37 o M48 belong to the right subpack.

The plots show how the SOH percentages are spread in the packs. As it had been stated in the previous sections a clear degradation path, based on the position, in the reduction of the capacity is not found. The thickest dark line has been calculated by adding the SOHs of the

modules with the same number, then this value has been divided by 3, as shown in the equation (6.1). The formula has been applied to all the 48 modules of the three battery packs.

$$AVG_{M1} = \frac{AVG_{M1B1} + AVG_{M1B2} + AVG_{M1B3}}{3} \quad (\%) \quad (6.1)$$

- AVG_{M1} Average SOH of the M1 (%)
- AVG_{M1B1} SOH of M1 of the first battery pack (%)
- AVG_{M1B2} SOH of M1 of the second battery pack (%)
- AVG_{M1B3} SOH of M1 of the third battery pack (%)

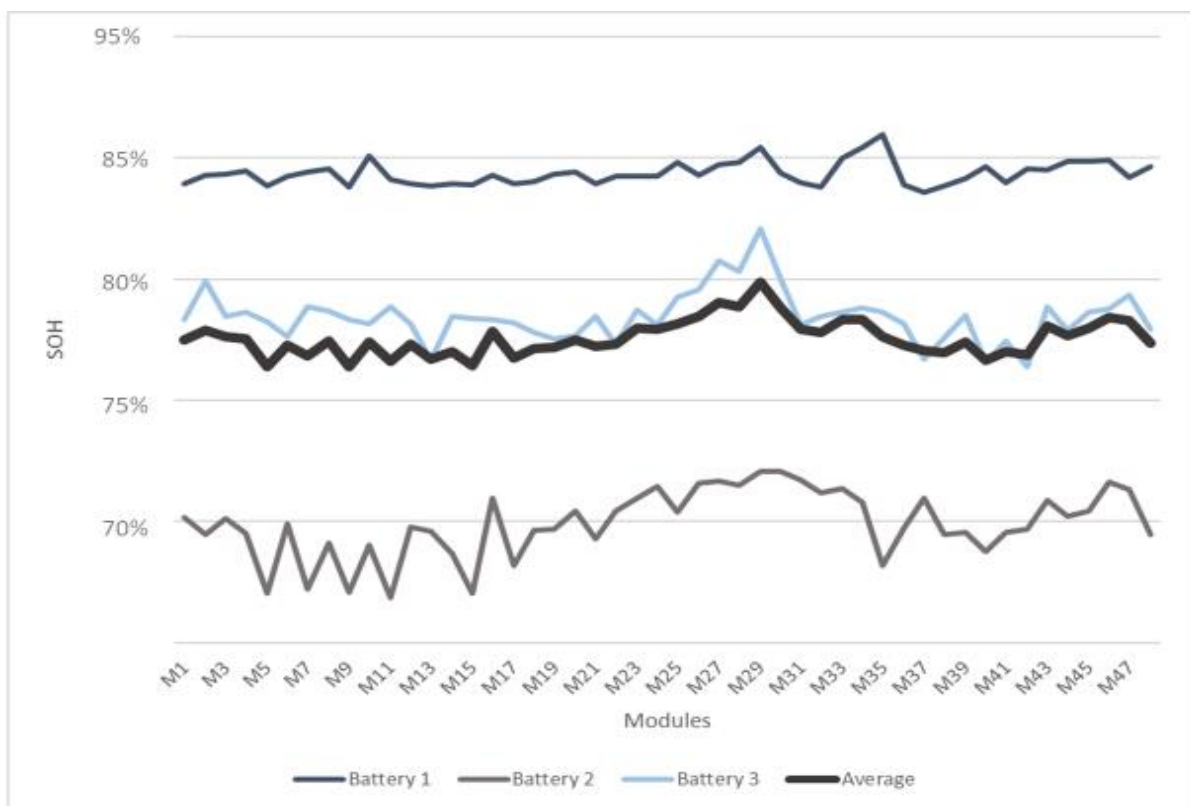


Figure 6.8 SOH percentages sorted by module number and divided in the three battery packs.

In Table 6.8 are shown the standard deviations (STD DEV) calculated for the main parameters presented in the previous sections of this chapter. The values are sorted by battery pack and in the last column are calculated the values for all the 144 modules that have been tested. The standard deviation values have been calculated according to the formula presented in equation (6.2) Vgl. Marco Codegone (Metodi matematici per l'ingegneria) 1995⁶⁸.

⁶⁸ Vgl. Marco Codegone (Metodi matematici per l'ingegneria) 1995.

$$\sigma = \sqrt{\frac{1}{N} \cdot \sum_{N=1}^N (x_i - \mu)^2} \quad (6.2)$$

σ	Standard deviation
N	Number of terms in the sample
x_i	Parameter being evaluated
μ	Mean value

Table 6.8 Standard deviation values of the main parameters sorted by battery packs.

	Standard Deviation			
	BP #1	BP #2	BP #3	Overall
STD DEV SOH	0.4926%	1.3941%	1.0434%	6.040%
STD DEV SD	0.8688%	0.8989%	0.8330%	2.558%
STD DEV R_0	34.362%	44.903%	38.269%	43.979%
STD DEV R_{tot}	33.960%	47.145%	39.124%	46.893%

The results shown in Table 6.8 summarize the trends of the main parameters considered. It can be seen that the σ , with respect to the SOH, generally increases with the decrease of the available remaining capacity. Indeed, the highest standard deviation for the SOH is found for the second battery pack. The same trend of σ is found when the standard deviations of R_0 and R_{tot} . In these cases, the lowest values of σ are found in the first battery pack, respectively 34.362% and 33.690%, which has the highest SOH percentages. The data in Table 6.8 confirm the evaluations made in previously at the beginning of this subsection. Indeed, the increase in the degradation (capacity fade), brings more aleatorily in the values of the main parameters (SOH, self-discharge, R_0 and R_{tot}).

6.2.2 EEC parameters

In the next subsections of this chapter are shown the differences in the values of the EEC parameters of the module of the Nissan Leaf 2011 Edition. The comparison is based on the data presented in Main results (6.1), with regards to the modules with the maximum and minimum SOH percentages among the three battery packs. In Table 6.9 and Table 6.10 are listed the main characteristics of the modules that have the overall maximum and minimum SOH among the three battery packs.

Table 6.9 Data of the module with the overall highest SOH percentage between the three battery packs.

Maximum SOH	
Battery pack	#1
Subpack	Left
Module #	M35
SOH	90.970%

Table 6.10 Data of the module with the overall lowest SOH percentage between the three battery packs.

Minimum SOH	
Battery pack	#2
Subpack	Rear
Module #	M11
SOH	71.848%

In the following subsections are presented the values of the different EEC parameters, with the maximum values (Max) that refer to the module M35 of the first battery pack. The minimum values (Min) refer to the module with the least SOH percentage, M11 from the second battery pack.

6.2.3 R_0

The first element of the EEC circuit is R_0 and as shown in the previous sections, its values are in the range of m Ω s. In Figure 6.9 are shown the measurements of the modules with the maximum and minimum SOH of the three packs. The trends of the variation of the resistive parameters of the EEC are presented in chapter 3 (State of the art), and in the researches Vgl. Böttiger et al. (Systematic experimental pulse test investigation for parameter identification of an equivalent based lithium-ion battery model) 2017⁶⁹ and Vgl. Madani et al. (An Electrical Equivalent Circuit Model of a Lithium Titanate Oxide Battery) 2019⁷⁰.

⁶⁹ Vgl. Böttiger et al. (Systematic experimental pulse test investigation for parameter identification of an equivalent based lithium-ion battery model) 2017.

⁷⁰ Vgl. Madani et al. (An Electrical Equivalent Circuit Model of a Lithium Titanate Oxide Battery) 2019.

The extractions of the parameters have been performed with the data provided by the pulse tests. As expected, the values of R_0 of the module with the highest SOH (M35, BP #1) are lower than the values of the ones of the module (M11, BP #2).

Indeed, most of the time the plots with the dashed line, referring to the lowest SOH, are above the solid ones. In particular, this occurs for the SOC's lower than 60%. The higher differences are found a 5% and 10%, where all the solid and dashed lines have very different values. The differences decrease with the increase of the SOC, and at the highest SOC, 95%, the values are comprised between 1.5 and 2 m Ω , with the only exception of the measurement taken with 0.5 C on the M11 (dashed red line), that has a value above 2.5 m Ω .

Given the results of Figure 6.9 the phenomenon of the increase in the values of R_0 with the decrease of the SOH is confirmed. In some cases, the increase is quite limited, or there is none, but in other cases is more severe, with the value of R_0 which doubles.

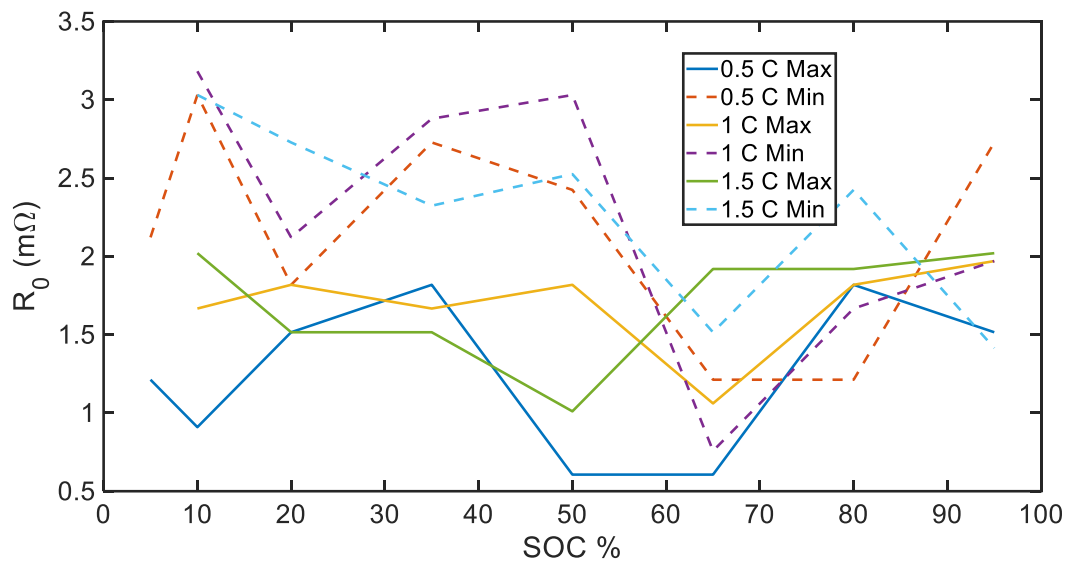


Figure 6.9 Comparison of the plots of the values of R_0 of the modules with the maximum and minimum SOH.

6.2.4 R_1

In Figure 6.10 are shown the values of the second resistive parameter of the EEC circuit, R_1 . As well as, for R_0 , the plots refer to the measurements performed on the modules that have the highest, M35, BP #1, and the lowest, M11, BP #2, SOH.

The trends found in Figure 6.9 are confirmed by the ones shown in Figure 6.10. Thus, the values R_0 of the module with the lowest SOH, plots with the dashed lines, have generally higher values compared with the ones of the M35.

However, even though the trends are similar to the ones found for R_0 , the difference in the values of Max and Min (comparing the measurements with the same C-rate), are smaller than the ones previously found. The values measured with 1.5 C (solid green line for Max SOH,

dashed light blue line for Min SOH), are quite close to each other, and in some cases the two plots cross each other (at 50% SOC, 0.5 m Ω).

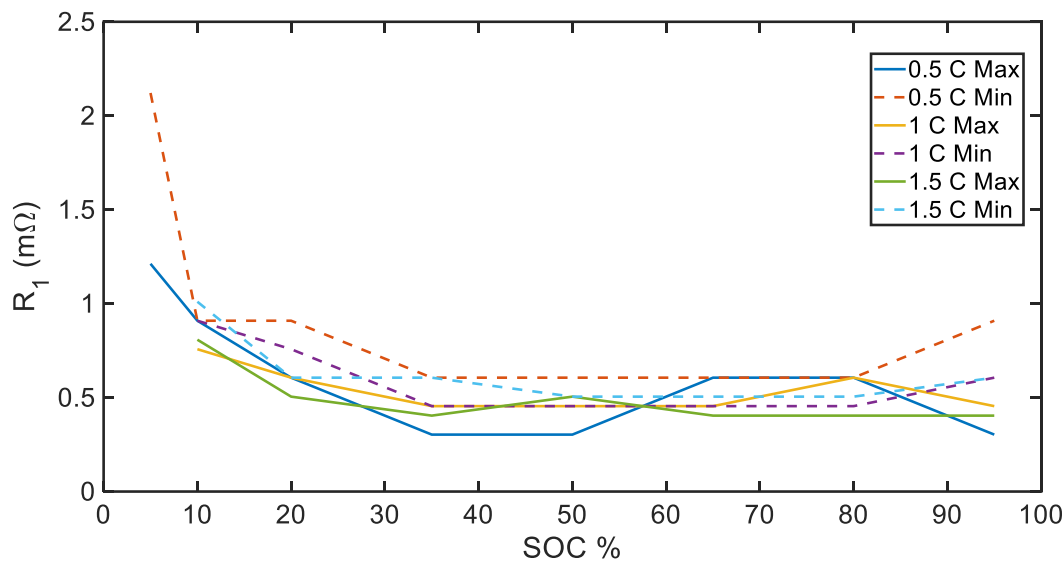


Figure 6.10 Comparison of the plots of the values of R_1 of the modules with the maximum and minimum SOH.

For what concerns the change in the values R_1 , with respect to the SOC level, it can be assessed that the trend is the following. At lower SOC levels (5%-20%) is where the values of R_1 are the highest, compared to the ones found at higher SOC levels. The peaks are found at the lowest SOC, 5%, then the values drop with the increase of the SOC. Then, from 20% to 60%/70%, depending on the degradation and on the C-rates used for the measurements, there is a general reduction in the values R_2 . Lastly, in the section from 60%/70% to 95% the measurements experience a limited increase. The maximum value is reached with 0.5 C at 5% for the module with the least SOH, and it corresponds to 2.252 m Ω (dashed red line). On the other hand, the minimum value is obtained three times, at 35%, 50%, and 95% with 0.5 C for the module with the highest SOH.

6.2.5 R_2

The measurements of the last resistive element of the EEC circuit are presented in Figure 6.11. R_2 is the resistance of the second RC parallel branch. The results are presented as it occurred for the previous elements of the EEC, R_0 and R_1 . The behaviour of R_2 is similar to ones found for R_0 and R_1 , with the values coming from the module with the least SOH, M11 BP #2, that are greater than the ones of M35 BP #1.

Another similar behaviour is the fact that the values change according to a pattern, with the lower SOC levels, from 5% to 30%, that experience higher values. In the plots of R_2 , from 30% to 80%, the values of the measurements of the highest SOH, experience a plateau. Indeed, the values of R_2 remain constant for all the SOC levels and for all the C-rates used (solid curves). In the same SOC range, for what concerns the M11, which has the least SOH, the values are not constant, but the trend is the same to the one found for M35. The higher range

of SOC experiences an overall increase in the values of R_2 , with the only exception of the measure taken on M11 with 0.5 C (red dashed line).

The different trends found for the resistive parameters can be found in all of the, with some trends that are more accentuated than others (increase of the values of the resistance with the decrease of the SOH).

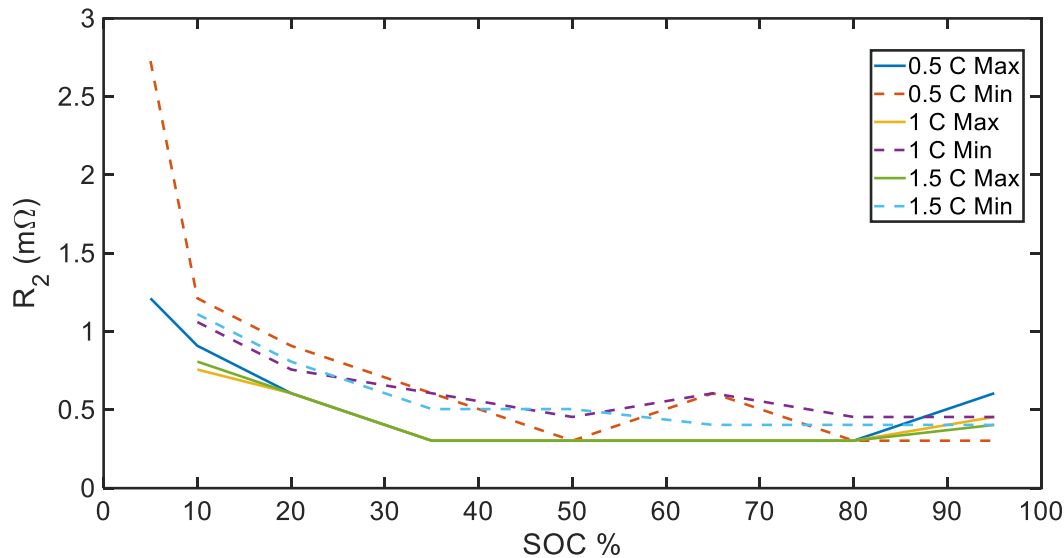


Figure 6.11 Comparison of the plots of the values of R_2 of the modules with the maximum and minimum SOH.

6.2.6 C_1

The first RC branch is composed by R_1 and by C_1 , the latter is the first capacitive parameter for which are evaluated the trends with respect to the SOH, the C-rate and the SOC. Indeed, in Figure 6.12 are presented the curves that refer to the two modules, the one which has the highest SOH, M35 BP #1, and the least, M11 BP #2. The changes in the values are evaluated over the SOC levels, by comparing the different measurements taken with three different C-rates (measurements performed during the pulse tests).

As it has been stated in chapter 3 (State of the art), for Li-Ion batteries the usage and the resulting degradation increases the value of the capacity parameters. Therefore, in this subsection it is expected to observe a general rise in the values of C_1 and C_2 .

As presented in Figure 6.12, the solid lines, representing the measurements of the module M35, are above the dashed line, representing the module M11. Only in three cases, the measurements at 65% and 80% with 0.5 C, and 1 C at 80% for module M35, had lower values than the one performed on M11. These trends follow the ones presented Vgl. Böttiger et al. (Systematic experimental pulse test investigation for parameter identification of an equivalent

based lithium-ion battery model) 2017⁷¹ and Vgl. Madani et al. (An Electrical Equivalent Circuit Model of a Lithium Titanate Oxide Battery) 2019⁷² and they determine that to a decrease in the SOH percentages it follows a general increase in the values of the capacity C_1 .

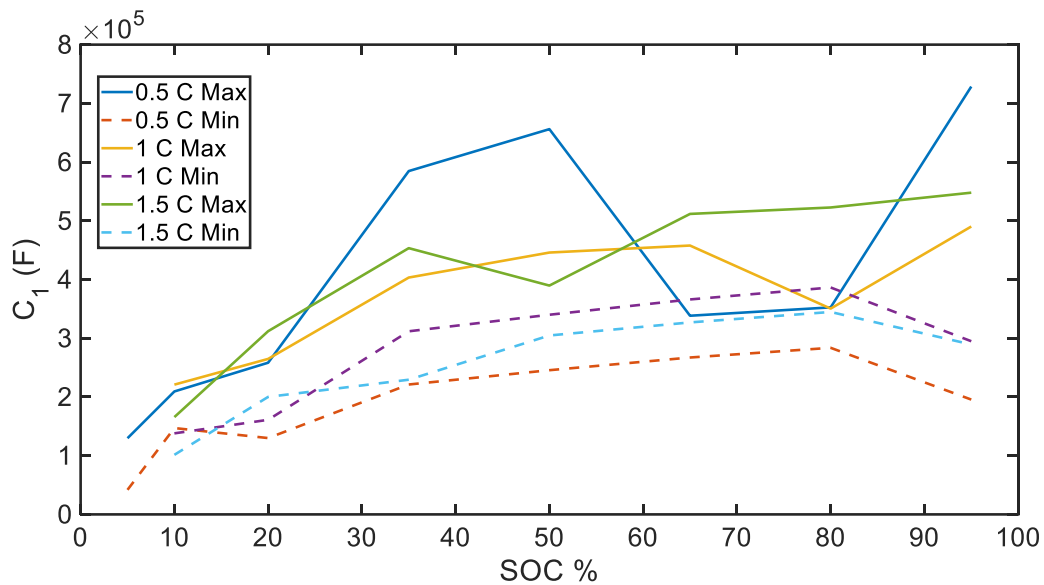


Figure 6.12 Comparison of the plots of the values of C_1 of the modules with the maximum and minimum SOH.

For what concerns the trend over the SOC, there are some differences between the maximum SOH and the minimum SOH cases. Regards to the maximum SOH, the values of C_1 increase with the increase of the SOC. This occurs for all the C-rates evaluated, 0.5 C, 1 C, and 1.5 C. The minimum values are found at 5% and at 10%, then there are increasing trends for all the C-rates. Their peaks are all found at 95%, but before that SOC level for all the C-rates there are some drops (the most severe occurred to the 0.5 C curve, between 50% and 80%).

The values of C_1 for the module with the least SOH follow a similar path, the least values are found at the lowest SOC, then all the plots increase their values. It is interesting to notice that as occurred for the highest SOH module, the higher values of C_1 are found at high SOC. However, contrary to the maximum SOH case, the highest values are found at 80% and not at 95%.

Comparing the dashed lines, minimum SOH, with the solid lines, maximum SOH, it can be seen that the trend of the first ones is smoother and it is not as much as scattered.

⁷¹ Vgl. Böttiger et al. (Systematic experimental pulse test investigation for parameter identification of an equivalent based lithium-ion battery model) 2017

⁷² Vgl. Madani et al. (An Electrical Equivalent Circuit Model of a Lithium Titanate Oxide Battery) 2019

6.2.7 C_2

Figure 6.13 shows the trends of the last capacitive element of the EEC over the SOC at different C-rates. As occurred for the other capacitive parameter, C_1 , the values of C_2 of the module with the higher SOH are greater than the ones of the minimum SOH. In this case there is only one exception and it occurs at the highest SOC evaluated, 95%. Indeed, at 95% the value of C_2 of the module M35 measured with 0.5 C has values smaller than the one measured on the M11 with the same C-rate.

The two modules have some differences in the trends. Thus, the one with the higher SOH, solid plots, experience a great increase with the increase of the SOC. For all the three C-rates the peaks are reached at 80%, with values that are very close to each other, around $8 \cdot 10^5$ F. At 95% all the three curves have a sudden drop, the lower was the C-rate the deeper was the drop. It has to be noticed that the three plots of the maximum SOH have the same trends and values very close to each other.

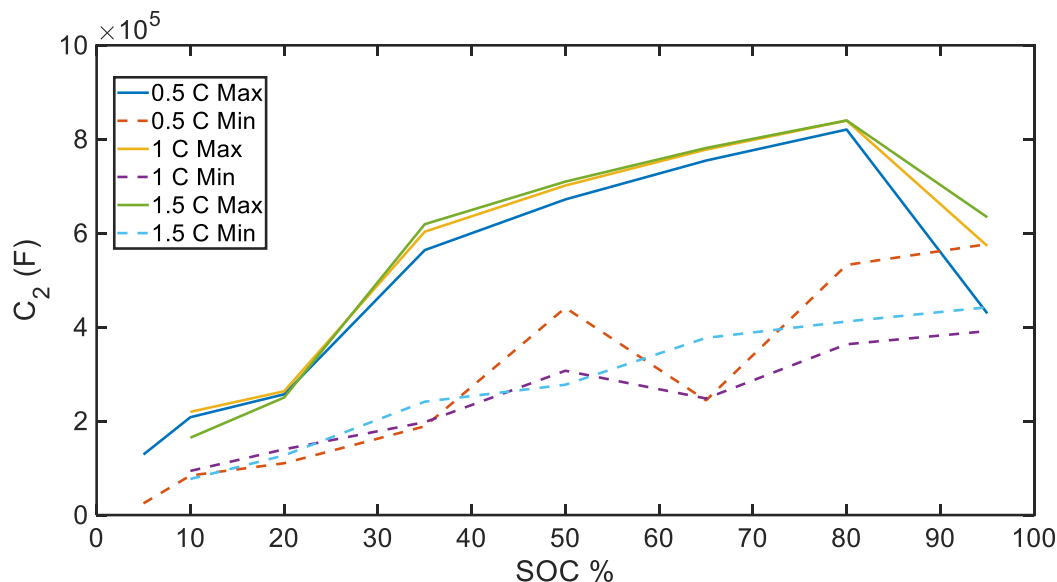


Figure 6.13 Comparison of the plots of the values of C_2 of the modules with the maximum and minimum SOH.

For what concerns the module with the minimum SOH, the trends are similar to each other. All the plots experience an increase with the increase of the SOC level. However, reached 50% the plots have different performances, with the curve of 0.5 C (dashed red line) that rises and drops and rises again, reaching the maximum value for the minimum SOH module, $5.9 \cdot 10^5$ F. The values of the curves of the maximum SOH module have in most of the cases twice the values of the minimum SOH.

6.2.8 R_{tot}

R_{tot} represents resistive behaviour of the EEC model of the module. As presented in the previous sections, R_{tot} get its value from the algebraic sum of the three resistive elements R_0 , R_1 and R_2 . Since its value is the result of the sum of the three elements, its trends are going to be

related to the trends of the three parameters, presented in 6.2.3, in 6.2.4, and in 6.2.5, respectively for R_0 , R_1 and R_2 .

In Figure 6.14 are presented six plots, three for the module with the maximum SOH (solid lines) and three for the module with the minimum SOH (dashed line). As expected, the dashed lines are generally above the solid ones, determining that the decrease in the SOH leads to an increase in the value the total equivalent resistance of the module.

From the lowest SOC considered, 5%, to 60% the values of the module with the minimum SOC are higher than the ones of the maximum. Above 60% all the plots rise, and they cross each other, then they have a peak at 95%. Even though the results of R_0 , R_1 , and R_2 are mixed, the pattern found for R_1 and R_2 , presented in 6.2.4 and in 6.2.5 can still be detected. Indeed, the higher values of the curves are found at the lowest SOC, then the plots decrease until 40%-50%-60%, depending on the C-rate, are reached. After those points there is a general increase trend for all the plots, with only two curves that decrease a little.

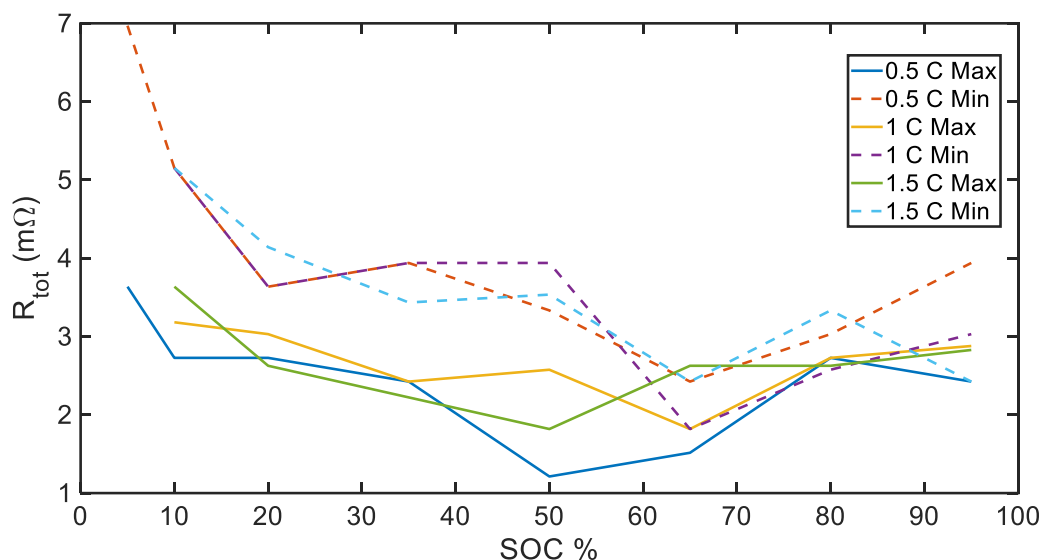


Figure 6.14 Comparison of the plots of the values of R_{tot} of the modules with the maximum and minimum SOH.

6.3 Distributions over the SOH

Given the results and the trends presented and shown in the previous sections 6.1 (Main results) and 6.2 (Overall results) this section aims to summarize the behaviour of some the parameters that have been considered. From the data presented have been created different distributions of the values of the parameters over the available remaining capacity of the modules of the three battery packs. The first two figures represent the distributions of R_{tot} in different conditions. In the last part of the section is evaluated the distribution of the self-discharge rate of found for the three batteries.

Thus, Figure 6.15 represents the distribution of the values of R_{tot} at different SOC levels (10%, 50% and 95%) over the available remaining capacity of the modules. The measurement of R_{tot}

are all from the pulse tests performed using a C-rate of 1.5 C, the measurements are from the three battery packs. Thus, the points plotted in Figure 6.15 are 144 for each color (representing the different measurements of R_{tot}), 432 points in total. It has to be taken into account that 144 is also the number of points that are inside every pane.

The data are also sorted by battery packs, to have a better overview of the trends present in the figure (blue pane for BP #2, orange pane for BP #3, and green pane for BP #1). The three packs are sorted by the three panes, but the division could have been performed by just using the available remaining capacities.

From the figure it can be seen that, for the measurements performed at the highest SOC level, 95%, the highest values are found. Indeed, the green dots, representing the 95% level, are generally in the top area of the panes for every battery pack. This behaviour is more accentuated in the third battery pack and first battery pack, which have respectively SOHs between 81% and 88% and 88% and 91%. For the second battery pack the phenomenon is less appreciable, because the dots are more spread. However, the higher values of R_{tot} are found at 95% of SOC.

Considering the second higher SOC level, 50% (blue dots), the results are different. The majority of the dots are placed in the lower regions of each pane. This means that the values of R_{tot} , measured at 50% SOC (always using a C-rate of 1.5 C, 99 A), have the least values, with respect to the ones measured at 10% and 95%. This behaviour is constant for all the three battery packs, even though for BP #2 and BP #1 is less appreciable than in BP #3. This could be due to the fact that the modules coming from BP #1 have not experienced a great degradation and therefore the internal resistance values have not changed their values. On the other hand, the modules of BP #2 have a SOH which is beyond the EOL threshold (80%).

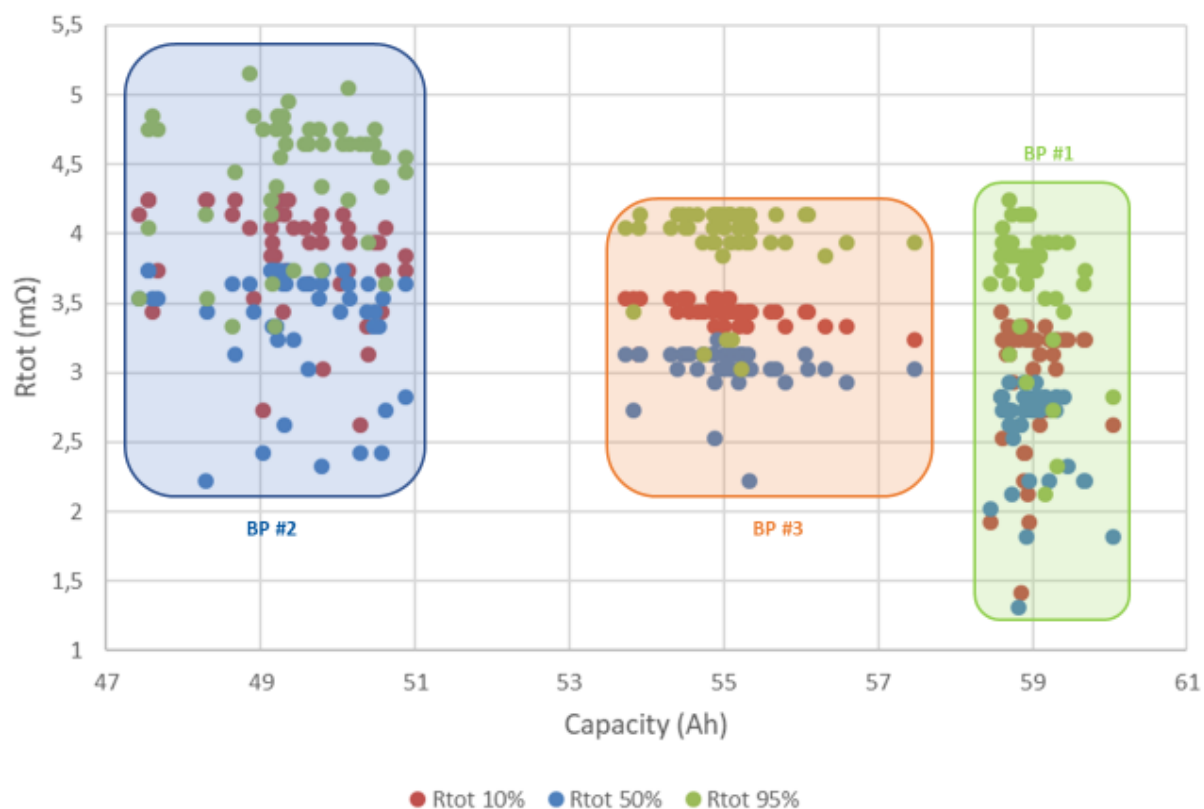


Figure 6.15 Distribution of R_{tot} at different SOC levels, sorted by battery pack, over the available remaining capacity.

The last SOC level evaluated for R_{tot} is 10%, for this level the values are shown with the red dots. This voltage level has values in between the ones found for 50% and 95%. As occurred for the 50% level, the values for BP #2 and BP #1, respectively blue and green panes, are scattered. For the third battery pack, red pane, the values are more constant in their values.

In Figure 6.16 are presented the distributions of R_{tot} over the available remaining capacity for the three battery packs. Figure 6.16 shows how the SOH (available remaining capacity) influences the values of the total internal resistance (R_{tot}) of the modules. As shown, the three distributions of the three battery packs have similar trends, but the values are different. Thus, the highest number of points of the first battery pack (red dots) is concentrated below, at 3 mΩ. The distribution regarding the first pack is narrow, this is due to the fact that the SOH range of the first battery pack is quite limited (between 88% and 91%).

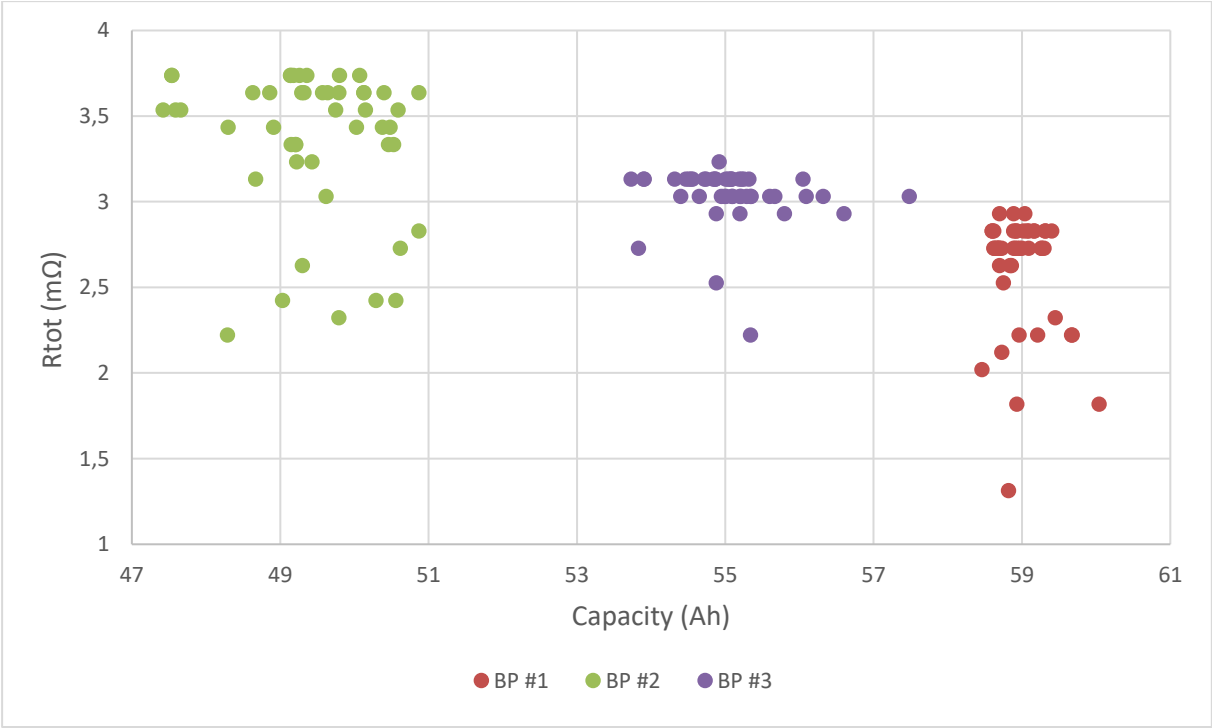


Figure 6.16 Distribution of R_{tot} ($m\Omega$) over the available remaining capacity (Ah) sorted by battery packs.

In Figure 6.17 are presented the distributions of the self-discharge rates over the available remaining capacity for the three battery packs. The graph has a total number of 144 points, coming from the 48 modules of each of the three packs that have been tested (one SD rate per module).

It is very interesting to notice that Figure 6.16 (analyzing R_{tot}) and Figure 6.17 (analyzing self-discharge rate) have very similar trends in them. Indeed, the trends for the three battery packs are the same, the first battery pack has the lowest values for both the SD rate and R_{tot} . Then, with the third battery pack, violet dots in Figure 6.16 and in Figure 6.17 there is a general increase in the values of both the SD rate and R_{tot} . The second battery pack, which has the least values of SOH percentages (71%-77%), has the higher values of R_{tot} and of the self-discharge rate.

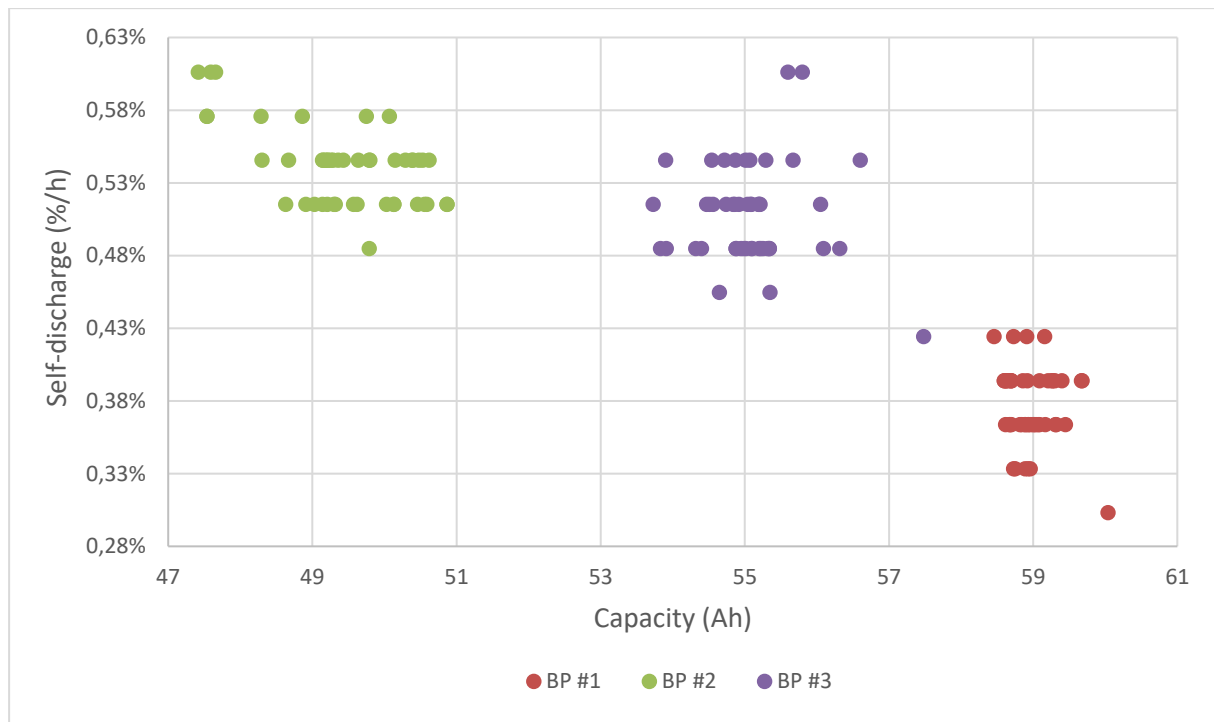


Figure 6.17 Distribution of the self-discharge rate (%/h) over the available remaining capacity (Ah) sorted by battery packs.

From the data presented in 6.2.3, in 6.2.4, in 6.2.5, in 6.2.6, in 6.2.7, and in 6.2.8 it can be assessed that the presented results confirm the theories illustrated in chapter 2 (General overview) and in chapter 3 (State of the art). Indeed, for the modules considered it can be stated that the degradation that goes along with the usage of the battery affects the parameters of the EEC of the model that simulates its behaviour.

Therefore, it can be assessed that the usage and the degradation of the battery go along with a general increase in the value of the total equivalent resistance of the EEC. This behaviour occurs at every SOC level and for every C-rate used (within the limits of these tests). This increase in the values of the resistances of the circuit, R_0 , R_1 , R_2 , leads to an increase the losses during the operation of the battery. With this increase in the losses, the temperature of the module (or cell) rises, leading to a higher possibility of reaching unsafe operating conditions. The increase of the internal temperature leads also to an increase of the resistance, linear relationship between temperature and ohmic resistance, thus increasing even more the losses and the temperature.

The usage and its subsequent degradation vary the values of the capacitive parameters of the EEC of the module. The capacitances of the EEC decrease their values with the decrease of the SOH of the module. Indeed, a module with a higher SOH has lower capacitive parameters compared to one that has a lower SOH. Thus, C_1 and C_2 have a direct correlation with the SOH, if one increases the other one does the same and vice versa.

The resistive parameters and the capacitive parameters have opposite trends regarding their variation to the variation of the SOH. When there is a decrease of the SOH of the module, the

resistances increase their values, while the capacitances decrease their values. With the changes in the values of the elements of the EEC it is clear that the operating conditions of the cell, the module, and the pack, could be very different from the nominal ones.

The relationship between the change in the SOH values and the consequent variation of the EEC parameters is evaluated in chapter 7 (Correlation between parameters and SOH). There a comparison of the correlation indexes is made, along with some evaluations and considerations with respect to the self-discharge rate and the SOH.

7 Correlation between parameters and SOH

Since in the previous sections of this chapter some relationships between the parameters have been found, in this section are considered the correlations of the different parameters evaluated. Indeed, the relationships between SOH and R_0 , SOH and R_{tot} , and SOH and self-discharge are studied in the next subsections. The correlation between the different parameters is calculated according the equation (7.1) presented in Vgl. Sheldon M. Ross (Introduction to Probability and Statistics for Engineers and Scientists) 2014⁷³.

The parameter β_{xy} represents the correlation between the parameters x and y . The value of β_{xy} is between -1 and +1, and its sign is very important. Indeed, if the parameter is negative the correlation is defined inverse, which means that the two parameters have opposite trends. If the value of x increases, y 's decreases, and vice versa. On the contrary, when the correlation index is positive, the trends are similar, if one parameter increases the other one does the same.

Another information that can be extracted from β_{xy} is how much the trends are similar between the two parameters that are being evaluated. The greater, considering its absolute value, is β_{xy} the higher is the degree of similarity of the two trends.

$$\beta_{xy} = \frac{\sum_1^N (x_i - \mu_x) \cdot (y_i - \mu_y)}{\sqrt{\sum_{N=1}^N (x_i - \mu_x)^2 \cdot \sum_{N=1}^N (y_i - \mu_y)^2}} \quad (7.1)$$

β_{xy}	Correlation index between x and y
x_i	First parameter x with i index
y_i	Second parameter y with i index
μ_x	Mean value of x
μ_y	Mean value of y

In the next subsections are evaluated the correlations found in the three battery packs that have been tested:

- SOH Self-discharge (7.1);
- SOH EEC parameters (7.2)

Section 7.2 illustrates the indexes for every parameter of the EEC model of the module, to have a better overview of the relationships that occur with the internal degradation processes of the modules. The results of the correlation indexes are then evaluated in the last sections

⁷³ Vgl. Sheldon M. Ross (Introduction to Probability and Statistics for Engineers and Scientists) 2014.

of the chapter, where the comparison of different tests cases is made, considering also the overall trends.

7.1 SOH Self-discharge

The first correlation index that is being evaluated is the one between the SOH and the self-discharge, measured at 100% for 30 minutes. As previously stated, Vgl. Ramoni et al. (End-of-life (EOL) issues and options for electric vehicle batteries) 2013⁷⁴, the self-discharge rate increases with the usage of the battery. For what concerns the available capacity, or SOH, it reduces with the usage of the battery pack Vgl. Ecker et al. (Calendar and cycle life study of Li(NiMnCo)O₂-based 18650 lithium-ion batteries) 2014⁷⁵. Considering these two trends, it can be determined that the correlation between the self-discharge and the SOH is inverse (when one increases the other one decreases and vice versa).

As shown in Figure 7.1 the indexes of the correlation have all negative values. The indexes that refer to the single battery packs have different values, with BP #1 and BP #3 that have the least values (considering their absolute values), respectively -0.1888 and -0.0603. On the other hand, the second battery pack has the highest index of the three, -0.5781.

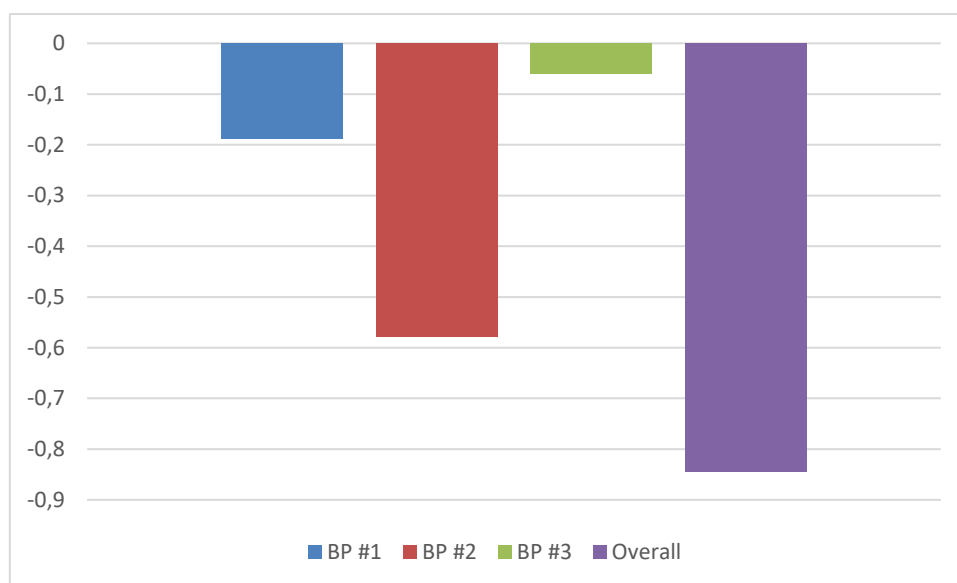


Figure 7.1 Comparison of the correlation indexes between SOH and self-discharge for the three battery packs.

Table 7.1 illustrates the indexes of the three battery packs and the overall index. All four values are negative, leading to the conclusion that for the modules object of the tests the reduction in

⁷⁴ Vgl. Ramoni et al. (End-of-life (EOL) issues and options for electric vehicle batteries) 2013.

⁷⁵ Vgl. Ecker et al. (Calendar and cycle life study of Li(NiMnCo)O₂-based 18650 lithium-ion batteries) 2014.

the SOH goes along with the increase of the self-discharge rate (measured at 100%). Indeed, for the overall cases, the most relevant statistically (144 modules), it has been reached a correlation index of -0.8440. With these results it is assessed that measuring the self-discharge rate, at 100%, gives a good estimation of the actual SOH of the modules. Of course, the accuracy of the estimation could be different based on the SOH of the modules. As shown in Table 7.1, with the same number of modules, 48, the results of the three packs are distant in their values. The correlation is quite high in the range 71%-78%, while it has the least values in the range 81%-88%.

The overall scenario has a wider range, going from 71% to 91% (the least of the second battery pack to the maximum of the first battery pack), and a great number of trials, for these reasons its correlation index is very high.

Table 7.1 Correlation indexes between SOH and self-discharge for the three battery packs.

Correlation indexes SOH-SD		
Battery pack	SOH range	Correlation index
BP #1	88%-91%	-0.1888
BP #2	71%-78%	-0.5781
BP #3	81%-88%	-0.0603
Overall	71%-91%	-0.8440

7.2 SOH and EEC parameters

As it occurred for the self-discharge in this section are calculated and evaluated the correlation indexes of the parameters of the EEC circuit (R_0 , R_1 , R_2 , C_1 , C_2 and R_{tot}) extracted with the pulse tests, with the SOH of the modules. The results are sorted by the parameters, with a subsection for each one. Then, they are sorted by battery pack. The assessments are divided according the following order:

- SOH- R_0 (7.2.1);
- SOH- R_1 (7.2.2);
- SOH- R_2 (7.2.3);
- SOH- C_1 (7.2.4);
- SOH- C_2 (7.2.5);
- SOH- R_{tot} (7.2.5).

With the trends of the correlation indexes it could be possible to assess a fast and reliable way to determine the SOH from the values of the EEC of the module. In the last section of the chapter are summarized the results collected for the different parameters, and a comparison is made.

7.2.1 SOH- R_0

In this subsection are evaluated the correlation that occurs between the parameter R_0 , extracted from the pulse tests, and the SOH of the different modules. To create the plots, it has been used the equation (7.1). In Figure 7.2, Figure 7.3, and Figure 7.4 are shown the trends of the correlation index at different SOC levels and with different C-rates for what concerns the first battery pack. The SOC's and C-rates are the same ones that have been used for the extraction of the parameters during the pulse tests. The trends are sorted by C-rates. The lines that represent 1 C and 1.5 C, respectively red and yellow, start from 0 because at 5% were not performed pulse tests with such C-rates, this occurred for all the three battery packs.

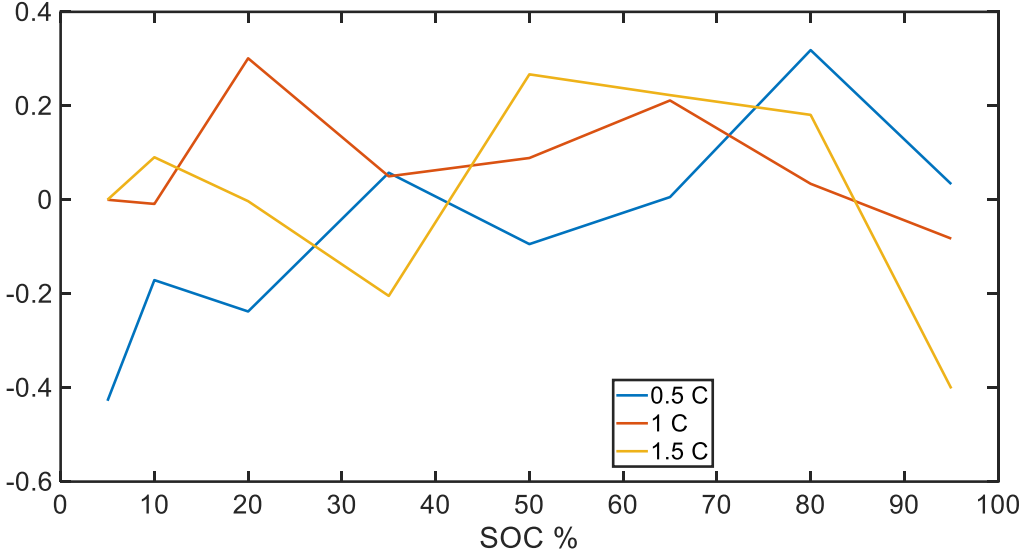


Figure 7.2 Correlation between SOH and R_0 for BP #1 using different C-rates and SOC levels.

As it can be seen from the three graphs, Figure 7.2 (BP #1), Figure 7.3 (BP #2), and Figure 7.4 (BP #3), the trends are quite different among them. Indeed, there are great fluctuations in the values of the correlation of the SOH values and the R_0 measurements. These results may be caused by the fact that the number of modules of one pack does not a statistical relevance.

It can be seen that the fluctuation in the values of the correlation could be due to the fact that the average SOH of the packs is still quite high (for BP #1 and BP #3 above the EOL threshold).

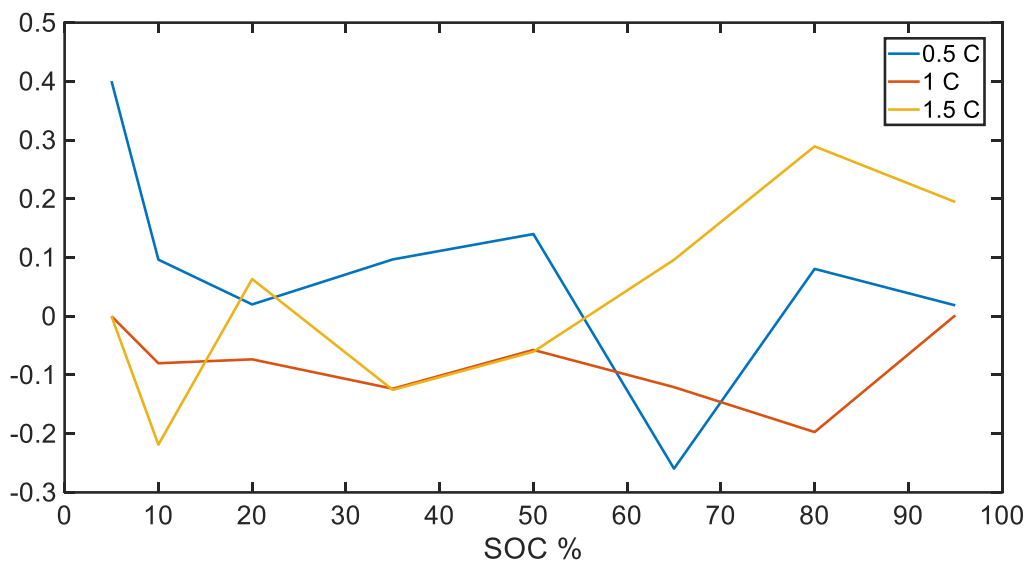


Figure 7.3 Correlation between SOH and R_0 for BP #2 using different C-rates and SOC levels.

As previously stated in the chapter, the values of the correlation that are expected for SOH- R_0 are negative. This is due to the fact generally the resistive parameters increase with the usage of the battery; while, at the same time, the available capacity (SOH) reduces, as presented in Vgl. Sarasketa-Zabala et al. (Cycle ageing analysis of a LiFePO₄/graphite cell with dynamic model validations: Towards realistic lifetime predictions) 2015⁷⁶. For these reasons the majority of the values of the correlation SOH- R_0 are negative. The results presented in Figure 7.2, Figure 7.3, and Figure 7.4 are used to make further evaluations in the next sections of this chapter. Indeed, the highest correlation parameters presented in this subsection will be object of a further study.

⁷⁶ Vgl. Sarasketa-Zabala et al. (Cycle ageing analysis of a LiFePO₄/graphite cell with dynamic model validations: Towards realistic lifetime predictions) 2015.

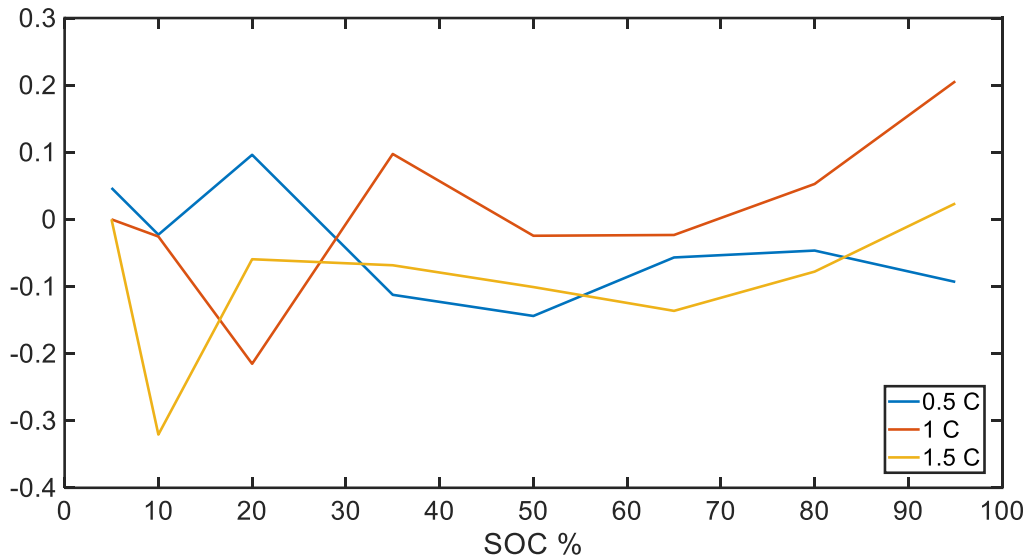


Figure 7.4 Correlation between SOH and R_0 for BP #3 using different C-rates and SOC levels.

7.2.2 SOH- R_1

In this subsection is evaluated the correlation between the SOH and R_1 the resistance of the first RC parallel branch of the EEC that simulates the behaviour of the module of the Nissan Leaf 2011 Edition. As well as for the correlation among SOH percentages and R_0 , the results are presented in the same order as the battery packs have been tested (BP #1 Figure 7.5 , BP #2 Figure 7.6, and lastly BP #3 Figure 7.7). In all the figures of this subsection the correlation indexes of 1 C and 1.5 C at 5% SOC have been set to 0; this had been done because at 5% were not performed the pulse tests with C-rates higher than 0.5 C.

Figure 7.5 shown the results of the correlation between R_1 and the SOH of the first battery pack. As found for R_0 the trend of correlation index does not follow a clear path for all the C-rates considered. However, it can be determined that the correlation of the first battery pack between the SOH and R_1 is negative. Indeed, the majority of the points plotted in Figure 7.5 are below 0. This leads to the idea that when a decrease in the SOH occurs the values of R_1 generally increase. It is interesting to noticed that the most consistent plot of the figure is the yellow one (1.5 C). The other C-rates considered 0.5 C (blue plot) and 1 C (red plot) have negative and positive values, which makes their trends less consistent and reliable for the estimation of the SOH from the measurement of R_1 .

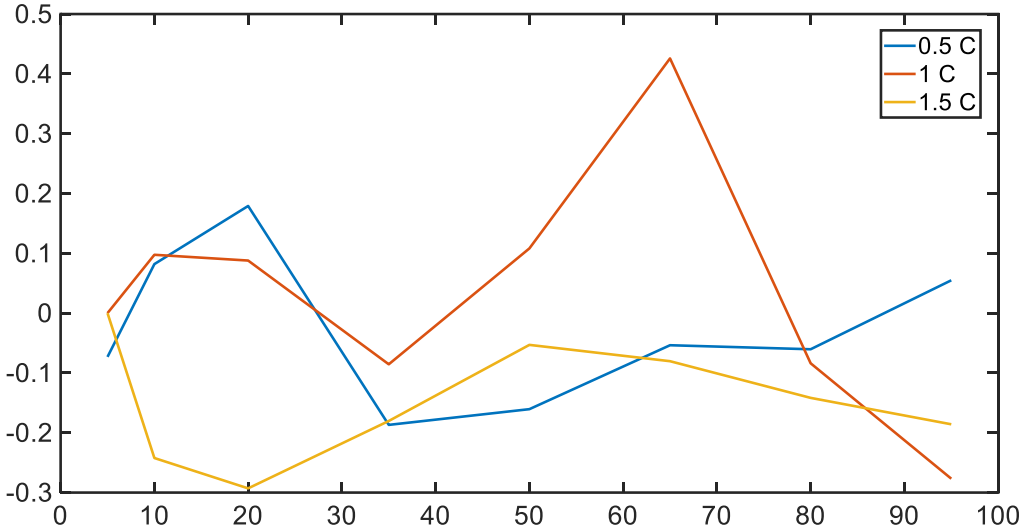


Figure 7.5 Correlation between SOH and R₁ for BP #1 using different C-rates and SOC levels.

Figure 7.6 report the correlation indexes for the second battery pack. The trends found in the first battery pack (Figure 7.5) are confirmed. Indeed, the majority of the point of the plots are negative, with a peak (negative) at 5% with 0.5 C. However, the Figure 7.6 does not present a consistent trend for any of the C-rates object of the test. These results could be caused by the excessive degradation of R₁ for the second battery pack, which has an average SOH of 74.911%.

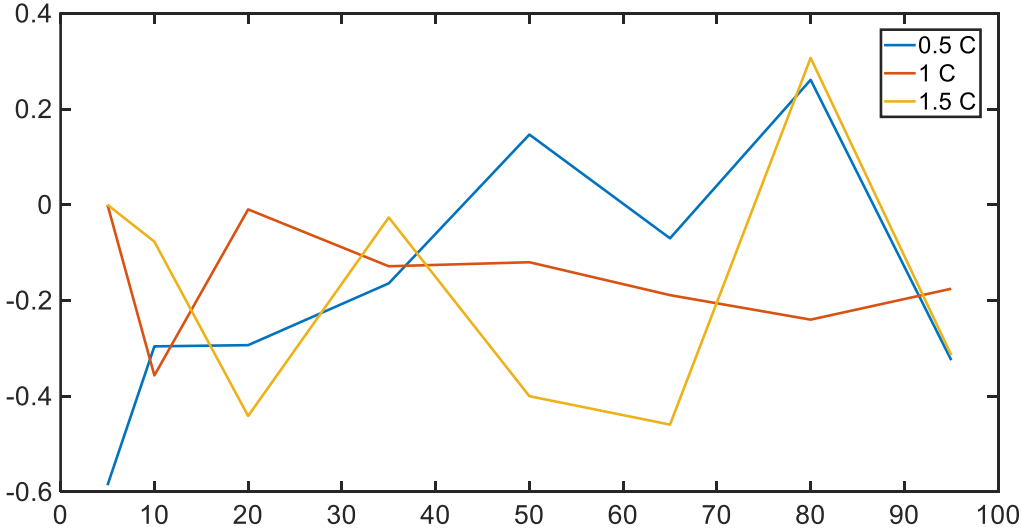


Figure 7.6 Correlation between SOH and R₁ for BP #2 using different C-rates and SOC levels.

In the next figure, Figure 7.7, are presented the trends for the correlation index of the third battery pack. As occurred for the previous packs, the correlation between the SOH of the modules and R₁ is sorted by C-rates. In the figure we can see that the trends for the highest C-rates (1 C and 1.5 C) are similar, with all the plots that have negative values. On the other

hand, the blue plot (0.5 C) has a various trend, with the curve that moves goes up and down with the increase of the SOC. Once again, given the results of the graphs presented in Figure 7.5, Figure 7.6, and Figure 7.7, the most consistent results have been found with the highest C-rate, 1.5 C.

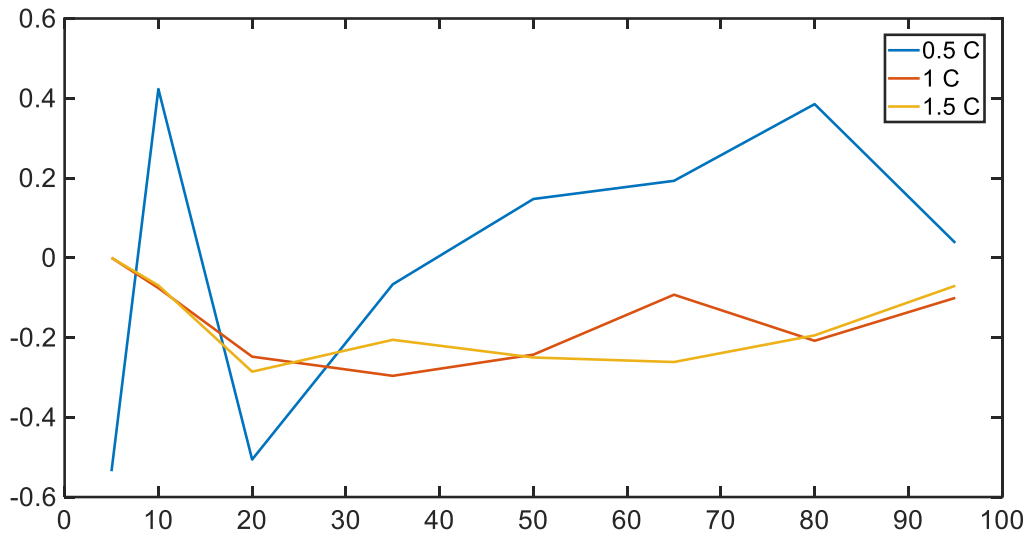


Figure 7.7 Correlation between SOH and R_1 for BP #3 using different C-rates and SOC levels.

7.2.3 SOH- R_2

This subsection evaluates the relationship between the third resistive element, R_2 , of the EEC of the module object of the testing. Figure 7.8, Figure 7.9, and Figure 7.10 show how the correlation between R_2 and the SOH varies in the different packs according to different SOC levels and C-rates.

In all the figures of this subsection the correlation indexes of 1 C and 1.5 C at 5% SOC have been set to 0; this had been done because at 5% were not performed the pulse tests with C-rates higher than 0.5 C.

Figure 7.8 reports the results for the first battery pack. As found for the other resistive parameters the correlation index with the SOH is negative for the majority of the test cases object of the evaluation. For what concerns the trends of the indexes, all the plots fluctuate very much between 0 and -0.2, with two peaks of the blue plot (0.5 C), one at 5% (negative) and one at 80% (positive). As said for the other elements previously evaluated for the first battery pack, due to the high average SOH (89.357%), it is quite difficult to see a clear trend in the correlation with the SOH.

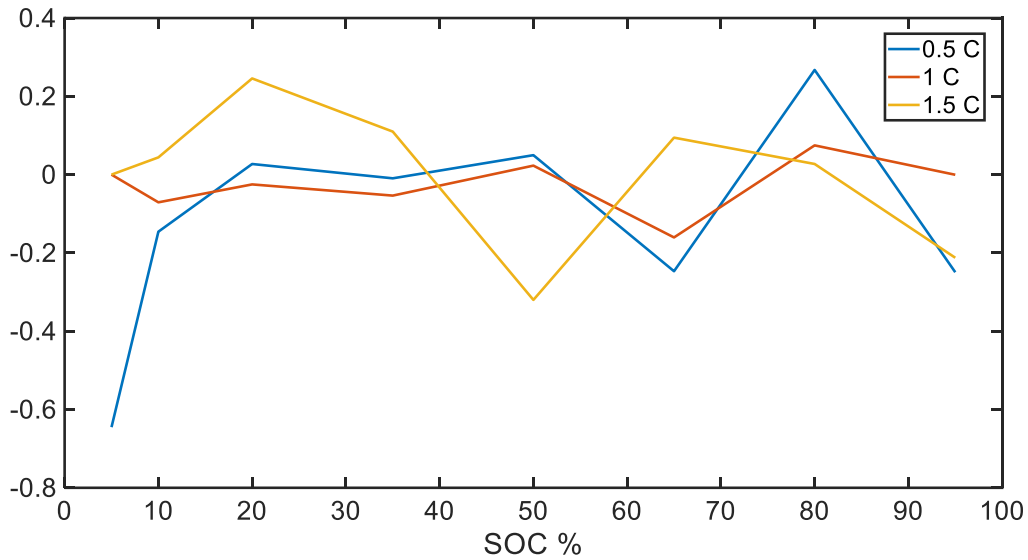


Figure 7.8 Correlation between SOH and R_2 for BP #1 using different C-rates and SOC levels.

The trends of the correlation indexes of the second battery pack (BP #2) are reported in Figure 7.9. On the contrary of the results of the first pack, Figure 7.8, the trends of the curves are more consistent, especially with the increase of the C-rate. Indeed, with the exception of the index at 95%, the plot of 1.5 C (yellow curve), has all negative values, with a peak of more than -0.6 at 10%. As well as for the first battery pack, the curve that represent 0.5 C (blue plot), fluctuates from negative to positive values.

As stated previously, the increase in the consistency of the curves could be related to the lower SOH, which signifies that the ongoing degradation phenomenon has varied the values of R_2 .

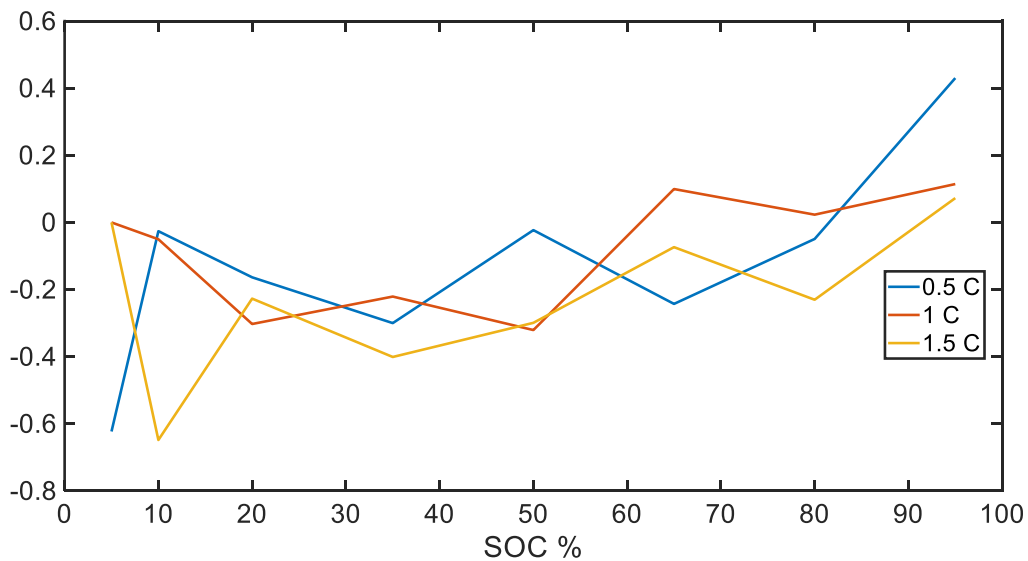


Figure 7.9 Correlation between SOH and R_2 for BP #2 using different C-rates and SOC levels.

The last evaluations for R_2 , based on the results of the third battery pack, are listed in Figure 7.10. The correlation indexes shown present very fluctuant trends, with alternate negative and positive peaks. The plot of the 0.5 C (blue curve), is the one that varies the most, with a minimum of more than -0.5 and a maximum of more 0.3. From Figure 7.10 is hard to find a relationship between the SOH and R_2 , this could be caused by the fact that the average SOH, 83.443%, is above the threshold set for the EOL, 80%, of Li-Ion batteries. In the next sections the relationship between R_2 and the SOH percentage is evaluated using all the data from the three battery packs.

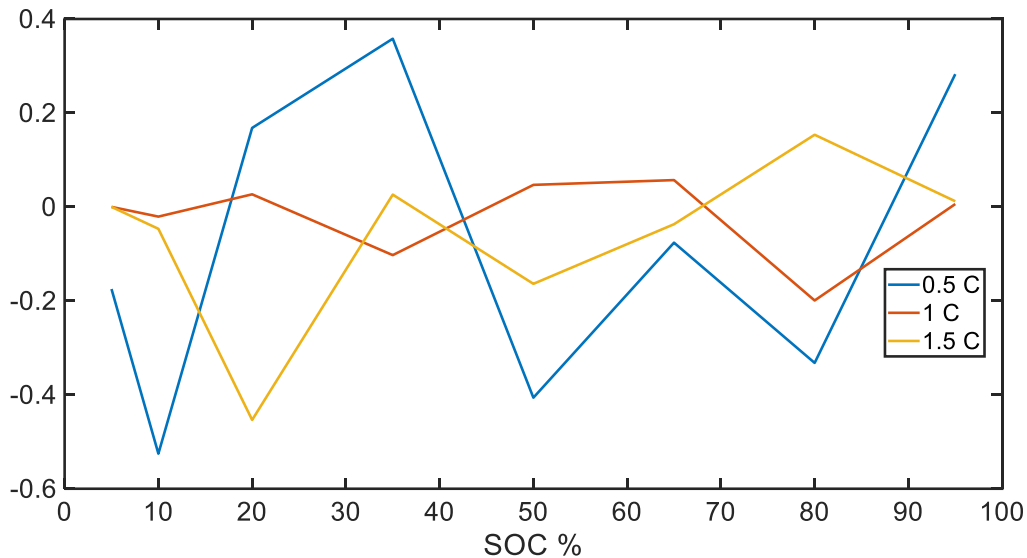


Figure 7.10 Correlation between SOH and R_2 for BP #3 using different C-rates and SOC levels.

7.2.4 SOH- C_1

C_1 is the capacitive element of the first RC branch of the EEC that represent the behaviour of the module. The correlation between the C_1 and the SOH is made in Figure 7.11, Figure 7.12, and Figure 7.13. As stated in Vgl. Sarasketa-Zabala et al. (Cycle ageing analysis of a LiFePO₄/graphite cell with dynamic model validations: Towards realistic lifetime predictions) 2015⁷⁷, the values of the capacitive elements generally decrease with the increase of the degradation, and therefore decrease of the SOH, of the battery. This direct relationship makes the correlation between C_1 and the SOH of the module positive.

In all the figures of this subsection the correlation indexes of 1 C and 1.5 C at 5% SOC have been set to 0; this had been done because at 5% were not performed the pulse tests with C-rates higher than 0.5 C.

Figure 7.11 illustrates the trends of the correlation indexes for the first battery pack. It can be noticed that the only plot that remains always positive is the one of the 1.5 C (yellow curve), which has a peak of 0.3 at 20%. The other two plots, 0.5 C (blue) and 1 C (red) shown go from

⁷⁷ Vgl. Sarasketa-Zabala et al. (Cycle ageing analysis of a LiFePO₄/graphite cell with dynamic model validations: Towards realistic lifetime predictions) 2015

negative to positive values, not showing consistent trends. Once again, the high average SOH, makes difficult to see a clear path in the correlation indexes.

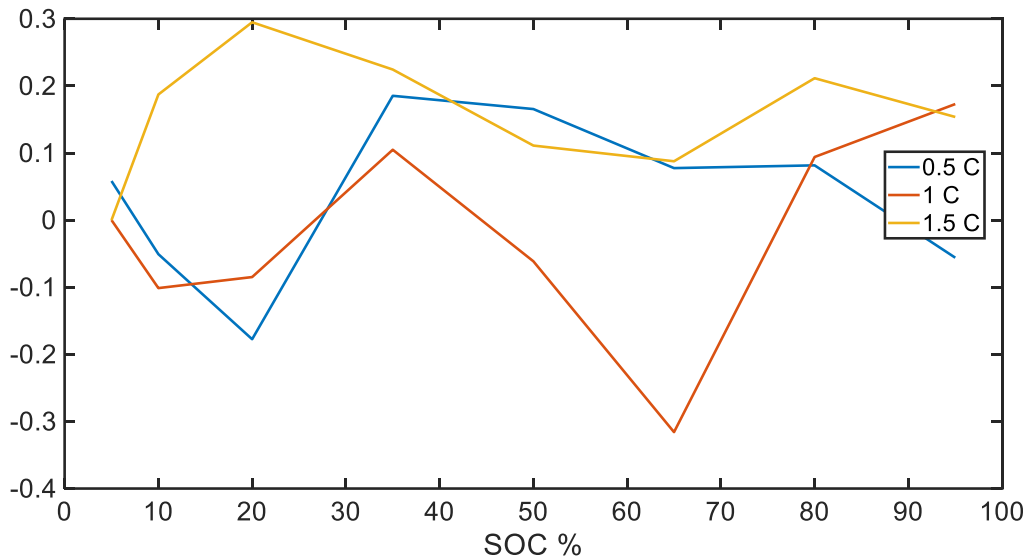


Figure 7.11 Correlation between SOH and C_1 for BP #1 using different C-rates and SOC levels.

Figure 7.12 illustrates the plots regarding the second battery pack. Here, even though the plots are a bit scattered, but the majority of the points have positive values. The only two exceptions come from the 0.5 C test, at 50% and 80%. The same trend was found in Figure 7.11 where most of the points were greater than 0. The trends of the plots of 1 C (red curve) and 1.5 C (yellow curve) are always positive, with the highest C-rate that has three high peaks (above 0.5) at 20%, 50% and 65%. These values show a good correlation between the SOH and the values of C_1 extracted with 1.5 C. Once again, as occurred for the other parameters of the EEC, the most consistent curve results to be the one based on the measurement made with 1.5 C.

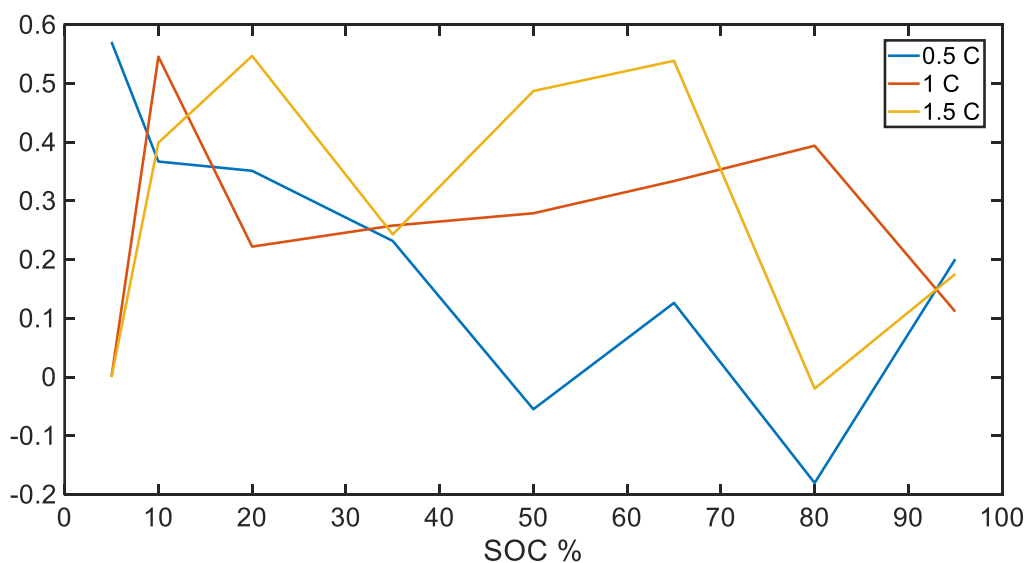


Figure 7.12 Correlation between SOH and C_1 for BP #2 using different C-rates and SOC levels.

In the last figure of this subsection, Figure 7.13, are shown the plots of the third battery pack. The highest correlation index, above 0.5, is found with 0.5 C (blue curve), however, its trend is quite various, with positive and negative values. On the other hand, the plots of the other two C-rates, 1 C (red curve) and 1.5 C (yellow curve), have smaller value, but they have more consistent trends. In particular, the yellow curve has the majority of the correlation indexes greater than 0.2. As occurred in for the other two battery packs, the correlation between the values of C_1 and the SOH percentages of the modules is confirmed to be direct.

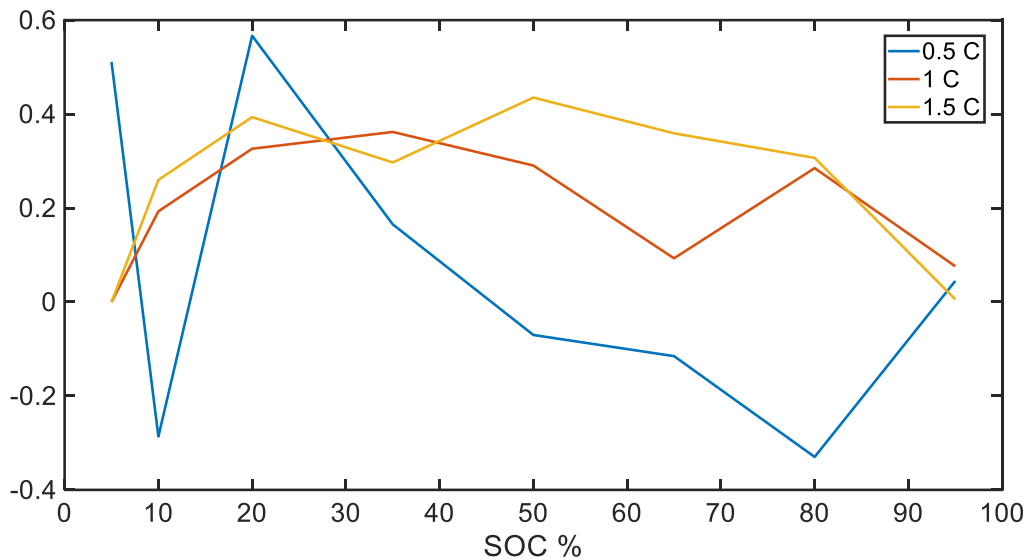


Figure 7.13 Correlation between SOH and C_1 for BP #3 using different C-rates and SOC levels.

7.2.5 SOH- C_2

The second capacitive element of the EEC is C_2 , which is the capacitance of the second RC branch. The trends of the correlation for the three battery pack are shown in Figure 7.14, Figure 7.15, and in Figure 7.16. For all the figures of this subsection the correlation indexes of 1 C and 1.5 C at 5% SOC have been set to 0; this had been done because at 5% were not performed the pulse tests with C-rates higher than 0.5 C.

As occurred for the first capacitive element of the EEC, C_1 , the values of the capacitances decrease with the increase of the degradation, and therefore decrease of the SOH, of the battery. This direct relationship makes the correlation between C_2 and the SOH of the module positive.

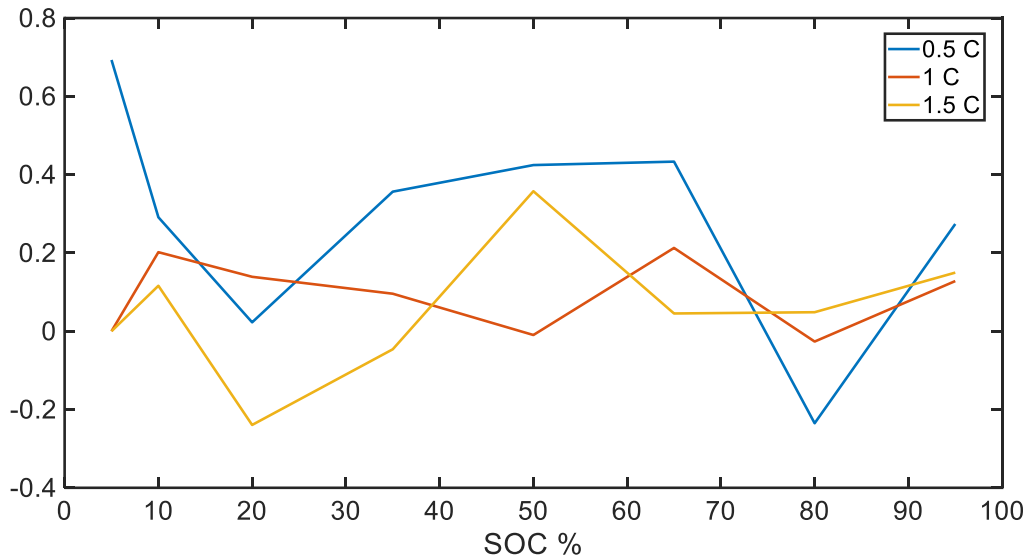


Figure 7.14 Correlation between SOH and C_2 for BP #1 using different C-rates and SOC levels.

Figure 7.14 illustrates the trends of the correlation indexes for the first battery pack. As occurred for other elements of the EEC the trends are not very consistent, especially the one regarding the lowest C-rate, 0.5 C (blue curve). Indeed, its plot has various peaks (the highest at 5%, at 0.7312), and fluctuates from positive to negative values, and vice versa. The trends of the higher C-rates are more stable, but they are not very consistent over the trail points. These behaviour lead to the conclusion that the modules of the first battery pack have not experienced enough degradation, and therefore enough variation in the values of C_2 , to have a good relationship between the SOH and the values of C_2 of the modules.

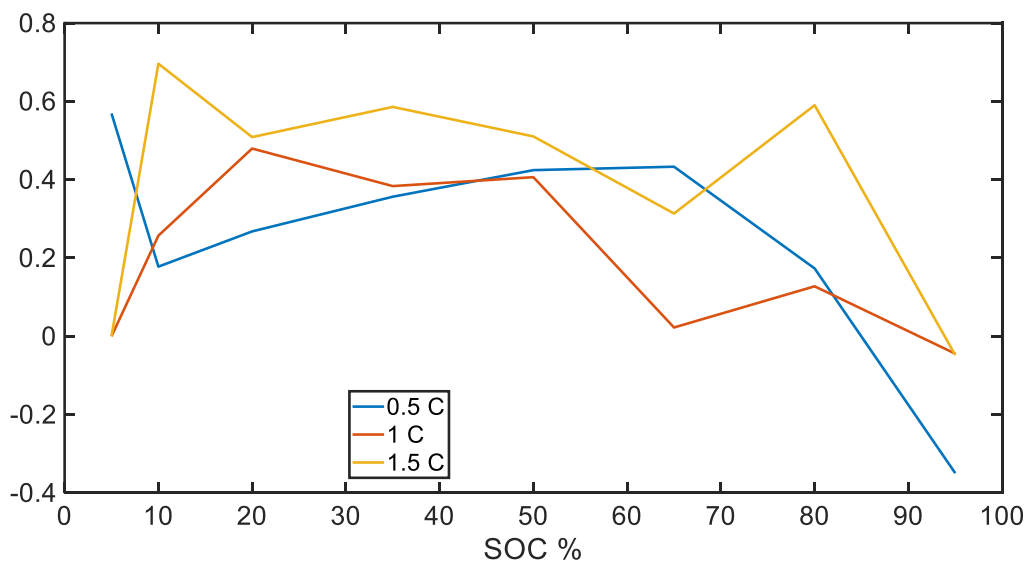


Figure 7.15 Correlation between SOH and C_2 for BP #2 using different C-rates and SOC levels.

Figure 7.15 is reporting the trends of the correlation indexes for the second battery pack. In the figure it can be seen how the correlation indexes are all above 0, with the only exceptions

of the ones at 95%. In addition, the point of the higher C-rate, 1.5 C (yellow curve) have great values, with several peaks above 0.50. The curve of 1 C (red curve) has a similar trend to the 1.5 C one, but the values of the indexes are generally lower. The lower C-rate, 0.5 C (blue curve) has great variation in its values, however in some points the indexes are high (at 5% the values is almost 0.60).

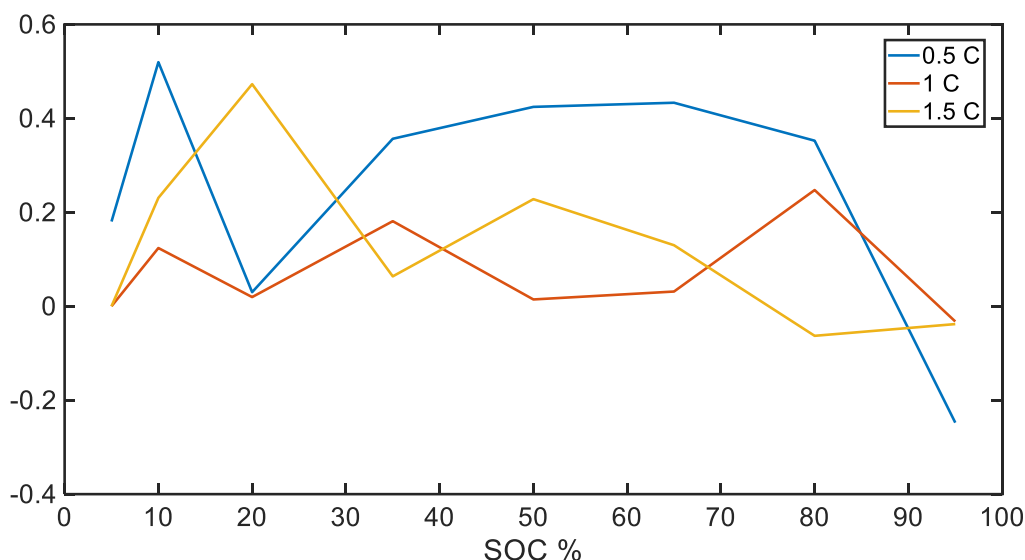


Figure 7.16 Correlation between SOH and C_2 for BP #3 using different C-rates and SOC levels.

In the last figure of this subsection, Figure 7.16, are listed the trends regarding the third battery pack. It is interesting to point out that at 95% there is an inversion in all the trends, with the correlation indexes that are below 0. The other points of the three curves are confirming the trends previously found in BP #1 and BP #2. The highest index, above 0.50 is found at 10% with 0.5 C.

As occurred in for the other two battery packs, the correlation between the values of C_2 and the SOH percentages of the modules is confirmed to be direct (increase in the value of C_2 with the decrease of the SOH of the modules).

7.2.6 SOH- R_{tot}

The last parameter for which are evaluated the correlation indexes with the SOH is R_{tot} . As stated in chapter 3 (State of the art), R_{tot} is the sum of the three resistive elements (R_0 , R_1 , and R_2) that compose the EEC circuit. Thus, Figure 7.17, Figure 7.18, and Figure 7.19 show the trends of the correlation indexes found in the three battery packs.

As occurred for the previous parameters evaluated in all the figures of this subsection the correlation indexes of 1 C and 1.5 C at 5% SOC have been set to 0; this had been done because at 5% were not performed the pulse tests with C-rates higher than 0.5 C.

Figure 7.17 regards the first battery pack. As occurred for some of the other resistive elements, the plots are quite scattered and it not possible to establish a clear trend in the correlation index. The reasons of this behaviour are multiplex, and one of them is the high value of the

average SOH of the first battery pack. Indeed, with such high SOHs the degradation processes that increase the value of the resistive elements have not started or they are small and not easily measurable.

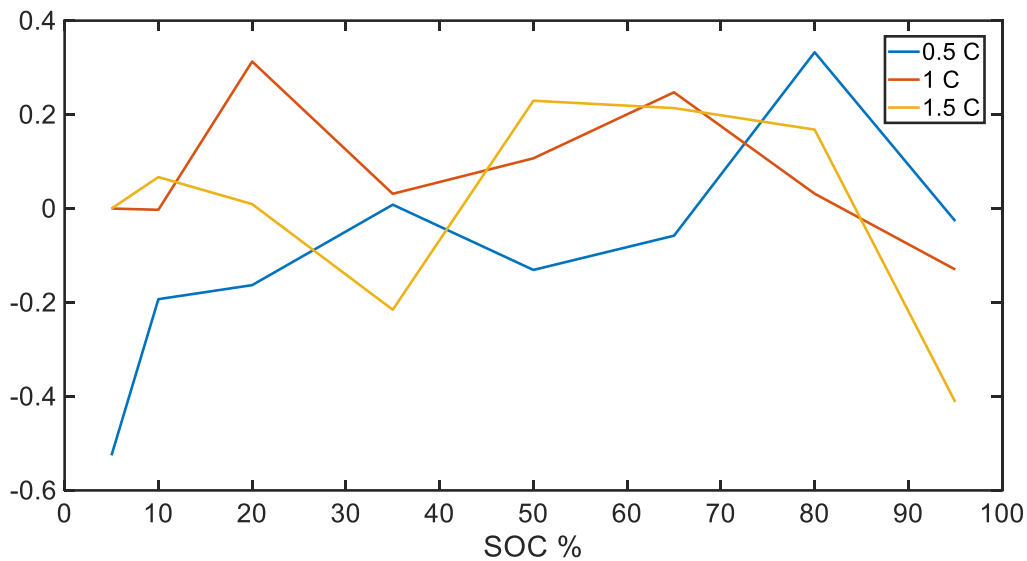


Figure 7.17 Correlation between SOH and R_{tot} for BP #1 using different C-rates and SOC levels.

Figure 7.18 is the second figure of this subsection, in there are presented the trends of the correlation between SOH and R_{tot} of the second battery pack. The trend for all the C-rates is negative, with most of the points of the curves that are below 0. However, the yellow plot, 1.5 C, has two positive peaks at 80% and 95%, respectively 0.3 and 0.2. It is difficult to identify a clear path in the trends, with only the curve regarding the 1 C (blue curve), that appears to have a consistent behaviour.

Since R_{tot} is the sum of the resistive elements of the EEC of the module the trends of the correlation indexes are quite similar to the ones found for the single elements.

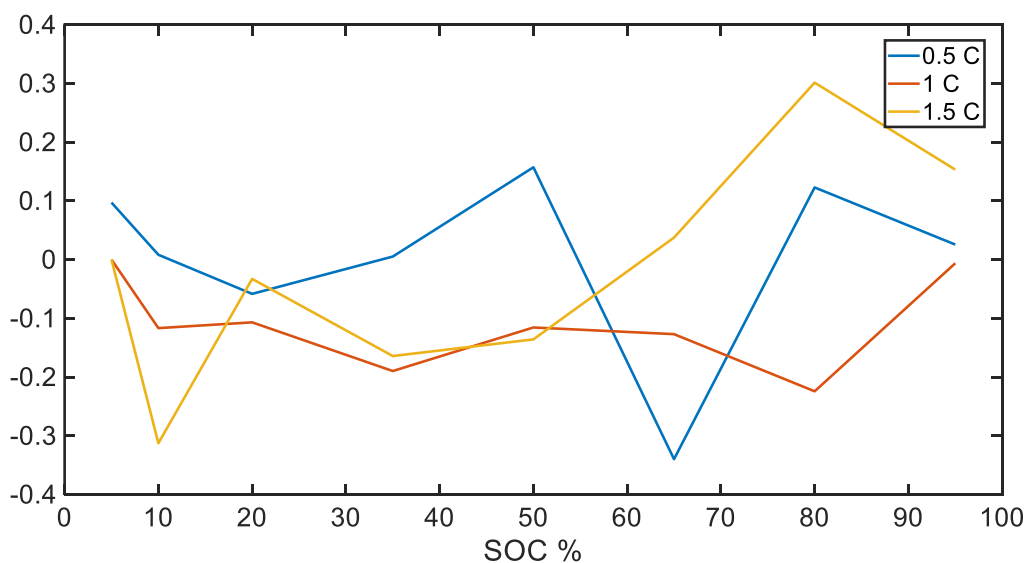


Figure 7.18 Correlation between SOH and R_{tot} for BP #2 using different C-rates and SOC levels.

In the last figure of this subsection are presented the results for the third battery pack. As stated for the other two cases, for the correlation between the SOH and R_{tot} is quite difficult to determine a clear path. Thus, as occurred previously, in Figure 7.19 the trends are scattered, with the plots that go from negative to positive values and vice versa. The only plot that remains always below 0, with the exception of the last point at 95%, is the one regarding the highest C-rate, 1.5 C (yellow curve). As it occurred in other cases, the highest values in the correlation indexes have been found when the highest C-rate has been used (1.5 C).

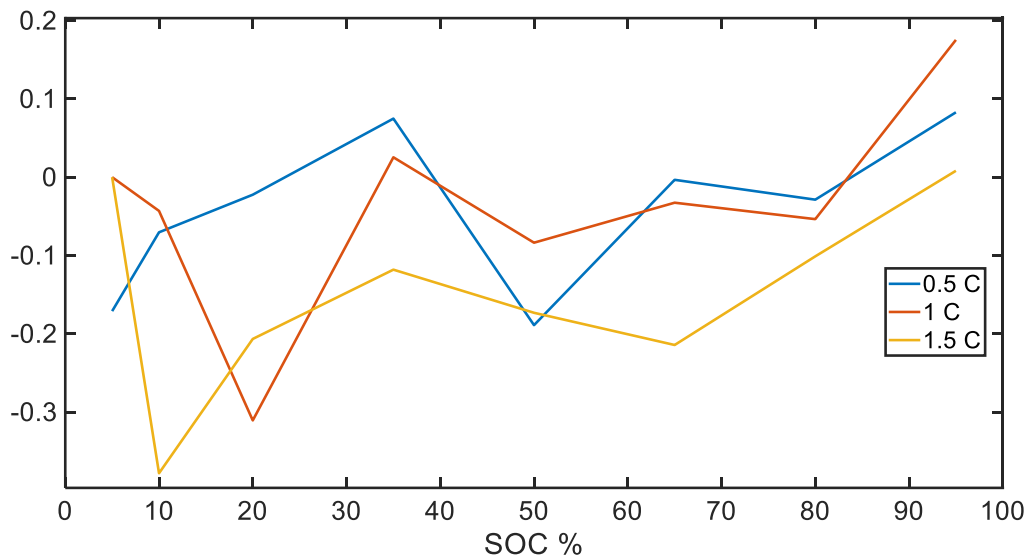


Figure 7.19 Correlation between SOH and R_{tot} for BP #3 using different C-rates and SOC levels.

7.3 Overall correlation trends

Correlation between the parameters of the EEC model of the modules and the SOH. The results are sorted by battery pack, then they are also divided according to different SOC levels (10%, 50% and 95%). These SOC levels have been chosen because they represent the widest range of the measurements that have been collected during the tests. In Figure 7.20, Figure 7.21 and Figure 7.22 are shown the correlation indexes. In order to have a better overview of the results the negative indexes have been changed to positive, by considering only their absolute values. The indexes that that to “Overall” represent the correlation index of the three battery packs combined together. It has been calculated to understand how much the number of modules included in the testing would affect the correlation between their parameters. Indeed, this index refers to 144 trials, while the other three, Battery 1, Battery 2 and Battery 3 refer to 48 trials.

All the indexes presented in Figure 7.20, Figure 7.21 and Figure 7.22 can be found, respectively in Table 7.2, in Table 7.3 and in Table 7.4.

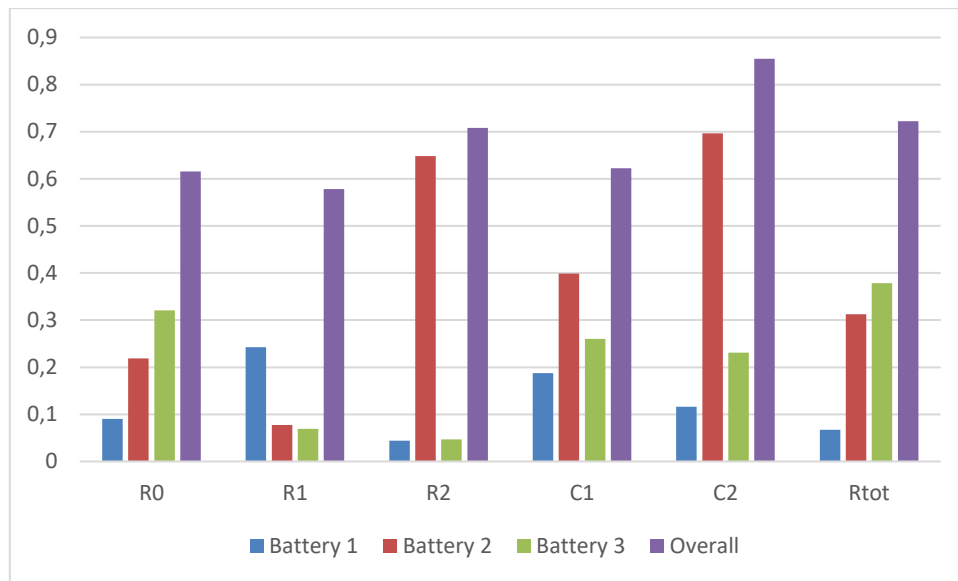


Figure 7.20 Correlation between the SOH and the parameters of the EEC measured at 10% using 1.5 C.

Figure 7.20 shows the correlation indexes between the SOH and the parameters of the EEC of the modules. They have been sorted by the battery packs, in order to evaluate the impact that the general SOH has on the results. Both Figure 7.20 and Table 7.2 refer to the parameters measured at 10% SOC using pulses of 1.5 C. As it can be noticed from the plot, the indexes that refers to Overall are the greatest. Indeed, in all the cases evaluated it has always had the highest values. As Table 7.2 shows, the highest value is found in the correlation between the SOH and C_2 , 0.8549. This value is positive, which indicates that the correlation is direct, the trend indicates that to the decrease of the SOH it corresponds a decrease in the value of C_2 . The same occurs for the other Capacitance of the EEC, C_1 , that has a correlation index of 0.6222.

Table 7.2 Correlation between the SOH and the parameters of the EEC measured at 10% using 1.5 C.

Correlation SOH EEC parameters at 10% with 1.5 C						
	R ₀	R ₁	R ₂	C ₁	C ₂	R _{tot}
BP #1	0.0905	-0.2422	0.0440	0.1872	0.1161	0.0670
BP #2	-0.2186	-0.0771	-0.6483	0.3991	0.6963	-0.3127
BP #3	-0.3207	-0.0694	-0.0467	0.2600	0.2308	-0.3781
Overall	-0.6157	-0.5785	-0.7080	0.6222	0.8549	-0.7221

For what concerns the resistive parameters of the EEC, the correlation indexes are negative. This means that when the SOH is decreasing R_0 , R_1 , R_2 and R_{tot} increase their values. As Table 7.2 shows, with some exceptions, the highest values in the correspondence are found

in the third battery pack. This is due to the fact that the capacity in the first pack is not very high (average SOH 89.357%) and therefore the processes of degradation are not severe yet. For what concerns the second battery pack, its average SOH, 74.911%, is below the EOL threshold (80%), this causes some of the correlation indexes to have smaller values (considering their absolute values).

For what concerns the highest indexes, of the scenario 10% with 1.5 C, they are found with C_2 and R_{tot} , when all the three battery packs are considered. However, all of the correlation indexes regarding the overall case are quite high, with the lowest found with R_1 , -0.5785.

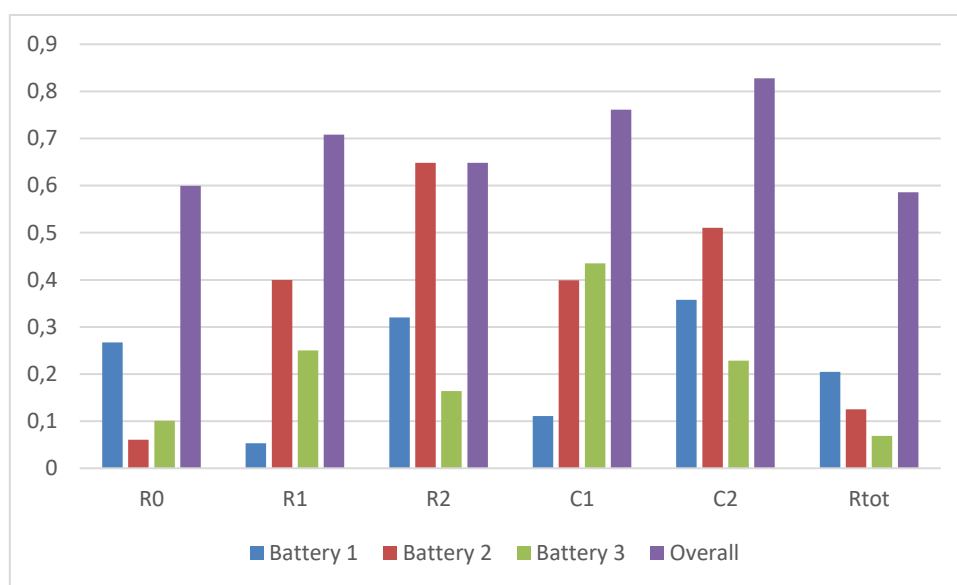


Figure 7.21 Correlation between the SOH and the parameters of the EEC measured at 50% using 1.5 C.

Figure 7.21 and Table 7.3 report the test case performed at 50% SOC with 1.5 C. As can be seen in Figure 7.21, the trends found in the scenario 10%-1.5 C are confirmed. Indeed, the case that combines the results of the three packs has the highest values of the correlation index. However, there is a case, R_2 , where the correlation index, considered by its absolute value, of the second battery pack (red bar), -0.6483, has the same value of the overall one, 0.6485, (purple bar). As found for the first scenario 10%-1.5 C the resistive parameters have negative correlation indexes, while the capacitive parameter ones are positive. In addition, the correlation between the capacitances C_1 and C_2 have the two highest indexes, respectively 0.7614 and 0.8281 the test cases.

As it was determined in the first case, 10% - 1.5 C, the correlation indexes of the overall case are quite high. Indeed, their values are all above 0.60, with two exceptions R_0 , -0.5994, and R_{tot} , -0.5858. As stated for the first case, the evaluation of the SOH of the modules, or the entire battery pack, could be performed with the use of the parameters of the EEC, measured at 50% using 1.5 C (66 A).

Table 7.3 Correlation between the SOH and the parameters of the EEC measured at 50% using 1.5 C.

Correlation SOH EEC parameters at 50% with 1.5 C						
	R ₀	R ₁	R ₂	C ₁	C ₂	R _{tot}
BP #1	0.2670	-0.0531	-0.3200	0.1111	0.3576	-0.2047
BP #2	-0.0604	-0.4000	-0.6483	0.3991	0.5105	-0.1254
BP #3	-0.1007	-0.2500	-0.1641	0.4351	0.2283	-0.0685
Overall	-0.5994	-0.7085	-0.6485	0.7614	0.8281	-0.5858

Figure 7.22 and Table 7.4 represent the evaluation of the correlation indexes performed at 95% using 1.5 C. As well as for the previous two study cases, the results are presented sorted by battery packs. At first sight it can be seen that the maximum values of the indexes are lower than the ones of the other cases. Indeed, all the correlation parameters are below 0.60, while for the 10%-1.5 C and 50%-1.5 C.

Other differences with the previous cases are the correlations with the capacitive elements of the EEC. Indeed, the relationships between C₁ and C₂ and the SOH was stronger in at lower SOC (10% and 50%). At 95% the indexes for C₁ and C₂ are 0.4180 and 0.3062, while in the first two cases reached 0.8281 (C₂ at 50% SOC), considering the overall scenario.

On the other hand, the resistive parameters kept the same trends, the indexes continued to be negative. Their absolute values go from the minimum 0.4387, R₀, to 0.5977, R₁, both of the values are of the overall case. Even though the trends of the resistive elements remained constant, as it occurred for the capacitive elements, their indexes generally decreased with respect to the previous cases.

An interesting result are the very low correlation indexes for the third battery pack (green bars), indeed, for all the parameters of the EEC the third battery pack results to have the least values. At 95% SOC the correlation indexes between the SOH and all of the EEC parameters are below 0.10, which is a very small value.

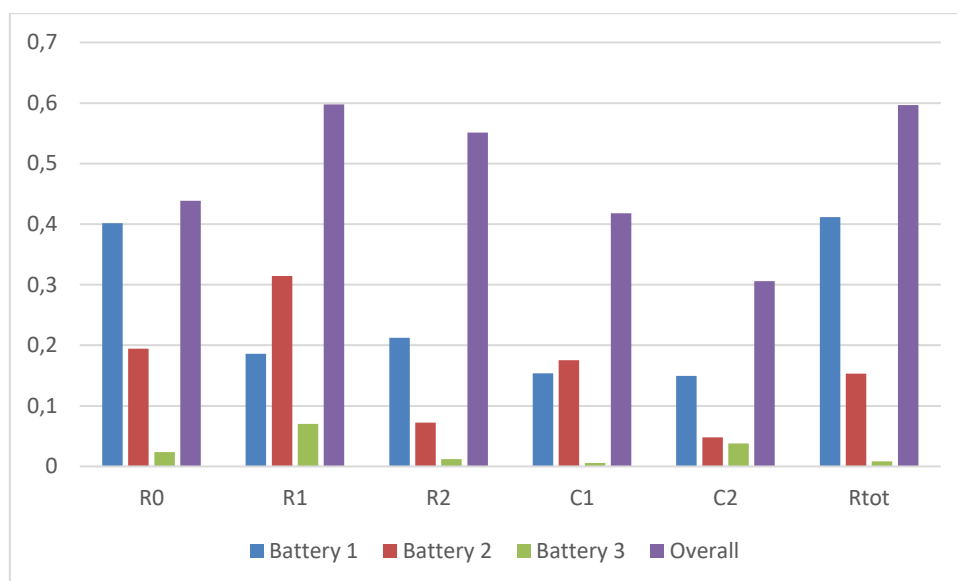


Figure 7.22 Correlation between the SOH and the parameters of the EEC measured at 95% using 1.5 C.

Table 7.4 Correlation between the SOH and the parameters of the EEC measured at 95% using 1.5 C.

Correlation SOH EEC parameters at 95% with 1.5 C						
	R ₀	R ₁	R ₂	C ₁	C ₂	R _{tot}
BP #1	-0.4016	-0.1858	-0.2123	0.1537	0.1497	-0.4119
BP #2	0.1946	-0.3142	0.0725	0.1755	-0.0482	0.1532
BP #3	0.0239	-0.0703	0.0120	0.0056	-0.0381	0.0084
Overall	-0.4387	-0.5977	-0.5511	0.4180	0.3062	-0.5969

Table 7.5 lists the highest correlation indexes for each parameter that has been extracted from the performed tests. In addition, the table reports the type of correlation (direct or inverse) that occurs between the SOH and those parameters. All the indexes refer to the overall study case (144 modules). This study case has been chosen because for all the parameters it presented the highest values, considering their absolute values, for the correlation of the parameters with the SOH of the modules.

Five out of seven correlations are inverse, which means that for those parameters (SD, R₀, R₁, R₂, and R_{tot}) the reduction in the SOH values would result in the increase of their values. Indeed, as shown in Figure 7.23, the bars corresponding to those parameters are plotted below the line representing 0. On the other hand, the remaining two parameters have a direct correlation with the SOH. Hence, to a decrease of the SOH it corresponds the increase of the capacitive parameters of the EEC (C₁ and C₂).

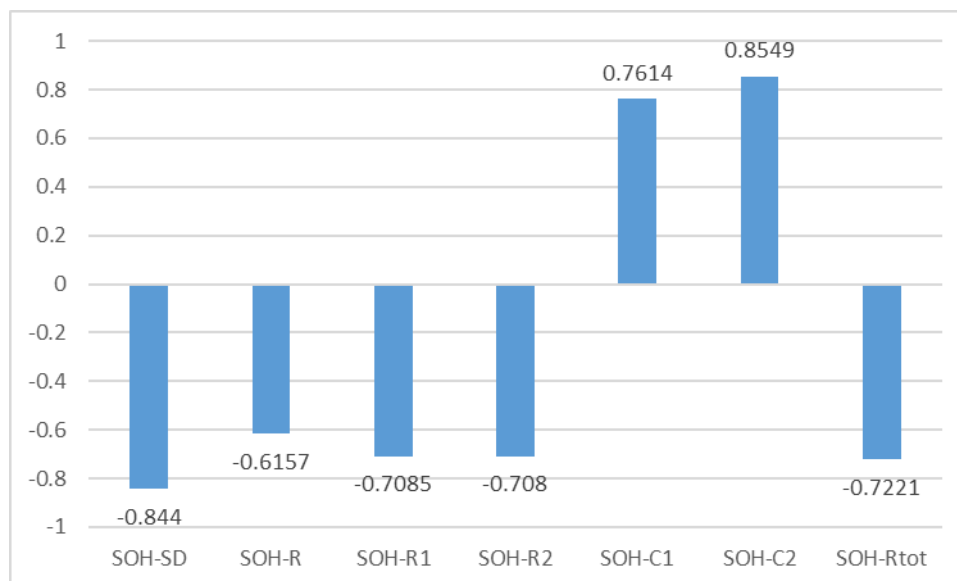


Figure 7.23 Highest correlation indexes for the different parameters extracted from the testing procedure.

Considering the absolute values, as can be seen from Table 7.5 and from Figure 7.23, the correlation indexes are quite high. Indeed, the lowest one is found for R_0 , -0.6157, which is an overall good correlation index. Then, there are the indexes for R_1 , R_2 , and R_{tot} , all of them are negative, respectively -0.7085, -0.7080 and -0.7221. The three highest correlation indexes are found for C_1 , self-discharge (SD), and C_2 , correspondingly 0.7614, -0.8440, and 0.8549. The highest index is found for C_2 , 0.8549, meaning that the change in the values of C_2 could be used to express and evaluate the variation in the SOH percentages.

Table 7.5 Summary of the highest correlation indexes (absolute values) found for the overall case study, between SOH and the parameters extracted from the tests.

Parameters	Type of correlation	Index
SOH- C_2	Direct	0.8549
SOH-SD	Inverse	0.8440
SOH- C_1	Direct	0.7614
SOH- R_{tot}	Inverse	0.7221
SOH- R_1	Inverse	0.7085
SOH- R_2	Inverse	0.7080
SOH- R_0	Inverse	0.6157

Given the results listed in Figure 7.20, Figure 7.21, Figure 7.22, Figure 7.23, Table 7.2, Table 7.3, Table 7.4, and Table 7.5, different evaluations can be made. First of all, as it was ex-

pected, the increase in the number of trials has increased the indexes of the correlation between the SOH and the parameters of the EEC of the module. In all the test cases that had been evaluated the overall's indexes (144 modules) had the highest correlation, compared to the single battery packs (48 modules).

In some cases, there was a great difference between the results of the single pack and the overall. This result could be caused by different factors. In some cases, the SOH of the pack has not reached the threshold at which the internal degradation processes vary the parameters of the battery, and therefore the phenomena are difficult to experience. At the same time, in other cases, the SOH could have already trespassed the limit at which the sudden change in the values occurs, thus making more difficult to determine a good relationship between the processes.

However, with the use of large datasets a strong relationship between the parameters of the EEC of the battery and the remaining available capacity. Along with the parameters of the EEC, the self-discharge rates can be used to assess the SOH with a good reliability.

All the presented tests can be performed to have better and deeper results on the SOH of the battery. In addition, after a campaign of testing, the results can be used to speed up the testing processes, reducing the testing procedure. Indeed, evaluated the outcome and the results of the campaign, the testing procedure can be shaped accordingly.

For example, the number of pulse tests can be reduced or the SOC levels and the C-rates adjusted. With this technique, the amount of time of the tests can be managed differently, reducing the total duration. The tests can be also designed according the different second life uses (remanufacturing, energy storage, power smoothing etc.).

8 EEC Simulations

In this chapter the data extracted from the tests and then presented in chapter 6 (Results and discussion) and in chapter 7 (Correlation between parameters and SOH) are used to parametrize a EEC model. The model refers to the EEC model presented in chapter 2 (General overview), indeed, it is the same model on which the pulse tests have been based. The EEC model presented (second order) has been implemented in Simulink using look-up tables from Matlab.

Thus, the model, presented in section 8.1 (Simulink model) model has been built using Simulink blocks and Matlab scripts. With the use of this model different test cases (varying the C-rate and the SOC level for the charge) could be performed, enabling the possibility of further analysis of the characteristics of the battery under different stress levels and at different operating points.

Indeed, the simulation made possible the use of higher C-rates (up to 4 C, 264 A), which were not available during the testing campaign. The focus of the simulations is on the losses due to the internal resistances. Indeed, in the sections of this chapter are reported the analysis of the simulation's results. In section 8.2.1, are shown the losses on the 0-100% charge, then in section 8.2.2 are evaluated the internal losses occurring during the 20-80% charge. The final test case that has been simulated is the 35-65% charge, presented in section 8.2.3.

8.1 Simulink model

The Simulink model used for the simulations presented in this chapter is a dynamic model. Being a dynamic model, it can simulate the dynamics that occur when the battery is being used, but it does not take into account the possible internal degradation of the cell. The model has been parametrized with the data presented in Chapter 6. Since some of the measurements were not possible to perform during the final testing protocol (high C-rates), those values have been estimated and calculated based on the trends found.

For what concerns the parametrization of the model the parameters have been adjusted as shown in Table 8.1. The SOC levels have been divided in ranges (ex 20-35%) according to the data extracted from the pulse tests. The SOC levels inside the range will have the value of the closest measurement. For instance, the measurement at 25% does not exist, but there are the ones at 20% and at 35%, the closest SOC level for which the data have been collected is 20%. Therefore, the parameters used for the EEC model will be the same of the 20% SOC. Using this process, it is possible to simulate the behaviour as better as possible, given the available data. The resolution of this division has been set to 1%.

Table 8.1 Characterization of the SOC levels for the internal resistive parameters of the EEC model.

SOC range	SOC level for the parameters
SOC < 7% (only for C-rates lower than 0.5 C)	5%
8-15%	10
16-27%	20
28-42%	35%
43-57%	50%
58-72%	65%
73-87%	80%
SOC > 87%	95%

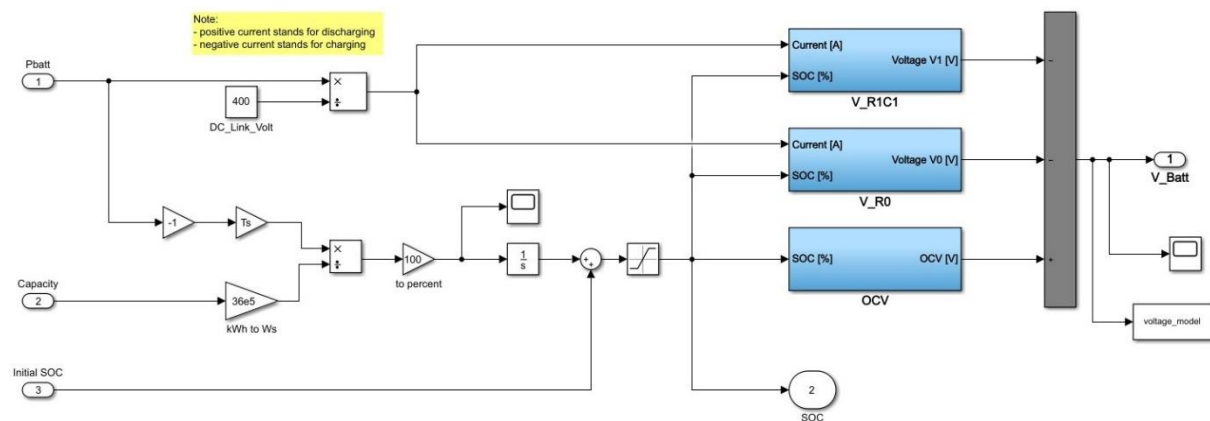


Figure 8.1 Simulink dynamic model of the EEC of the module of the Nissan Leaf 2011 Edition.

In order to evaluate the losses due to the internal resistive parameters (R_0 , R_1 , and R_2) of the module, equations (8.1) and (8.3) have been implemented in the Simulink model presented in Figure 8.1. The first equation (8.1) is used to calculate the instantaneous loss in terms of power. Equation (8.3) calculates the energy that has been dissipated due to the resistive parameters over a certain amount of time. As can be seen, both of the equations have the parameter I_{batt} that is squared, and it is then multiplied by the resistance (that can change according to the index i). In these cases, the index can be 0, 1, or 2, depending of which resistive parameter of the EEC is considered.

$$P_{L,i} = R_i \cdot I_{batt}^2 \tag{8.1}$$

- $P_{L,i}$ Power loss by the resistor i (W)
- R_i Resistance i (Ω)
- i Index of the parameter

I_{batt} Current of the battery (A)

$$E_L = \int_{t_1}^{t_2} R \cdot I_{batt}^2 dt = \int_{t_1}^{t_2} P_L dt \tag{8.2}$$

E_L Energy loss due to the resistance R (W)

t_1 Start of the charge/discharge phase (s)

t_2 End of the charge/discharge phase (s)

Figure 8.2 illustrates how the dynamic of the battery is evaluated for the first RC branch. The values recorded during the pulse tests are implemented in the look up tables for R_1 and C_1 , divided into the charge and discharge phases. Since the data extracted from the pulse tests are only with a discharge pulse, the look up tables for the charging and discharging states of the parameters (R_0 , R_1 , R_2 , C_1 , and C_2) have been created by using the data of the discharge pulse.

However, the lookup tables are in two dimensions, one for the different C-rates and the other one based on the SOC levels. As shown in the next paragraphs of this section, the characteristics of the parameters at high C-rates (greater than 1.5 C) have not been tested. For these reasons an evaluation of the change in the values of the parameters has been performed and presented.

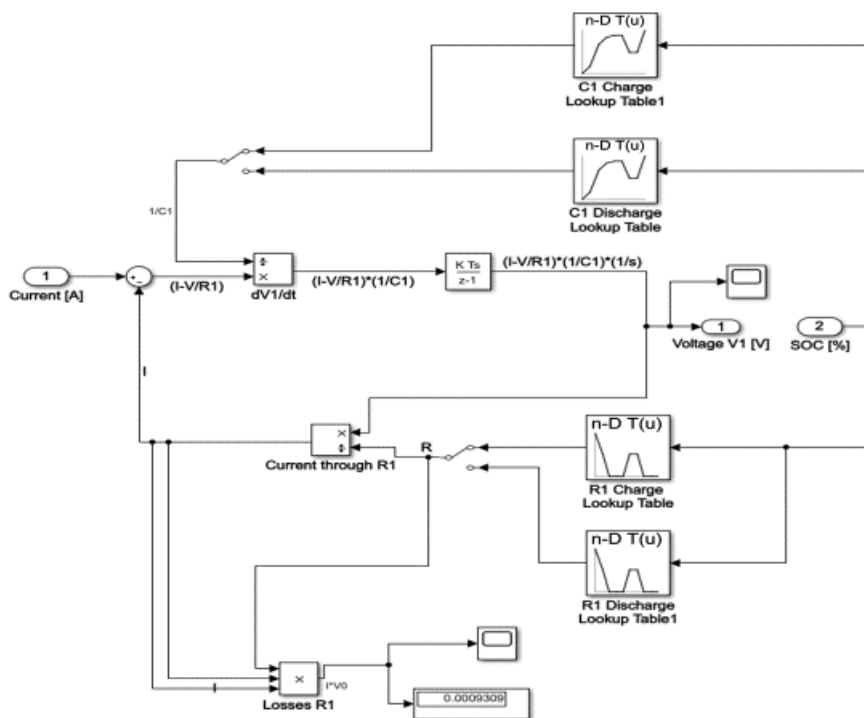


Figure 8.2 Particular of the Simulink model, it represents the behaviour of the R_1C_1 parallel branch during the use of the battery.

The values of R_{tot} of the module M11, from BP #2, remain quite constant when the C-rate increases. In some cases, 20% (red plot) and 80% (dark blue plot) there are limited increases in the values of R_{tot} . The value that changes the most is the one measured at 95%, which starts from 4 m Ω at 0.5 C and goes down to 2.5 m Ω at 1.5 C. In the other cases, the measurements of R_{tot} have values very similar.

Given the trends presented in Figure 8.3, in Figure 8.4, and in Figure 8.5, it is not possible to determine, with a good reliability, the trend of R_{tot} when the C-rates is higher than 1.5 C. For these reasons it has been decided that for the values of R_{tot} , when the C-rate is higher than 1.5 C is kept constant. Thus, the values of R_{tot} that have been used for C-rates greater than 1.5 C, 2 C and 4 C, are the same of the 1.5 C case. Then are presented the C-rates used in the different study cases and their conversion into current (measured in A). The C-rates have been chosen for various reasons, first of all 0.5 C, 1 C, and 1.5 C have been chosen because the data were available from the tests. Then, 2 C and 4 C have been chosen because they are the C-rates at which it is usually possible to charge the EVs from public charging stations (2 C gives total power of 48 kW, while 4 C 96 kW) Vgl. Spöttle et al. (Research for TRAN Committee - Charging infrastructure for electric road vehicles) 2018⁷⁸.

With a wide range of C-rates it is possible to have a better understanding of how much the internal parameters of the battery influence the energy losses that occur when the battery is being used. To have the parameters of the EEC for the C-rates that have not being tested the following procedure has been performed.

As occurred for some of the voltage levels not all the C-rates used in the simulations have data coming from real measurements. Indeed, for 0.1 C, 2 C, and 4 C have not been performed the pulse tests. For this reason, the parameters of the EEC for such C-rates are not available. In order to run the simulation, the datasets for those C-rates have been determined.

In Table 8.2 are listed the C-rates that have been used to perform the different simulations, as can be seen the lowest is 0.1 C, which corresponds to 6.6 A, while the greatest is 4 C, which is equal to 264 A. This wide range enable to understand the behaviour of the module under different operating conditions.

⁷⁸ Vgl. Spöttle et al. (Research for TRAN Committee - Charging infrastructure for electric road vehicles) 2018.

Table 8.2 List of the study cases performed during the simulations using the Simulink EEC model.

C-rates (C)	Current (A)
0.1 C	6.6 A
0.5 C	33 A
1 C	66 A
1.5 C	99 A
2 C	132 A
4 C	264 A

For the determination of the behaviour of the internal parameters of the EEC the data recorded during the tests have been used. Therefore, the evaluation is based on the data of 0.5 C, 1 C, and 1.5 C. From the values of the internal parameters it has been evaluated the trends occurring when the same parameter was measured with different C-rate.

In Figure 8.3, in Figure 8.4, and in Figure 8.5 are presented the measurements of R_{tot} at different SOC and with C-rates, respectively for BP #1 M35, BP #2 M11, and BP #3 M13. As shown, the effect of increasing the C-rate could have different results. In some cases the value of R_{tot} increases (10% SOC in Figure 8.3 and in Figure 8.5), in other cases the value remains constant (or with a small variation, ex 10% SOC in Figure 8.4). In some other cases, the value of R_{tot} decreases with the increase of the C-rate (95% SOC in Figure 8.4).

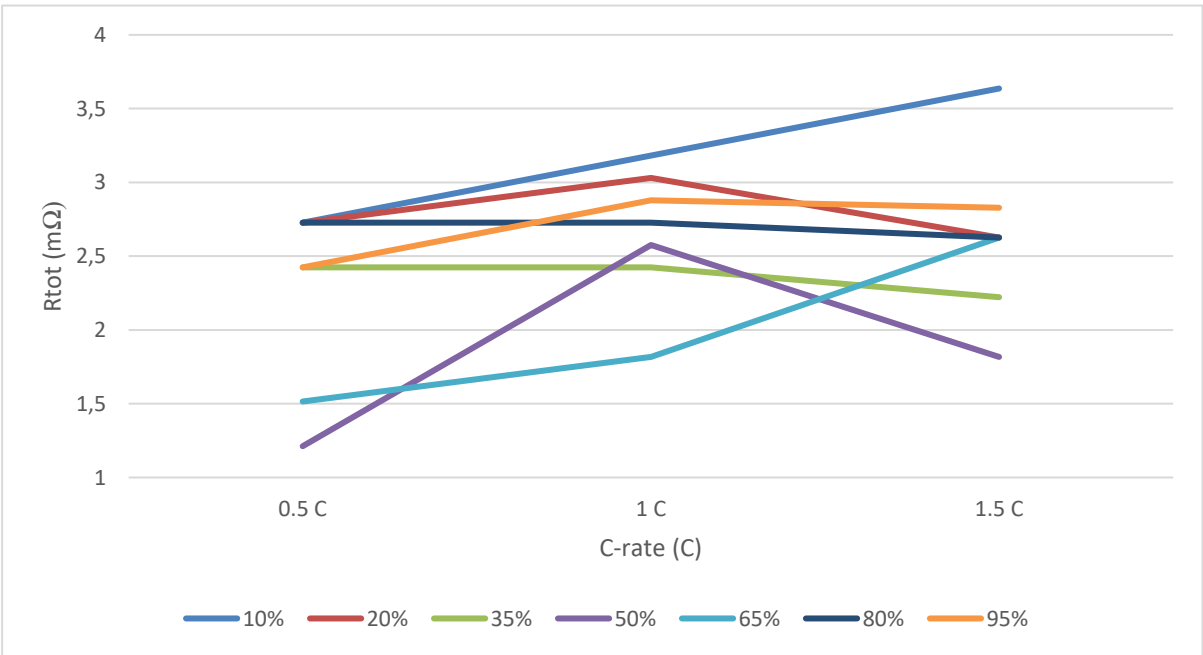


Figure 8.3 Trends of the change of the total resistance R_{tot} with at different C-rates for M35 BP #1.

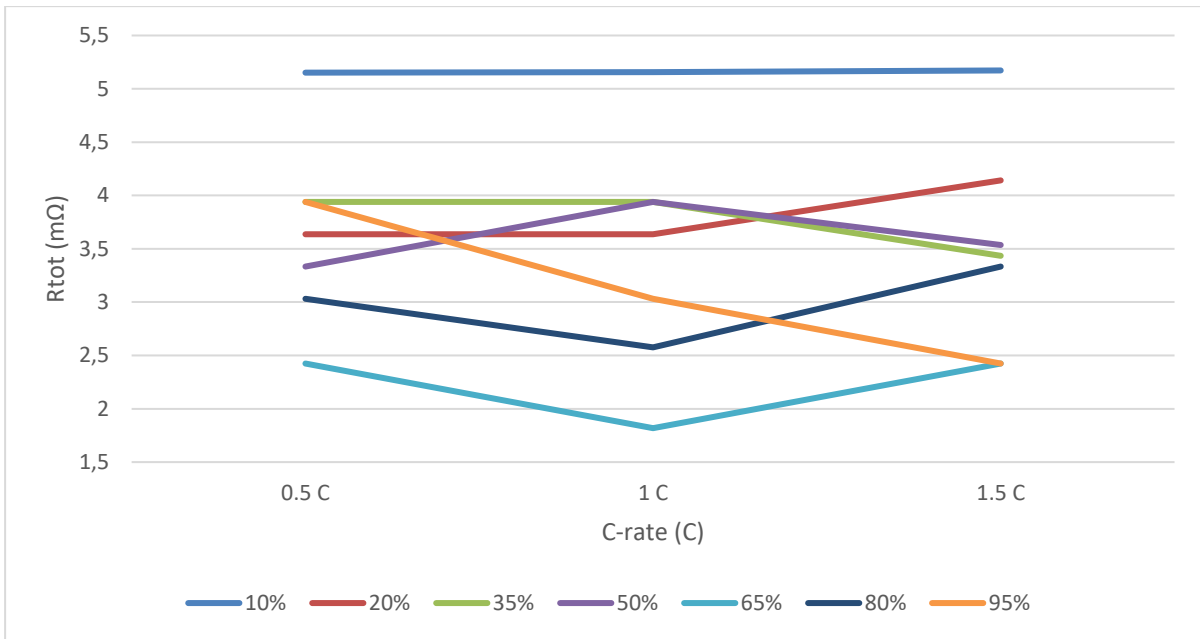


Figure 8.4 Trends of the change of the total resistance R_{tot} with at different C-rates for M11 BP #2.

The values of R_{tot} of the module M11, from BP #2, remain quite constant when the C-rate increases. In some cases, 20% (red plot) and 80% (dark blue plot) there are limited increases in the values of R_{tot} . The value that changes the most is the one measured at 95%, which starts from 4 $m\Omega$ at 0.5 C and goes down to 2.5 $m\Omega$ at 1.5 C. In the other cases, the measurements of R_{tot} have values very similar.

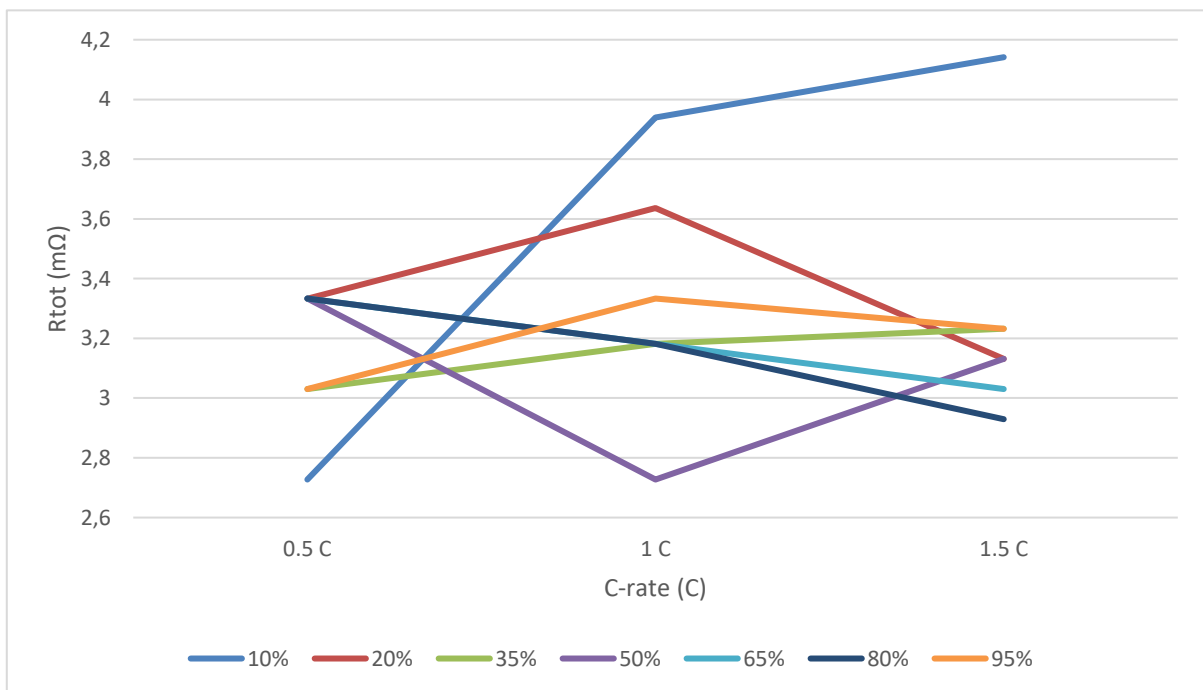


Figure 8.5 Trends of the change of the total resistance R_{tot} with at different C-rates for M13 BP #3.

Given the trends presented in Figure 8.3, in Figure 8.4, and in Figure 8.5, it is not possible to determine, with a good reliability, the trend of R_{tot} when the C-rates is higher than 1.5 C. For these reasons it has been decided that for the values of R_{tot} , when the C-rate is higher than 1.5 C is kept constant. Thus, the values of R_{tot} that have been used for C-rates greater than 1.5 C, 2 C and 4 C, are the same of the 1.5 C case.

To have a better overview of how the different modules react to the charging strategies, the Simulink has been parametrized with the data of three modules. In Table 8.3 are presented the three modules, as can be noticed each of the modules comes from a different pack, this has been chosen to have a more homogeneous situation. The modules have been chosen according to their SOH, indeed M35 has been chosen because its SOH is the highest, 90.970%. M11 has been chosen because its SOH is the lowest, 71.848%; the last module m13 has been chosen because its SOH is in between the two other SOH (81.667%).

The Simulink model has been parametrized using the values extracted from the test, therefore the parameters of the three modules have been implemented in three different Simulink models. With the use of these three modules the results of the simulations give a broader overview of the losses occurring during the charge at different SOH percentages.

Table 8.3 Modules used in the Simulink simulations.

Module number	SOH (%)	Capacity (Ah)-Energy (Wh)
B1 M35	90.970%	60.04 Ah - 454.85 Wh
B2 M11	71.848%	47.42 Ah - 359.24 Wh
B3 M13	81.667%	53.90 Ah - 408.34 Wh

8.2 Energy losses

In these sections are illustrated the simulations different test cases (different modules, charging boundaries, and C-rates), in order to determine the amount of energy that is lost while the battery is in use. The study cases simulated have been chosen to illustrate the different behaviour of the battery when the application varies. The scenarios evaluated are:

- full charge (0-100%) section 8.2.1;
- 60% charge (20-80%) section 8.2.2;
- 30% charge (35-65%) section 8.2.3.

The use of three different study cases for the charge enables the possibility of studying how the battery reacts to the different charges. In addition, since the second life uses are different in terms of power (remanufacturing, peak shaving, day storage, long term storage) the use of different C-rates gives an idea of the energy losses.

8.2.1 Full charge (0-100%)

In this section are presented the results for what concerns the full charge (0-100%) operated using different C-rates (from 0.1 C to 4 C). This test case has been studied to determine the behaviour of the module during a full charge with the use of different C-rates. The module is charge from 0% (5.4 V) to 100% (8.3 V) using a constant current (CC) for the whole process. This study case has been performed for the three modules (BP #1 M35, BP #2 M11, and BP #3 M13) and with all the C-rates (0.1 C, 0.5 C, 1 C, 2 C, and 4 C). The results of the energy loss during the processes are presented in Table 8.4, in Table 8.5, and in Table 8.6

Table 8.4 Results for the full charge of B1 M35 (90.97% SOH).

Energy dissipated for one charge (0%-100%)			
C-rate	Energy loss (Wh)	Duration (h)	Actual duration
0.1	1.3428	10	9.01 h (541 min)
0.5	5.0346	2	1.82 h (108 min)
1	10.2273	1	54 min
1.5	15.5153	0.66 (40 min)	36 min
2	19.6395	0.5 (30 min)	27 min
4	36.8283	0.25 (15 min)	13 min

In Table 8.4, in Table 8.5, and in Table 8.6 the column “duration” refers to the time needed to fully charge the module when the module is new, in the column “actual duration” is presented the time that is actually needed to fully charge it. The durations are different for the three modules because they have different SOHs, and this affects the total amount of energy that can be accumulated. If the C-rate is kept constant, a lower SOH gives a lower time to charge, but of course the amount of energy stored in the battery is lower.

Indeed, the lowest durations are found for the module B2 M11, which has the lowest SOH. On the contrary, the longest charging states are found for the module B1 M35, that has the greatest SOH among the modules that have been tested.

Table 8.5 Results for the full charge of B2 M11 (71.848%SOH).

Energy dissipated for one charge (0%-100%)			
C-rate	Energy loss (Wh)	Duration (h)	Actual duration
0.1	1.8197	10	7.20 h (430 min)
0.5	7.0563	2	1.43 h (86 min)
1	15.7720	1	43 min
1.5	20.8602	0.66 (40 min)	29 min
2	25.5539	0.5 (30 min)	15 min
4	55.8681	0.25 (15 min)	8 min

In Table 8.4, in Table 8.5, and in Table 8.6 are shown the values of the energy lost during the charges. Those values have been calculated using equation (8.3). As expected, the losses increase with the increase of the C-rate used to charge the battery. At the same time, the losses increase with the decrease of the SOH. This trend was expected, because the correlation between the SOH and the total internal resistance was found to be inverse (with the increase of one the other decreases). And as expressed with equation (8.1) and equation (8.3) the losses in terms of power and energy are directly proportional to the internal resistance R_{tot} .

Table 8.6 Results for the full charge of B3 M13 (81.667%SOH).

Energy dissipated for one charge (0%-100%)			
C-rate	Energy loss (Wh)	Duration (h)	Actual duration
0.1	1.7051	10	8.16 h (490 min)
0.5	6.3929	2	1.63 h (98 min)
1	11.9508	1	49 min
1.5	20.1802	0.66 (40 min)	33 min
2	22.1392	0.5 (30 min)	16 min
4	49.7368	0.25 (15 min)	8 min

The data presented in Table 8.4, in Table 8.5, and in Table 8.6 are expressed and summarized in Figure 8.6. There, the values of the Energy loss during the full charge (0-100%) are sorted by C-rates and modules of the battery packs. The blue bars refer to the module M35 that has the highest SOH, the red bars represent the module M11 which has the lowest SOH. The green bars refer to the last module object of the study, M13 from the third battery pack.

In all the test cases evaluated the highest values are found for M11, then there are the values of M13, and lastly the energy lost for M35.

However, there are some variations in the difference between the energy loss of the cases; for instance, at 1.5 C the energy for M11 and M13 have very similar values, whilst in the other cases the difference is greater. As expected, the losses due to the internal resistance increase with the increase of the C-rate (the power dissipated over the resistance is proportional to the square of the current).

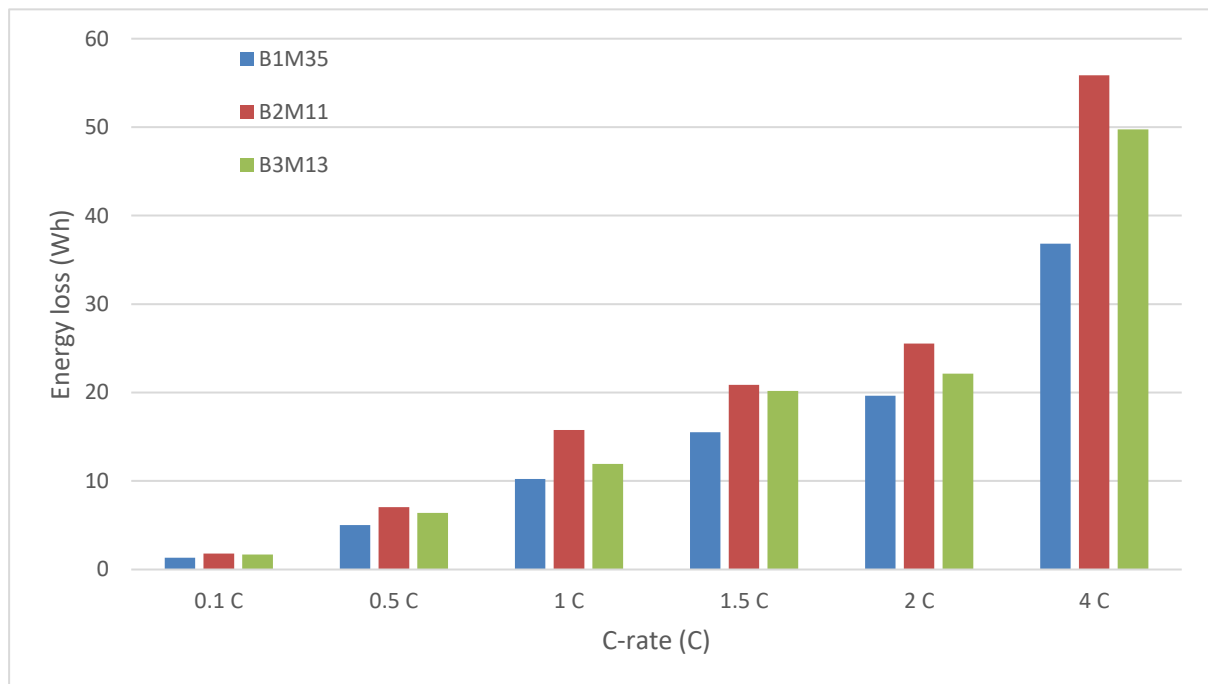


Figure 8.6 Comparison between the energy loss experienced by the module during a full charge using different C-rates.

8.2.2 20-80% Charge

The second study case that has been simulated for the charge of the battery is the 60% charge performed from 20% to 80%. This study case has been performed for all the C-rates listed in Table 8.2. Then the data referring to 0.1 C and 1 C have been analyzed and the composition of the losses has been evaluated. These two C-rates have been chosen because the first one refers to the daily storage for a residential PV+battery system Vgl. Farinet et al. (Battery Lifetime Analysis for Residential PV-Battery System used to Optimize the Self Consumption - A Danish Scenario) 2019⁷⁹, while the second refers to an automotive scenario, where the EV is

⁷⁹ Vgl. Farinet et al. (Battery Lifetime Analysis for Residential PV-Battery System used to Optimize the Self Consumption - A Danish Scenario) 2019.

charged using 1 C Vgl. Spöttle et al. (Research for TRAN Committee - Charging infrastructure for electric road vehicles) 2018⁸⁰.

In addition to the data presented in the cited papers this range comprehends 5 different real measurements performed during the pulse tests (20%, 35%, 50%, 65%, and 80%), which give more reliability to the simulations performed with the Simulink model.

The test cases that have been evaluated more closely for the range 20-80% are:

- 0.1 C (6.6 A) representing residential daily storage;
- 1 C (66 A) representing automotive charge.

In Figure 8.7 are shown the values of the energy losses for all the C-rates, sorted by the three modules used in the simulations. The trends found for the full charge (0-100%), in Figure 8.6, are found also in this type of charging procedure.

As happened for the full charge also in the 20-80% charge the values of the energy loss increase with the increase of the C-rate. These trends are due to the fact that the losses, as shown in equation (8.1) and equation (8.3) are proportional to the square of the current. In this test case the highest losses are found for the module M11, the one with the lowest SOH. This means that, even though the amount of energy to be stored in the module is smaller, (because the SOH is lower than the two other cases) the energy dissipated internally is greater (keeping constant the current).

⁸⁰ Vgl. Spöttle et al. (Research for TRAN Committee - Charging infrastructure for electric road vehicles) 2018.

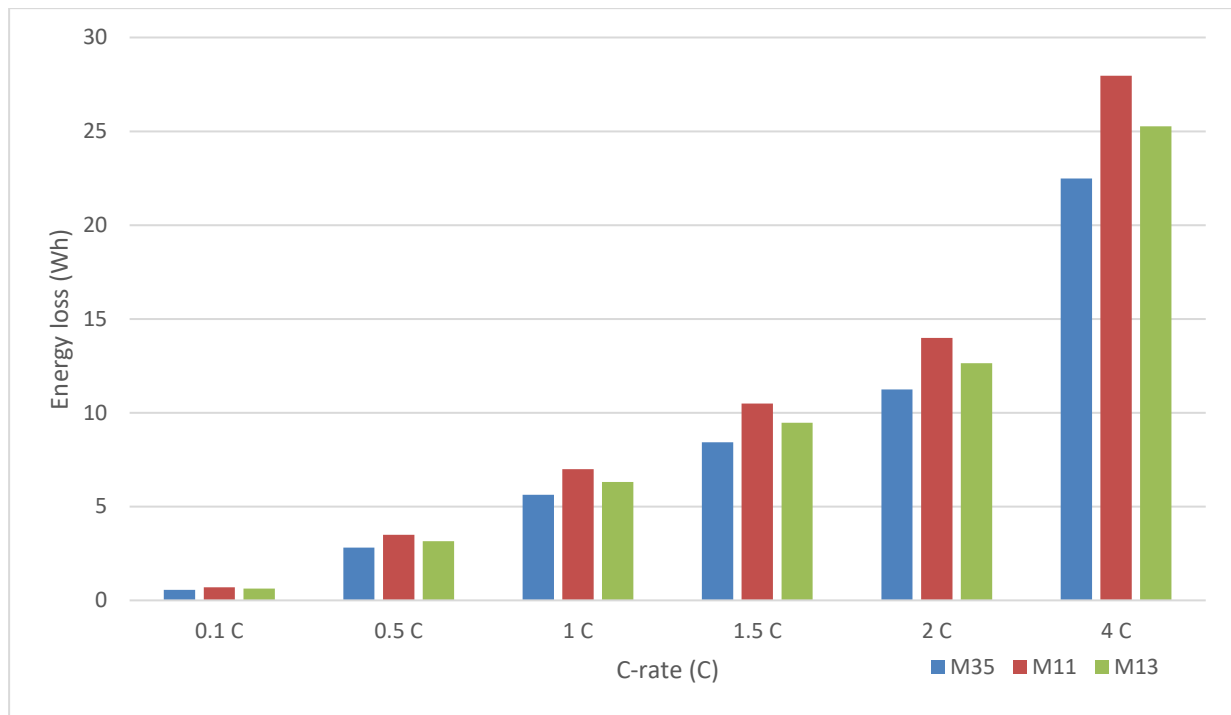


Figure 8.7 Energy losses due to the resistive parameters in the 20-80% charge with different C-rates.

In Table 8.7 is shown a comparison between the energy charged and the energy loss using 2 C of the three modules, for the charge 20-80%. Even though M11 has the lowest energy charged (28.45 Wh), it has the greatest value for the energy loss. This occurs because the SOH is low (71.848%) and the total internal resistance is high. On the contrary, for M35 is found the highest values for the energy charged, 36.02 Wh, and the lowest energy loss 11.24 Wh, the reason for this behaviour is that in general, as shown in section 7.2.6, the SOH has an inverse correlation with the total internal resistance R_{tot} .

The efficiency of the charging process, shown in the column on the right is calculated according equation (8.3). As shown, it is the ratio between the energy available at the end of the charge and the amount of energy needed to charge the module. As expected, the highest efficiency is found for M35, 96.06%, then there is M13 with 95.11%, the least efficiency is found for M11, 93.93%. This index, η , shows the amount of energy that is actually available at the end of the charging state.

$$\eta = \frac{E_A}{E_A + E_L} \quad (8.3)$$

η Efficiency of the charging process (%)

E_A Energy available after the charge (Wh)

E_L Energy lost during the charge (Wh)

Table 8.7 Comparison of the energy losses during the charge (20-80%) using 2 C.

Module	Energy Charged (20-80%)	Energy Lost (2 C)	η (%)
B1 M35	273.78 Wh	11.24 Wh	96.06%
B2 M11	216.23 Wh	13.98 Wh	93.93%
B3 M13	245.79 Wh	12.63 Wh	95.11%

The first (0.1 C) and the third (1 C) section of Figure 8.7 are evaluated in the next part of this section, to understand the behaviour of the module under two different study cases.

For what concerns the charge with 0.1 C, this represents the charge that could occur for a residential system that integrates a rooftop PV and a Battery Energy Storage System (BESS). With this type of situation, the average power coming from the PV could be set to 1/10 of the battery, determining an average C-rate of 0.1 C Vgl. Liu et al. (A Charging Strategy for PV-Based Battery Switch Stations Considering Service Availability and Self-Consumption of PV Energy) 2015⁸¹.

Figure 8.8 reports the losses for the charge 20-80% when a C-rate of 0.1 C (6.6 A) is used. The three bars represent the three modules used for the simulations. Each bar is then divided in three sections, each one represents the losses of the single resistive parameters. The blue one represents R_0 , the red one R_1 , and the last one, green, R_2 . Using this division is possible to estimate the weight that each resistive parameter has in the total losses.

As can be seen from Figure 8.8, for all the three modules, the highest amount of the losses is due to R_0 , which is the cause of more than 2/3 of the losses for all the simulations. Indeed, the greatest percentage is found for M13, where 71.44% of the losses is due to R_0 . The weight of R_1 is lower, its values go from 16.44%, for M13, to 19.85% of M35. The influence of R_2 is smaller than the ones found for R_0 and R_1 , indeed, its losses are around 13% for all the cases. These trends confirm the characteristics presented in the previous sections, hence, the importance and the weight of the parameters with higher indexes decreases with the increase of the index. The amount of energy dissipated on the R_{tot} for the three cases is reported in Table 8.8.

⁸¹ Vgl. Liu et al. (A Charging Strategy for PV-Based Battery Switch Stations Considering Service Availability and Self-Consumption of PV Energy) 2015.

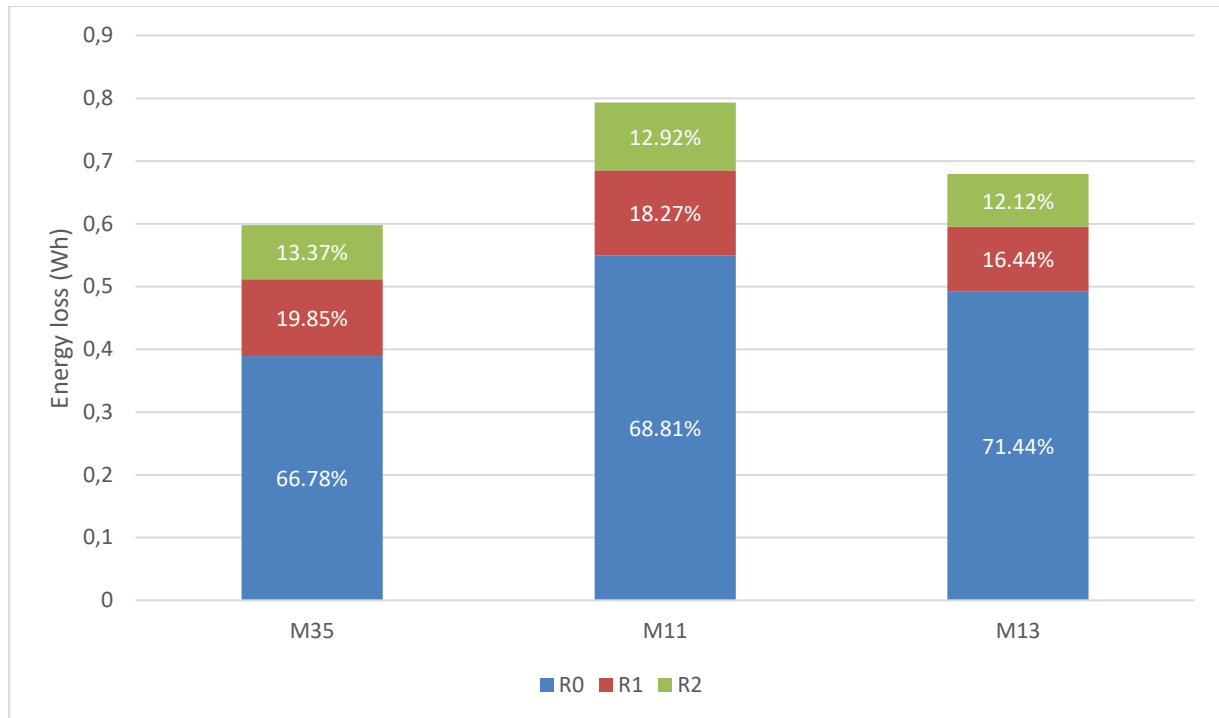


Figure 8.8 Energy losses due to the resistive parameters R_0 , R_1 , and R_2 , in the 20-80% charge with 0.1 C (6.6 A).

In Table 8.8 are presented the values of the energy loss for the charge 20-80% performed using 0.1 C. As occurred in the previous case the highest values for the energy loss is found for M11, which to charge 216.23 Wh requires an additional 0.793 Wh. Even though the other two modules have a higher amount of energy charged, the losses are lower (0.598 Wh for M35 and 0.679 Wh for M13) than the one found for M11. The same trend found in Table 8.8 was found also in Table 8.7.

Table 8.8 Comparison of the energy losses during the charge (20-80%) using 0.1 C.

Module	Energy Charged (20-80%)	Energy Lost (0.1 C)	η (%)
B1 M35	273.78 Wh	0.598 Wh	99.782%
B2 M11	216.23 Wh	0.793 Wh	99.634%
B3 M13	245.79 Wh	0.679 Wh	99.724%

The efficiency η , calculated according equation (8.3), has very high values, all above 99%. This means that if the batteries are operated with low C-rates the losses due to the internal resistive parameters do not affect their operation.

The last case evaluated for the 20-80% charge is the one regarding the C-rate of 1 C. This simulation has been performed to simulate a possible charge for automotive purposes Vgl.

Spöttle et al. (Research for TRAN Committee - Charging infrastructure for electric road vehicles) 2018⁸². Indeed, the range 20-80% is where the majority of the batteries that equip EVs are used.

As done for the 0.1 C case, in Figure 8.9 are shown the divisions of the losses due to R_0 , R_1 and R_2 . The losses due to R_0 , for M35 and M11, have the same value in percentage, respectively 65.22% and 65.71%, which are values close to the ones found for 0.1 C, shown in Figure 8.8.

For what concerns the losses caused by R_1 , the weight goes from 14.41% of M13 to 18.72% of M35. As occurred for R_0 these values are close to the ones found for the charge performed with 0.1 C. For the last resistive parameters, R_2 , the percentages found for M35 and M11 are greater than the ones found for 0.1 C. The range of the losses goes from 12.82% of M13 to 18.10% of M11. However, division of the losses between the three resistive parameters is in accordance to the one found for the other C-rate used. Indeed, a rough estimation of the losses is that circa 2/3 of the losses are due to R_1 , and the remaining part is equally divided in R_1 and R_2 (circa 1/6 each).

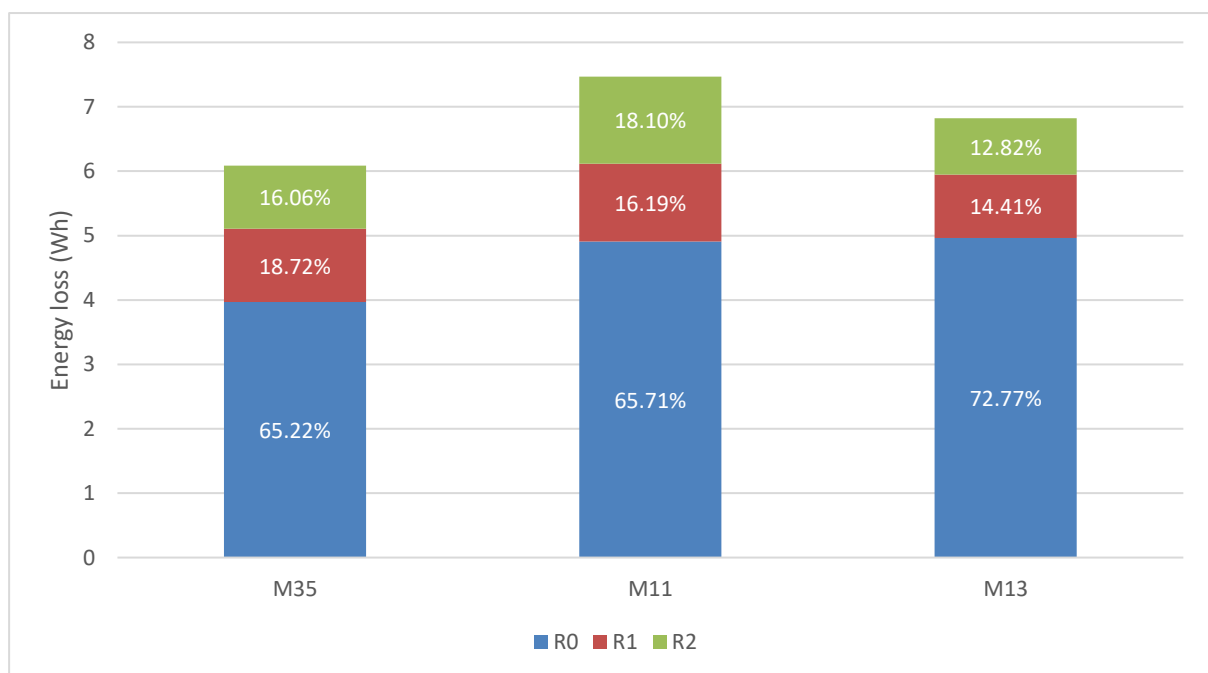


Figure 8.9 Energy loss due to the resistive parameters R_0 , R_1 , and R_2 , in the 20-80% charge with 1 C (66 A).

Table 8.9 reports the amount of energy that is being lost during the charge of the three modules. The columns “Energy Charged” represents the amount of energy that has been actually

⁸² Vgl. Spöttle et al. (Research for TRAN Committee - Charging infrastructure for electric road vehicles) 2018.

stored in the battery in the range 20-80%. The column in the right “Energy Lost” shows the amount of additional energy that has to be provided to the module in order to charge the amount shown in the center column. The highest loss is found for module M11, which needs additional 7.469 Wh to charge 216.23 Wh.

Table 8.9 Comparison of the energy losses during the charge (20-80%) using 1 C.

Module	Energy Charged (20-80%)	Energy Lost (1 C)	η (%)
B1 M35	273.78 Wh	6.084 Wh	97.826%
B2 M11	216.23 Wh	7.469 Wh	96.661%
B3 M13	245.79 Wh	6.822 Wh	97.299%

The efficiency indexes of the charging process, η , can be calculated by using equation (8.3), are reported in the right column of Table 8.9. The values are lower than the 0.1 C case (in Table 8.8), but the trends are confirmed, the highest value is found for M35, then M13 and lastly M11. The difference between the maximum efficiency, 97.826% and the least 96.661% is small, however, the energy losses can be great over the time of use.

8.2.3 35-65% charge

The lowest charge range simulated is of 30% and it goes from 35% to 65%. This range has been chosen because it is the smallest range that included three SOCs with real measurements (35%, 50% and 65%). In this way the results of the simulations are more reliable. As occurred for the 20-80% range all the C-rates have been used for the simulations. However, the focus has been set to some of them. The C-rates that have been studied the most for this test case are:

- 0.5 C (33 A) representing a large PV plant;
- 1 C (66 A) representing an automotive case;
- 4 C (264 A) representing an extreme case.

The results of the simulations of these test cases give an idea of how the internal losses of the battery change according to different the applications Vgl. Marcos et al. (Storage requirements for PV power ramp-rate control) 2014⁸³.

The overall results for all the C-rates (0.1 C, 0.5 C, 1 C, 2 C, and 4 C) are presented in Figure 8.10. In the figure the same trends found for the previous ranges (0-100% and 20-80%), presented in section 8.2.1 and in section 8.2.2, are found. Indeed, the energy losses increase with the increase of the C-rate. As occurred for the two other charge ranges the highest values are

⁸³ Vgl. Marcos et al. (Storage requirements for PV power ramp-rate control) 2014.

found for the module M11 (red bars). The lowest values for the energy loss are found for the module M35 (blue bars), strengthening the idea that to a high SOH corresponds a more efficient operating condition.

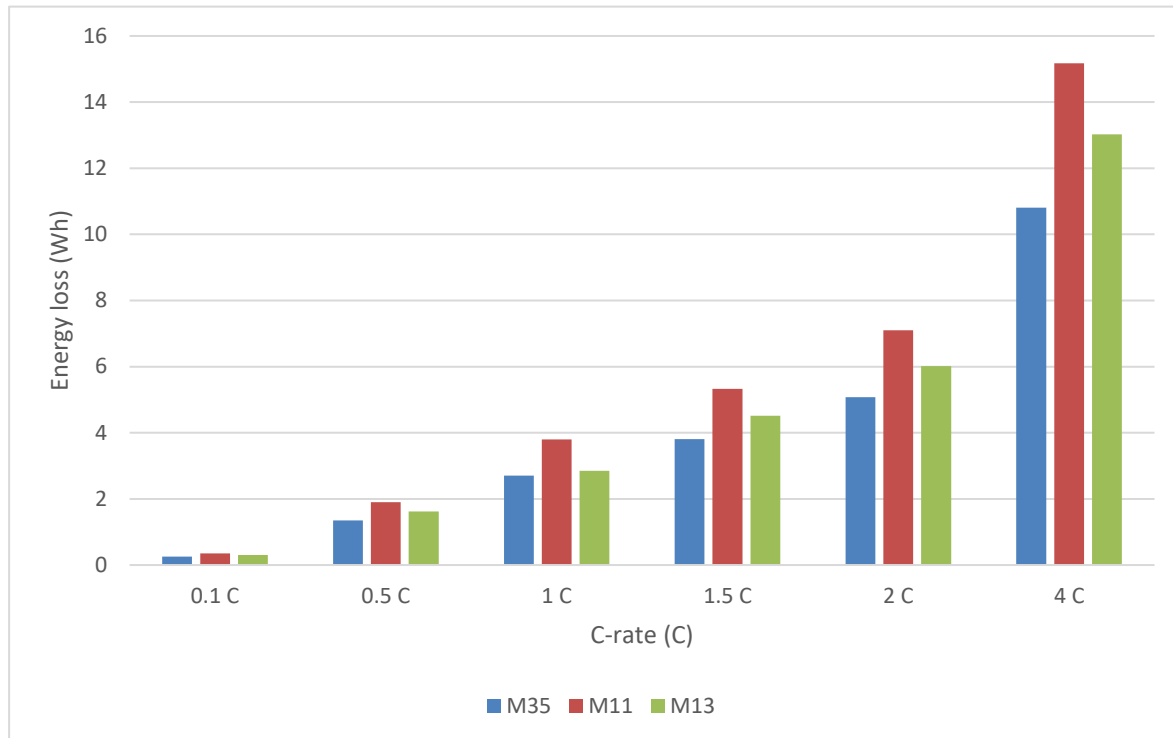


Figure 8.10 Energy losses due to the resistive parameters in the 35-65% charge with different C-rates.

The first test case for which is run the simulation is the 35-65% charge using a C-rate of 0.5 C. This C-rate has been chosen to simulate the condition of a large PV plant (equipped with a storage system), which has a mean power of half of the one for which is rated the storage system. In this case the power coming from the battery can be used for a power smoothing operation.

In Figure 8.11 are presented the results of the simulation 35-65%, as occurred for the other SOC ranges, the module that have been used to parametrized the Simulink model are B1 M35 (left bar), B2 M11 (center bars), and B3 M13 (right bars). In this case, the weight of the R_0 , plotted in blue, is quite high for the cases M11 and M13. Hence, their values are higher than 70%, respectively 73.05% and 71.39%. On the other hand, the percentage of the losses for R_0 for module M35 is 64.28%, similar to the values found in previous scenarios. However, even though there are some differences between the weight of R_0 , the trend in the division of the losses for this case is similar to the ones found for the other SOC ranges. The previous overall distribution of the losses is confirmed also in this case.

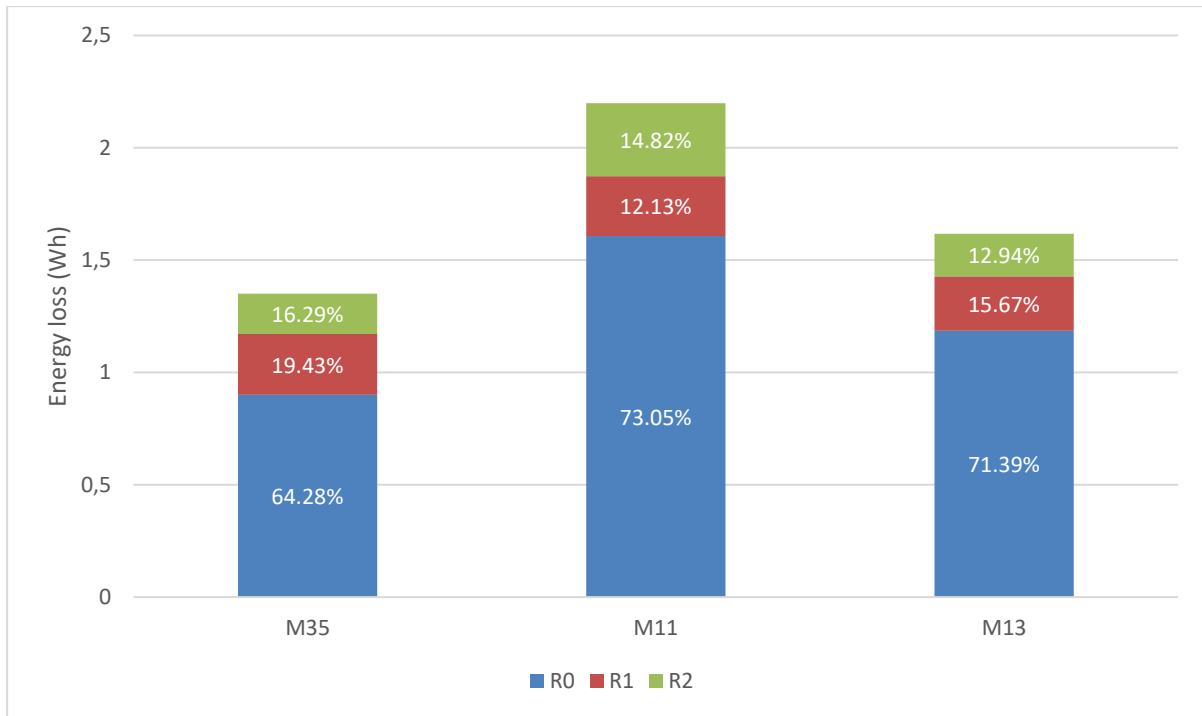


Figure 8.11 Energy loss due to the resistive parameters R_0 , R_1 , and R_2 , in the 35-65% charge with 0.5 C (33 A).

In Table 8.10 are presented the results of the 30% charge for the three modules. The amount of energy charged, listed in the second column, are different for the three modules, because their SOHs are different. However, the comparison between their behaviors can be done by using the efficiency of the charge index, η .

Therefore, the module M13, from the third battery pack, has been charged from 35% to 65% with 110.319 Wh, of which 2.199 where dissipated on the resistive parameters. This brought the efficiency of the charge to 98.24%. The other efficiency indexes are 99.02% for M35 and 98.24% for M13. As occurred for the other cases, the highest efficiency is found for the module with the highest SOH (and the least losses) M35. The efficiency indexes for this case, with 0.5 C are quite high, indeed, all of them are above 98%.

Table 8.10 Comparison of the energy losses during the charge (35-65%) using 0.5 C.

Module	Energy Charged (35-65%)	Energy Lost (0.5 C)	η (%)
B1 M35	136.89 Wh	1.351 Wh	99.02%
B2 M11	108.12 Wh	2.199 Wh	98.01%
B3 M13	122.89 Wh	1.617 Wh	98.24%

The second case simulated for the range 35-65% has been performed using a C-rate of 1 C. This has been done to estimate the behaviour of the battery in automotive cases, when the battery pack has SOCs values close to 50%. In Figure 8.12 and in Table 8.11 are presented

the results of this simulations. As for the other cases, three modules have been used to parametrize the Simulink model. As occurred for the first C-rate evaluated in this section (0.5 C), the energy loss due to R_0 is above 70% for both M11 and M13. At the same time, the energy loss due to R_0 , for M35 is 65.67%. These three situations are the same that were found for the previous C-rate (in terms of percentages).

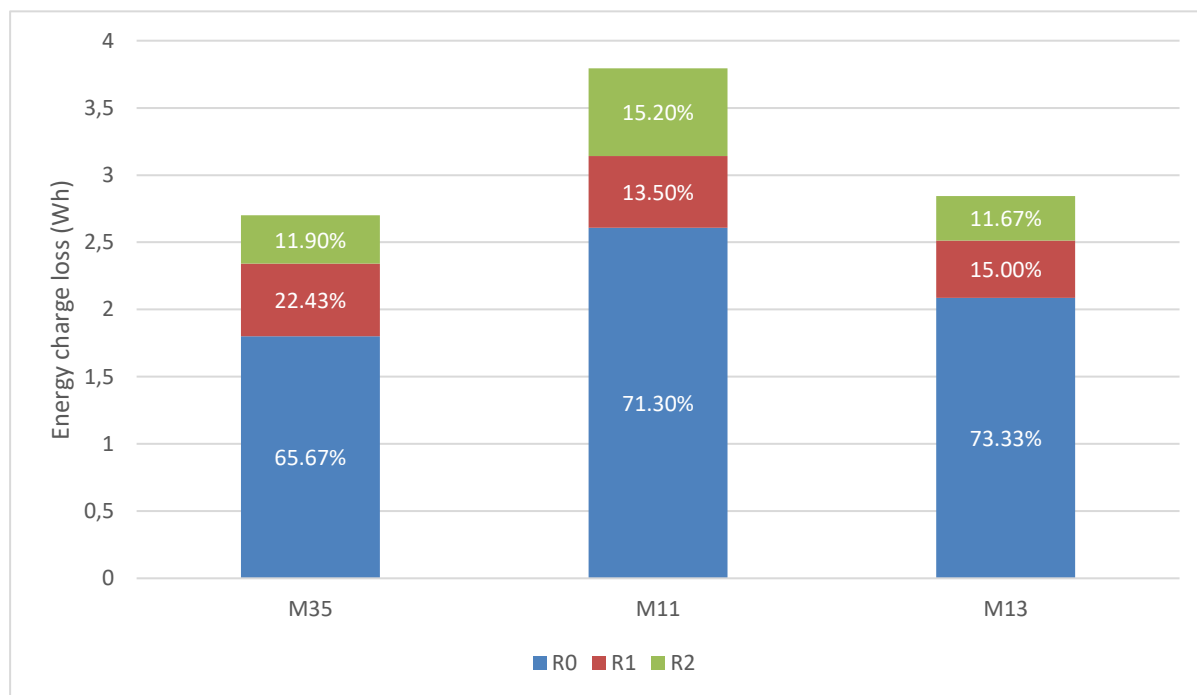


Figure 8.12 Energy loss due to the resistive parameters R_0 , R_1 , and R_2 , in the 35-65% charge with 1 C (66 A).

As can be thought the efficiency of the charging process has lower values than the previous case, indeed, the energy charged is the same, but the energy loss, which is at denominator in equation (8.3), increases. Hence, in Table 8.11 are presented the results, with the charging efficiency indexes that are lower than the previous case, reaching at maximum 98.06%. The least value is found with M11, which has 96.61% as efficiency index.

Table 8.11 Comparison of the energy losses during the charge (35-65%) using 1 C.

Module	Energy Charged (35-65%)	Energy Lost (0.5 C)	η (%)
B1 M35	136.89 Wh	2.702 Wh	98.06%
B2 M11	108.12 Wh	3.794 Wh	96.61%
B3 M13	122.89 Wh	2.845 Wh	97.74%

The last study case that has been simulated with the Simulink model is the charge between 35% and 65% using 4 C (264 A). This scenario has been chosen as an extreme case of the battery (for instance a very fast charge from a public charging station).

In Figure 8.13 are presented the results of the simulation performed using 4 C. In this case, the weight (the percentage of its losses) of R_0 are similar to each other, with values that go from 64.10% of the module M13 to 68.75% of the module M11.

For what concerns R_1 , red section of the bars, M35 and M13 have similar percentages, respectively 20% and 20.19%. On the other hand, its weight for M11 is only 14.06%.

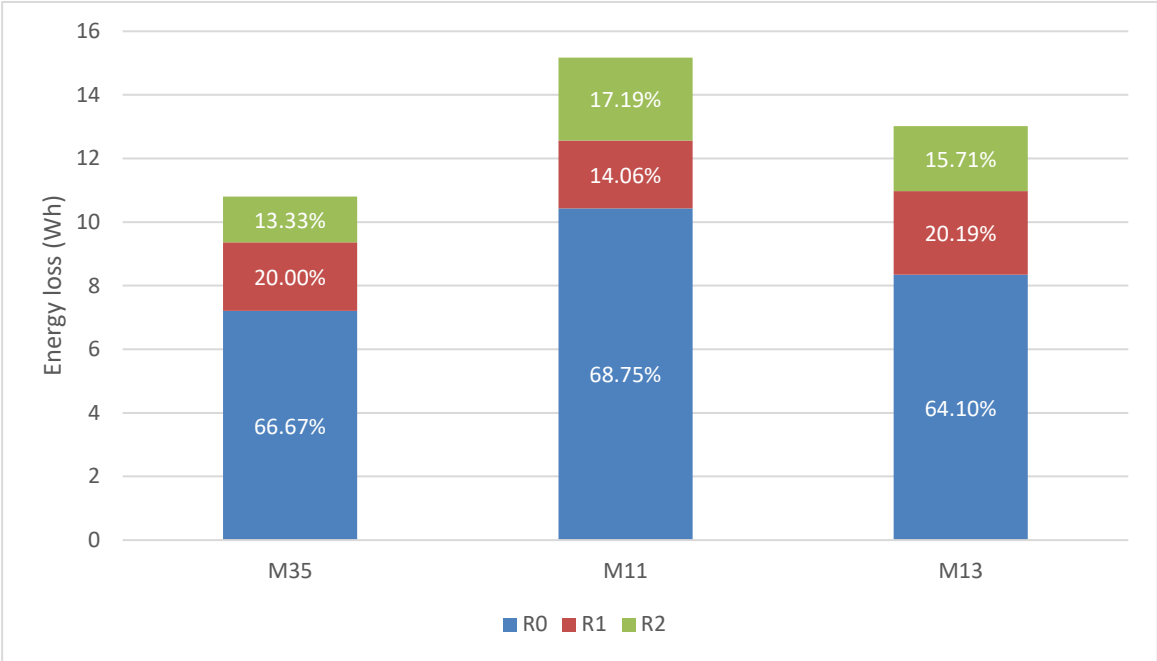


Figure 8.13 Energy loss due to the resistive parameters R_0 , R_1 , and R_2 , in the 35-65% charge with 4 C (264 A).

In Table 8.12 are presented the efficiency indexes for the simulations. As can be noticed their values are quite low, compared to the ones previously presented in this section. However, the amount of energy charged, between 35% and 65% remained constant. This is due to the fact that even though the energy charged remained the same, the energy lost due to the internal resistive parameters increased, thus decreasing the efficiency of the charging process.

For instance, to charge 108.12 Wh (30% of the capacity of M11) in the module M11 additional 15.174 Wh are required, to overcome the losses due to the internal resistances (R_0 , R_1 , and R_2). With 4 C as C-rate the indexes are around 90%, with the maximum found for M35, 92.68%. The least is found for M11, 87.69%, 5% less than the best case.

Table 8.12 Comparison of the energy losses during the charge (35-65%) using 4 C.

Module	Energy Charged (35-65%)	Energy Lost (0.5 C)	η (%)
B1 M35	136.89 Wh	10.807 Wh	92.68%
B2 M11	108.12 Wh	15.174 Wh	87.69%
B3 M13	122.89 Wh	13.020 Wh	90.42%

As stated in the different sections of this chapter, the results of the simulations show that the SOH level directly influences the efficiency of the battery. These differences in the efficiency increased with the increase of the C-rate, reaching 5% for the case 35-65% with 4 C. With the use of the simulations, the operation of the modules under different SOC charge ranges (0-100%, 20-80%, and 35-65%) and C-rates (0.1 C, 0.5 C, 1 C, 2 C, and 4 C) can be evaluated. Indeed, the three modules that have been tested have very various SOH, going from 71.484% of M11, to 90.970% of M35 passing through 81.667% of the module M13. Using these broad parameters, the trends and the behavior of the modules can be assessed with a higher degree of accuracy.

Given the results it can be stated that for high power (where the C-rate is high) and mobile applications, the internal resistance R_{tot} has to have limited values, because the energy losses would greatly affect the performances. Of course, for the remanufacturing of the battery packs for automotive applications, the SOH has to be the greatest possible, with values higher than 80%. It is assessed that along with a high SOH go low internal resistive parameters and a low self-discharge rate. The best modules for second life uses are the ones with the least internal resistance R_{tot} .

On the other hand, for static applications, such as power smoothing, power balancing, residential energy storage, can be used modules with a higher internal resistance R_{tot} . Of course, the sizing, in terms of capacity, of the battery storage would have to be designed according to the parameters of the used cells or modules.

9 Conclusions and future work

In this final chapter of the thesis are reported the main conclusions and findings of the study that has been performed. In addition, in the second section of the chapter are shown some ideas and some insights for future studies and researches on testing batteries for EVs and their second life uses.

9.1 Conclusions

The market share of the EVs is rapidly growing as it will continue to do so, according to the previsions made by several institutes and companies. Along with the increase of the number of EVs the request for battery packs will rise. In addition to that, the RES will require energy storage systems and most of them will be using batteries based on Li-Ion technology.

In this scenario, the batteries used in automotive applications could provide part of the energy capacity needed. To re-utilize the automotive used battery packs for any second life use, it is necessary to test them and evaluate their main characteristics. To do so, the packs have to be disassembled and the modules/cells that compose them have to be tested singularly. Using this technique, the output gives results that are more reliable and precise. In this thesis are presented different tests, that are then implemented in a testing protocol for used EV battery packs.

The testing of battery packs for automotive applications is time-consuming and requires expensive and specific equipment. With the testing protocol developed during the research, presented in section 5.6 (Final testing protocol), the main parameters regarding the module of the battery pack of the Nissan Leaf 2011 Edition can be extracted. The duration of the entire testing protocol varies according to the initial SOC and to the SOH of the modules object of the test. However, the average duration of the test was of 8 hours (it may vary due to the SOH and the SOC of the module at the start of the test). This testing protocol can be performed on other Li-Ion battery packs, by adjusting some of the parameters (voltage levels, relaxation time, C-rate, etc.).

The results presented in chapter 6 (Results and discussion), in chapter 7 (Correlation between parameters and SOH), and in chapter 8 (EEC Simulations) give an overview of the work that has been carried out in this research. In chapter 6 are reported the trends in the variation of the internal parameters of the modules of the Nissan Leaf 2011 Edition. The range of SOH found in the three packs is of 20%, going from 71% (found in the second battery pack) to 91% (found in the first battery pack), which gives a good overview of the possible conditions of the used modules coming from the battery packs of EVs. Even though the three battery packs that have been tested have been found different SOHs, the trends and the behaviors found are common and similar for all of them.

The resistive parameters of the EEC circuit, R_0 , R_1 , and R_2 all increase their values with the increase of the usage of the battery (and its consequent drop in the SOH). These increases of the resistances bring another variation. Indeed, the value of the self-discharge (measured at 100% SOC) increases with the decrease of the SOH of the modules.

For what concerns the capacitive parameters of the EEC, the trends are opposite from the ones found for the resistive parameters. Hence, with the decrease of the SOH the capacitances C_1 and C_2 decrease their values. These general trends occur at the different SOC levels and with the C-rates tested. Therefore, with the reduction of the SOH, the resistive parameters increase their values, while the capacitive ones decrease theirs.

The main findings presented in chapter 6 can be summarized in the following list:

- An overall increase of the resistive parameters of the EEC with the decrease of the SOH;
- An overall decrease of the capacitive parameters of the EEC with the decrease of the SOH;
- An overall increase of the self-discharge rate (at 100%) with the decrease of the SOH;

In chapter 7 are shown the correlation indexes between the SOH and the parameters extracted from the tests. The trends found in the results of chapter 6 have been analyzed, to have a better understanding of the relationships that occur between the parameters extracted from the testing protocol. The correlation indexes have shown a good relationship between the parameters of the EEC and the SOH of the modules. For the resistive parameters, and for the self-discharge, the correlation indexes are negative, meaning that the correlation is inverse. On the other hand, for the capacitive parameters the indexes are positive, meaning that the correlation between the SOH and the capacitances is direct.

In the list below are summarized the main findings of obtained from chapter 7:

- Correlation index SOH- R_0 , negative
- Correlation index SOH- R_1 negative
- Correlation index SOH- R_2 negative
- Correlation index SOH- C_1 positive
- Correlation index SOH- C_2 positive
- Correlation index SOH-SD negative

Hence, it can be stated that the testing protocol designed and developed for the test of the battery packs gives good results and it is reliable. Indeed, the results are conform to one of other researches, presented in chapter 3 (State of the art). This testing protocol enables us to extract the parameters of Li-Ion batteries with good reliability and has a short duration in time (compared to the ones presented in other papers and researches).

The simulations presented in chapter 8 confirm the trends found in chapter 6 and in chapter 7. Indeed, the decrease in the available capacity (SOH) goes along with a decrease in the efficiency of the charging processes. In all the study cases that have been simulated the energy losses due to the resistive parameters increase with the decrease of the SOH of the modules.

For what concerns the second life uses of the modules/cells that compose the pack the division has been made according to two parameters. The first one is the SOH, which highly characterizes the possible second life uses of the modules. Thus, the modules with a high SOH (above 85%) can be used for remanufacturing of EV battery packs. The modules with lower

SOHs (below 85%) can be used for other purposes, such as residential energy storage, peak shaving, power smoothing, and large energy storage for renewable energy sources.

9.2 Future work

As well as for all the studies and researches there is always room for improvement and future line of work. As stated in the first chapter, Introduction, this study has some limitations, these are due to different causes, such as time limitations, equipment limitations, number of batteries available and so on. In addition to these elements, new strategies and ideas could be applied to develop and design new testing protocols for EV battery packs.

In the following list are reported some of the possible lines of work for future researches and studies:

- Increase the resolution of the tests;
- Increase the number of battery packs object of the testing;
- Widen the SOH ranges of the samples;
- Increase the C-rates and the number of SOC levels for the pulse tests;
- Different SOC levels for the self-discharge test;
- Electrochemical Impedance Spectroscopy (EIS);
- Perform tests on the cell level;
- Model that includes more parameters.

Certainly, to the presented list of the possible implementations of the test could be added other different examinations and protocols, as well as different strategies of testing.

Even though the three battery packs object of the research give a good range in the SOH (from 71% to 91%), it would be ideal to collect the data from other SOH levels. This could provide a better understanding of the variation in the values of the internal parameters. To do so it is necessary to increase the number of battery packs tested. It would be interesting and relevant to test the modules (or cells) coming from a brand-new battery pack, to set a starting point for the parameters of the EEC.

The testing protocol presented in section 5.6 (Final testing protocol), has a good range in the SOC levels (8) and a good range in the C-rates (3), which describe quite well the overall behaviour of the battery. However, due to equipment (maximum current) and time limitations, it has not been possible to increase the number of tests. In future researches, it could be possible to start from the results of this study and to test some, or all, the SOC levels with higher C-rates.

In addition, to the higher number of study cases for the pulse tests, an improvement can be done for what concerns the test for the self-discharge. In this study it has been evaluated at 100% SOC, it would be interesting to test it at different SOC levels, in the low (below 10%) and medium (50%) ranges. This would provide other data and parameters that could increase the precision of the tests, in addition this could lead to additional correlation in the parameters.

In this project, due to the limitations of the testing equipment, it has not been performed the test of the Electrochemical Impedance Spectroscopy (EIS). This test could give another point of view on the internal parameters of the battery. By comparing the results of the EIS with the results of the pulse tests other trends and behaviors of the battery could be found. With the comparison of the results from the EIS and the pulse tests, it could be possible to find other correlation indexes between the SOH and the internal parameters of the battery. This could be very helpful in cases of very severe degradation of the cells.

In addition to the previous options, it is possible to widen the tests to the cell level. In this study, the tests have been performed on the module level, due to the requirements of the project. However, going to the lower level of the system, the cell level, could provide an additional point of view on the ongoing processes occurring to the battery. With the data of the tests performed at the cell level it could be possible to experience small variations in the internal parameters that with the module level are quite limited and therefore cannot be noticed and analyzed.

Considering the simulations, the model can be improved by adding other variables, for instance the temperature can be included. In addition to that, it would be interesting to simulate the behaviour of the module under different condition for its entire lifespan, by using a model that simulates also the degradation that occurs with the usage.

V Bibliography

AESC Corp 2011:

Specifications Nissan Leaf 2011 Edition. <https://www.envision-aesc.com/en/product.html>

Andre, D; Meiler, M; Steiner, K; Walz, H; Soczka-Guth, T; Sauer, D. U.:

Characterization of high-power lithium-ion batteries by electrochemical impedance spectroscopy. II: Modelling. In: *Journal of Power Sources*, Jg. 2011, 2011, Nr. 196

Bo Liu; Maolin Yin; Qirong Lin; Lin Lin; Shuai Yuan; Jie Ma; Ti Guan:

Control Strategy of BESS for Smoothing Fluctuation, Jg. 2017

Böttiger, M; Paulitschke, M; Bocklisch, T.:

Systematic experimental pulse test investigation for parameter identification of an equivalent based lithium-ion battery model. In: *Energy Procedia*, Jg. 135, 2017, S. 337–346.

Braco, E; Martin, I. S; Sanchis, P; Ursua, A.:

Characterization and capacity dispersion of lithium-ion second-life batteries from electric vehicles: 2019 IEEE International Conference on Environment and Electrical Engineering and 2019 IEEE Industrial and Commercial Power Systems Europe (EEEIC / I&CPS Europe). 2019 IEEE International Conference on Environment and Electrical Engineering and 2019 IEEE Industrial and Commercial Power Systems Europe (EEEIC / I&CPS Europe), 11/06/2019 - 14/06/2019: IEEE 2019 - 2019, S. 1–6.

Brennan, J. W; Barder, T. E.:

Battery Electric Vehicles vs. Internal Combustion Engine Vehicles. A United States-Based Comprehensive Assessment USA, November, 2016

Casals, L. C; García, B. A; Aguesse, F; Iturrondobeitia, A.:

Second life of electric vehicle batteries: relation between materials degradation and environmental impact. In: *Int J Life Cycle Assess*, Jg. 22, 2017, Nr. 1, S. 82–93.

Davide Andrea:

Battery Management Systems for Large Lithium-Ion Battery Packs. for large Li-Ion battery packs USA: Artech House on Demand, 2010

Diouf, B; Pode, R.:

Potential of lithium-ion batteries in renewable energy. In: *Renewable Energy*, Jg. 76, April 2015, S. 375–380.

Ecker, M; Nieto, N; Käbitz, S; Schmalstieg, J; Blanke, H; Warnecke, A; Sauer, D. U.:

Calendar and cycle life study of Li(NiMnCo)O₂-based 18650 lithium-ion batteries. In: *Journal of Power Sources*, Jg. 248, 2014, S. 839–851.

Farinet, D; Vacca, L; Maurer, M; Spataru, S. V; Stroe, D.-I.:

Battery Lifetime Analysis for Residential PV-Battery System used to Optimize the Self Consumption - A Danish Scenario. In: *In proceedings IEEE ECCE 2019*

V Bibliography

Galeotti, M; Cinà, L; Giammanco, C; Cordiner, S; Di Carlo, A.:

Performance analysis and SOH (state of health) evaluation of lithium polymer batteries through electrochemical impedance spectroscopy. In: Energy, Jg. 89, 2015, S. 678–686.

Gray, T; Wishart, J; Shirk, M.:

2011 Nissan Leaf VIN 0356 Plug-In Hybrid Electric Vehicle Battery Test Results 2016

Hans Eric Melin:

The lithium-ion battery end-of-life market – A baseline study, 2019

Hongwen, h; Xiong, R; Jinxin, F.:

Evaluation of Lithium-Ion Battery Equivalent Circuit Models for State of Charge Estimation by an Experimental Approach. In: Energies, Jg. 2011, 2011

Hu, X; Xiong, R; Egardt, B.:

Model-Based Dynamic Power Assessment of Lithium-Ion Batteries Considering Different Operating Conditions. In: IEEE Trans. Ind. Inf., Jg. 10, 2014, Nr. 3, S. 1948–1959.

Jiao, N; Evans, S.:

Business Models for Sustainability: The Case of Second-life Electric Vehicle Batteries. In: Procedia CIRP 2016, Nr. 40, S. 250–255.

Kampker, A; Wessel, S; Fiedler, F; Maltoni, F. (Hrsg.):

Remanufacturing of electric vehicles batteries up to the cell level. International Conference on Remanufacturing (ICoR), 23-25 June 2019

Keeli, A; Sharma, R. K.:

Optimal use of second life battery for peak load management and improving the life of the battery: 2012 IEEE International Electric Vehicle Conference. 2012 IEEE International Electric Vehicle Conference (IEVC), 04/03/2012 - 08/03/2012: IEEE 2012 - 2012, S. 1–6.

Keysight Technologies:

Evaluate Lithium Ion Self-Discharge of Cells in a Fraction of the Time Traditionally Required [Year derived is missing!]

Li, Z.:

Systematic analysis of an automatic disassembly process of automotive batteries. Master's Thesis 2018

Lie, T. T; Prasad, K; Ding, N.:

The electric vehicle: a review. In: International Journal of Electric and Hybrid Vehicles, Jg. 9, 2017, Nr. 49

Liu, N; Chen, Q; Lu, X; Liu, J; Zhang, J.:

A Charging Strategy for PV-Based Battery Switch Stations Considering Service Availability and Self-Consumption of PV Energy. In: TRANSACTIONS ON INDUSTRIAL ELECTRONICS, Jg. 62, 2015

V Bibliography

Madani, S; Schaltz, E; Knudsen Kær, S.:

An Electrical Equivalent Circuit Model of a Lithium Titanate Oxide Battery. In: Batteries, Jg. 5, 2019, Nr. 1, S. 31.

Marco Codegone:

Metodi matematici per l'ingegneria Turin, Italy: Zanichelli Editore, 1995

Marcos, J; Storköl, O; Marroyo, L; Garcia, M; Lorenzo, E.:

Storage requirements for PV power ramp-rate control. In: Solar Energy, Jg. 99, 2014, S. 28–35.

Martinez-Laserna, E; Sarasketa-Zabala, E; Stroe, D.-I; Swierczynski, M; Warnecke, A; Timmermans, J. M; Goutam, S; Rodriguez, P.:

Evaluation of lithium-ion battery second life performance and degradation: 2016 IEEE Energy Conversion Congress and Exposition (ECCE). 2016 IEEE Energy Conversion Congress and Exposition (ECCE), 18/09/2016 - 22/09/2016: IEEE 2016 - 2016, S. 1–7.

Masson, G; Kaizuka, I; Cambiè, C.:

A Snapshot of Global PV (1992-2017). International Energy Agency, Paris, France,. In: IEA 2017

Petzl, M; Danzer, M. A.:

Advancements in OCV Measurement and Analysis for Lithium-Ion Batteries. In: IEEE Trans. Energy Convers., Jg. 28, 2013, Nr. 3, S. 675–681.

Ramoni, M. O; Zhang, H.-C.:

End-of-life (EOL) issues and options for electric vehicle batteries. In: Clean Techn Environ Policy, Jg. 15, 2013, Nr. 6, S. 881–891.

Sarasketa-Zabala, E; Gandiaga, I; Martinez-Laserna, E; Rodriguez-Martinez, L. M; Villarreal, I.:

Cycle ageing analysis of a LiFePO₄/graphite cell with dynamic model validations: Towards realistic lifetime predictions. In: Journal of Power Sources, Jg. 275, 2015, S. 573–587.

Seok Choi, S; Lim, H. S.:

Factors that affect cycle-life and possible degradation mechanisms of a Li-ion cell based on LiCoO₂. In: Journal of Power Sources, Jg. 2002, 2002, Nr. 111, S. 130–136.

Sheldon M. Ross:

Introduction to Probability and Statistics for Engineers and Scientists, 5 Aufl. USA: Academic Press, 2014

Shih, H; Lo, T.-C.:

Electrochemical Impedance Spectroscopy for Battery Research and Development. In: Technical report 31 1996

Spöttle, M; Jörling, K; Schimmel, M; Staats, M; Grizzel, Logan, Jerram, Lisa; Drier, W; Gartner, J; Thomas, M; Ratcliff, C; Borka, A.:

V Bibliography

Research for TRAN Committee - Charging infrastructure for electric road vehicles Bruxelles, 2018

Stroe, A.-I; Stroe, D.-I; Knudsen Kær, S; Swierczynski, M.:

Generalized Characterization Methodology for Performance Modelling of Lithium-Ion Batteries. In: Batteries, Jg. 2016, 2016, Nr. 2

Stroe, A.-I; Stroe, D.-I; Swierczynski, M; Teodorescu Remus; Knudsen-Kaer, S.:

Lithium-Ion Battery Dynamic Model for Wide Range of Operating Conditions. The Cheile Gradistei Fundata Complex, Braşov, Romania, 25-27 May, 2017 Piscataway, NJ: IEEE, 2017

Stroe, D.-I.:

Master of Research (MRES) - Introduction to Battery Models, Jg. 2018, 2018

Tim Fronzek:

New ID.3 and future ID. models to be equipped with batteries offering the highest capacity – and an eight-year warranty, 2019

Yuping Wu:

Lithium-Ion Batteries: Fundamentals and Applications. Electrochemical Energy Storage and Conversion , 2015

Zimmerman, A. H.:

Self-discharge losses in lithium-ion cells. In: IEEE Aerosp. Electron. Syst. Mag., Jg. 19, 2004, Nr. 2, S. 19–24.

NISSAN NORTH AMERICA, I.:

2011 Leaf First Responder's Guide , 1 Aufl. , 2011

van Schalkwijk, W; Scrosati, B.:

Advances in Lithium Ion Batteries. Introduction 2002, S. 1–5.